LA-UR-20-29243
Approved for public release; distribution is unlimited.

Title: Heavily Confined PBX 9501 Experiment Report FY2020

Author(s): Holmes, Matthew David; Broilo, Robert M.; Rettinger, Ryan Charles; Barnes, Andrew Thomas; Heatwole, Eric Mann; Erickson, Michael Andrew Englert; Feagin, Trevor Alexander; Rae, Philip John; Pederson, Michelle Nicole; Dickson, Peter; Parker, Gary Robert Jr.

Intended for: Report

Issued: 2020-11-10

Heavily Confined PBX 9501 Experiment Report FY2020

Holmes, Matthew D.
Broilo, Robert M.
Rettinger, Ryan
Barnes, Andrew
Heatwole, Eric M.
Englert-Erickson, Michael A.
Feagin, Trevor A.
Rae, Philip
Pederson, Michelle
Dickson, Peter
Parker, Gary R.

Los Alamos National Laboratory
M-6 Explosives Applications and Special Projects
High Explosives Thermal and Mechanical Response Team

October 16, 2020

Abstract

Most accidental insults to explosives are invariably thermal in nature—either direct thermal via application of heat or indirect thermal when mechanical energy is converted to heat. The key question is whether the initial thermal insult transitions into a violent explosive response. If the ultimate violence attained is moderate, nearby personnel may be harmed or killed, but Inadvertent Nuclear Detonation (IND) will not occur. However, if the explosive ultimately transitions from deflagration to detonation (DDT) then IND becomes a concern.

PBX 9501 is not an insensitive high explosive (IHE). It has been conclusively demonstrated that mechanically and thermally damaged PBX 9501 can readily DDT in heavy confinement. However, it is currently unknown whether *pristine* explosive—i.e. thermally and mechanically undamaged— is capable of DDT.

Three experiments were conducted in order to determine whether very heavily confined pristine PBX 9501 is capable of DDT. All experiments used identical 6-inch diameter spherical charges of PBX 9501 confined in a 350 lb. hardened steel vessel with >2.5-inch thick walls. The first, primary experiment tested pristine PBX 9501 and was thermally ignited at the center of using a laser over optical fiber. Two additional baseline experiments were performed for comparison: the second test was initiated at the center using a detonator; the third test was bulk heated until self-ignition (cookoff).

Velocimetry data in combination with hydrocode simulations suggest that a classical detonation wave did not develop in the pristine, thermally ignited PBX 9501. Reaction violence was approximately equivalent—in terms of ultimate energy output—as a full detonation, but the acceleration of metal fragments occurred more slowly than in a detonation-driven scenario.

Table of Contents

Figures

1. Introduction

This report documents three experiments performed in 2020 with 6-inch diameter spherical charges of PBX 9501 in a massively confined geometry.

The purpose of the test was to determine whether pristine PBX 9501 is capable of DDT in a very conservative over-test, and to compare the violence of pristine material to thermally pre-damaged material.

The first test used pristine PBX 9501, thermally ignited at the center of the charge using an infrared laser delivered via optical fiber. The second test used pristine PBX 9501 and was deliberately detonated from the center of the charge. The third test used heated, thermally damaged PBX 9501 and was heated until self-ignition (cookoff).

1.1. Accident Hazard Motivation

There are numerous conceivable accident scenarios involving weapon processes or transport that may deliver an insult to the high explosive charge. Some examples include mechanical impact, engulfing fire, and electrical discharge. Regardless the type of event, the nature of the insult delivered to the explosive in most accident scenarios is ultimately *thermal* in nature. The hazard is that the stimulus may be converted to heat, and if sufficiently concentrated it may raise the temperature of the explosive to ignite a deflagration. After ignition, the range of possible post-ignition response ranges in violence from benign quench, up to and including detonation.

In order for a non-shock insult delivered during an accident scenario to ultimately result in detonation, the explosive must undergo the deflagration-to-detonation transition (DDT). Explosives differ in their propensity to DDT. Consider that the TATB explosive component in PBX 9502 has never been observed to DDT, even in highly conservative, worse-case conditions[1]. The inability to undergo DDT is the primary attribute that qualifies it as an Insensitive High Explosive (IHE)[2].

The question of whether or not pristine PBX 9501 is capable of DDT is particularly relevant for safety determinations. If the main charge explosive does not detonate, an Inadvertent Nuclear Detonation (IND) cannot occur (sub-detonative levels of violence may, in the worst case, disperse non-aerosolized fragments of Special Nuclear Material—SNM). Therefore, if DDT can be ruled out for a particular non-shock accident scenario, IND can be eliminated as a possible outcome.

LANL established a decade ago that PBX 9501 which is both heavily-confined and thermally-damaged is capable of DDT[3]. Parker et. al. have conducted considerable additional DDT research since, exploring the mechanism for DDT in quasi-one-dimensional geometries for various PBX compositions[3].

However, the question of whether *pristine* PBX 9501 is capable of DDT (*pristine* is defined as thermally and mechanically un-damaged at the time of ignition) remains unanswered. PBX 9501 is probably the most studied explosive in history. Hundreds—perhaps thousands—of sub-detonative experiments have been conducted with pristine PBX 9501 over the past half-century to ascertain the response to accident scenarios. Despite this rich dataset, the authors are unaware of a single test in which *pristine* PBX 9501 was observed to DDT.

Hazard analyses of insults to main charge CHE commonly assume that any ignition results in a full detonation. This is a quite conservative assumption, considering that detonation of pristine PBX 9501 has never been observed to result from an ignition. Indeed, this assumption may be overly conservative by a margin far larger than required for adequately mitigating the risk. Historically, this assumption was necessary due to the limited predictive capability for post-ignition violence. Though the modeling capability for post-ignition violence remains insufficiently robust for use in nuclear weapon safety determinations, significant progress has been made towards understanding the factors that dominate post-ignition violence. This increased knowledge provides an opportunity to improve the level of conservatism required for a safety basis. With sufficient scientific basis, it may be possible to revise the assumption that ignition ineluctably leads to detonation.

1.2. The Role of Confinement

Many factors contribute to the propensity for an explosive to DDT. However, it is widely accepted that, of the many factors, confinement is *required* for PBX 9501 to DDT. An unconfined charge of pristine PBX 9501 ignited on the surface will burn benignly, and cannot transition to detonation. This is not a statistical result; it is physically based. There exists no mechanism for a surface deflagration of an unconfined charge of PBX 9501 to DDT.

The main charge of CHE in a weapon geometry experiences a certain amount of confinement; the confinement increases the ultimate violence that can be attained by an initially deflagrating charge. It is unknown at present what maximum violence may be attained by a thermally ignited pristine charge of PBX 9501 in a weapon. It is not practical to perform the quantity of test with high-fidelity weapon assemblies that would be necessary to obtain the statistics required to support a 1×10^{6} hazard level. "Over-tests" must be performed, in which any factors that increase the likelihood of detonation are contrived to be "worse", by a margin, than in an actual weapon.

Ideally, the level of conservatism performed in the over-test would be realistic and relevant, i.e. greater than the weapon by a quantifiable but not excessive margin. It is difficult however to precisely characterize and quantify the confinement provided by a weapon geometry. Confinement, with regard to its effects on explosive reaction, is a complicated, multi-faceted concept. The mass of explosive, masses and types of surrounding materials (collective we shall refer to this as the "case"), and properties of the case including ductility, toughness, strength, strain-hardening and strain-rate dependence, free-volume ullage of the case, all affect the confinement, and not always with linear or even monotonic dependencies.

It is much easier however to design an experiment with *considerably* higher confinement than that present in a weapon geometry. The confinement is the most important attribute of the Heavy experiment described in this report, and sets it apart from previous deflagration experiments. We are aware of no other tests with the level of confinement in this design.

It should be reiterated that the Heavy experiment was not designed to achieve a confinement that is realistic or representative of a weapon environment; the confinement in this design is the maximum confinement given practical considerations for test assembly and execution. The primary constraints on the level of confinement were weight, manufacturability of the steel vessel components, and the ability for workers to LANL workers to handle and assemble the vessel components.

The philosophy behind the Heavy test, with its massive over-confinement, is that it may provide results that side-step the confinement debate. If an explosive can deflagrate inside this confinement without transitioning to detonation, it provides a strong argument—with excessive margin—that the explosive will not DDT in a weapon-relevant configuration. However, the experiment does not support the converse claim: if the explosive is observed to DDT in this confinement, it does not indicate that the explosive will DDT in a weapon-relevant configuration, which possesses significantly less confinement.

1.3. Cookoff

High Explosive (HE) that is subjected to an accidental fire experiences a thermal insult that can lead to self-heating and thermal runaway. The thermal runaway and consequent self-ignition is termed "cookoff."

When boundary temperature on the explosive is high enough that the explosive ignites at the surface, the situation is termed a "fast" cookoff. The *slow* cookoff scenario requires the boundary temperature to be tuned such that self-heating of the explosive eventually dominates the ignition time and location. In the ideal slow cookoff scenario, the ignition location self-centers within the charge. This scenario produces higher violence than a fast cookoff, for multiple reasons: the additional time at elevated temperature promotes thermal damage, which is known to exacerbate violence, the overall temperature is already higher at the moment of cookoff, and the center ignition is more confined, inertially, by the surrounding mass of explosive. The slow cookoff scenario is therefore considered a more conservative thermal insult and is typically used for "over-test" experiments.

The ultimate goal of cookoff research efforts is to develop the capability to predict the time-to-cookoff and location of cookoff given a set of known thermal boundary conditions.

While the primary goal of the Heavy experiment reported here is to ascertain the violence attained by pristine 9501 in heavy confinement, a secondary goal is to perform a cookoff experiment in the same confinement, for a baseline comparison against the pristine material, and to exercise the existing capabilities of 9501 thermal modeling.

1.4. Previous Heavy Tests with PBX 9502

M-6 personnel designed the Heavy Test apparatus in 2014 to reproduce, with additional confinement and diagnostics, a historical 1979 qualification test for PBX 9502 performed by Larry Hatler[4]. The historical Hatler test was a simple go/no-go test with few diagnostics. We re-designed the Hatler vessel and performed a test series in 2014 and 2018. There were two purposes for that test series: a) establish a baseline qualification standard for existing in-use lots of PBX 9502, b) provide model verification and validation data for a thermal cookoff model of PBX 9502. Reports for that test series are found in references [1,5]. The design for those tests is used with minor modifications for the PBX 9501 experiments reported here.

1.5. CISME experiments FY 2018

In 2018 M-6 performed the CISME (center-ignited spherical mass explosion) experiment series with pristine charges of PBX 9501. The results for this test are documented in reference [6]. The mechanical confinement for that test consisted of 4 mm thick stainless-steel hemispherical shells containing a 10-inch diameter solid spherical charge (in the largest test). The charge was centrally ignited using a laser pulse, fiber optically delivered to a small charge of thermite down a blind hole.

The violence observed in the 10-inch diameter CISME test was surprisingly benign. The bolts holding the metal shells together were sheared, the shells were ejected intact, and a small amount of explosive was deflagrated before reaction quenched. Most of the explosive was recovered as large broken chunks afterward, with relatively little evidence of reaction.

Prior to the CISME test series, it is this author's opinion that the outcome of a Heavy experiment with pristine PBX 9501 would have almost surely resulted in DDT. However, the unexpectedly benign result from the 10-inch diameter, moderately confined CISME experiment indicated that only a small fraction of the 9501 near the ignition point reacted—causing fracture and acceleration of the pristine 9501 fragments; the majority of the initial charge was recovered in seemingly unaffected chunks. It became necessary to perform a PBX 9501 Heavy experiment in order to further confine reaction that might result in DDT in pristine 9501. As mentioned, if the Heavy experiment is observed to cause DDT in pristine PBX 9501, it will be the first reported experiment to do so.

2. Design

This section will detail design elements that are common to all of the Heavy vessel experiments. Design details specific to individual experiments will be covered in the results sections for each individual experiment.

2.1. Explosive

Explosive was uniaxially pressed from PBX 9501 molding prills (lot BAE08H145-15) into 12-inch diameter billets and turned down on the lathe to 6.00-inch diameter spheres. A 0.125-inch diameter hole was drilled to the center of the sphere. Final charge weights were 3.408 kg and density 1.839 g/cc (**Appendix A**).

2.2. Vessel

The vessel consists of three components: the bowl, the insert, and the lid (Figure 1). The minimum thicknesses of steel between the inner cavity and outer surfaces of the bottom, sides, and top are 2.75, 2.92, and 3.17 inches, respectively. These components were machined by Yeamans Machine Shop in Los Alamos.

All parts are made of 4340 chromoly steel. These components were rough machined, hardened to 38-40 HRC (Appendix F), then finish machined to the final dimensions.

As mentioned earlier, the design for this vessel was motivated by a historical qualification test organized by Larry Hatler[7]. Hatler's vessel used an insert and a bolted lid, but the insert was unthreaded. Our threaded insert, thicker walls, and hardened 4340 steel all increase the confinement over Hatler's design[1].

The insert is threaded into the bucket with 6.5-8-UNS-2A thread, with a thread engagement depth of 3.375-inches. When fully seated, the insert sits 0.005-inches shy of the lid to ensure that the lid bolts flush to the bucket rather than the insert. Shallow grooves in the top of the insert provide gas passages to ensure that pressure is equalized across the face and threads of the insert.

The diameter of the cavity in the bowl is 6.156 inches. It is oversized relative to the charge diameter in order to permit an 8% by volume thermal expansion during heating.

Two o-ring grooves in the top face of the bowl provide a face seal to prevent leaking between the bowl and lid.

There are four penetrations into the cavity. On the bottom, a 0.125-inch diameter hole leads to a threaded cavity for mounting a pressure transducer. Two feedthrough ports for Autoclave Engineers (AE) high-pressure fittings (Appendix G) are cut into the side wall of the bucket, at the mid-plane of the bowl cavity, opposite each other. A 0.094-inch diameter hole provides access to the cavity. Another AE port is cut in the top of the lid, and a 0.094-inch diameter hole leads axially through both the lid and insert.

The total thickness of steel on the bottom, side, and top were 2.67 inches, 2.92 inches, and 3.18 inches, respectively. Key dimensions are called out in Figure 3.

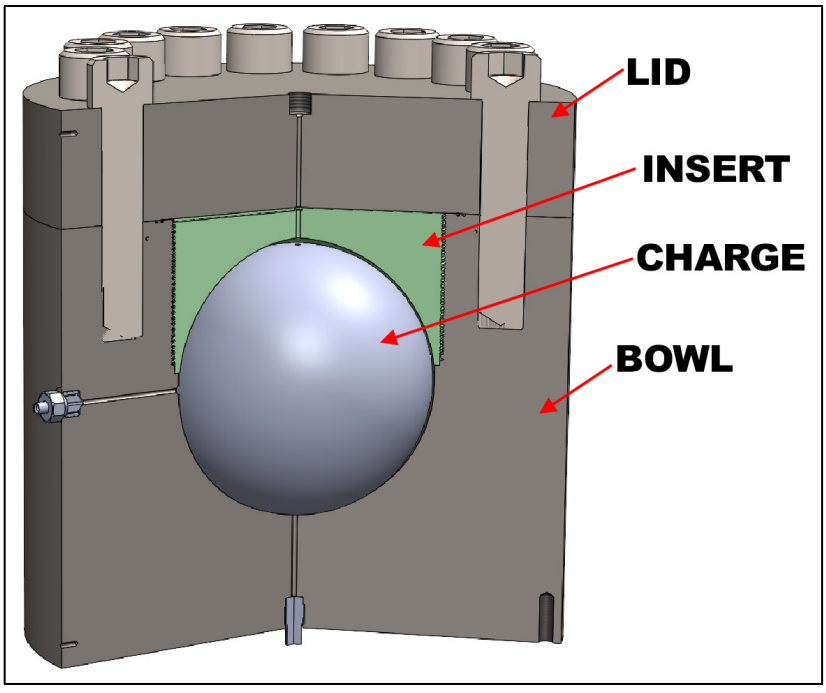

Figure 1. Cutaway diagram of vessel.

[1] One might question whether the addition of pressure ports for feedthroughs decreases the confinement. However, postmortem analysis of vessel fragments reveal that the pressure port is not a failure point during dynamic disassembly, indicating that the feedthroughs are not the weak link and thus do not decrease the confinement.

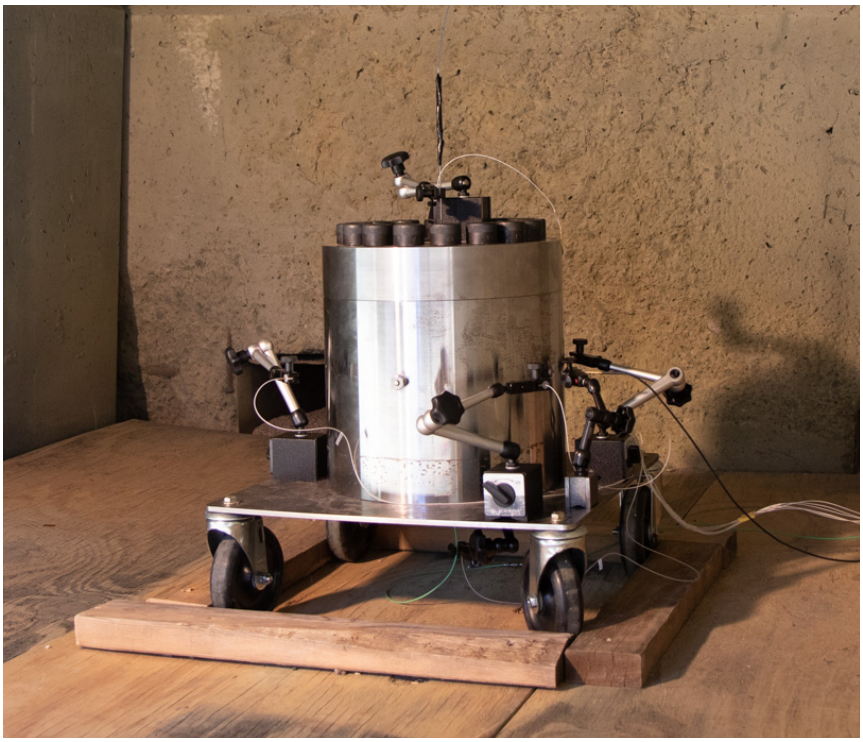

Figure 2. Photograph of shot ready for execution in the block house on the firing mound.

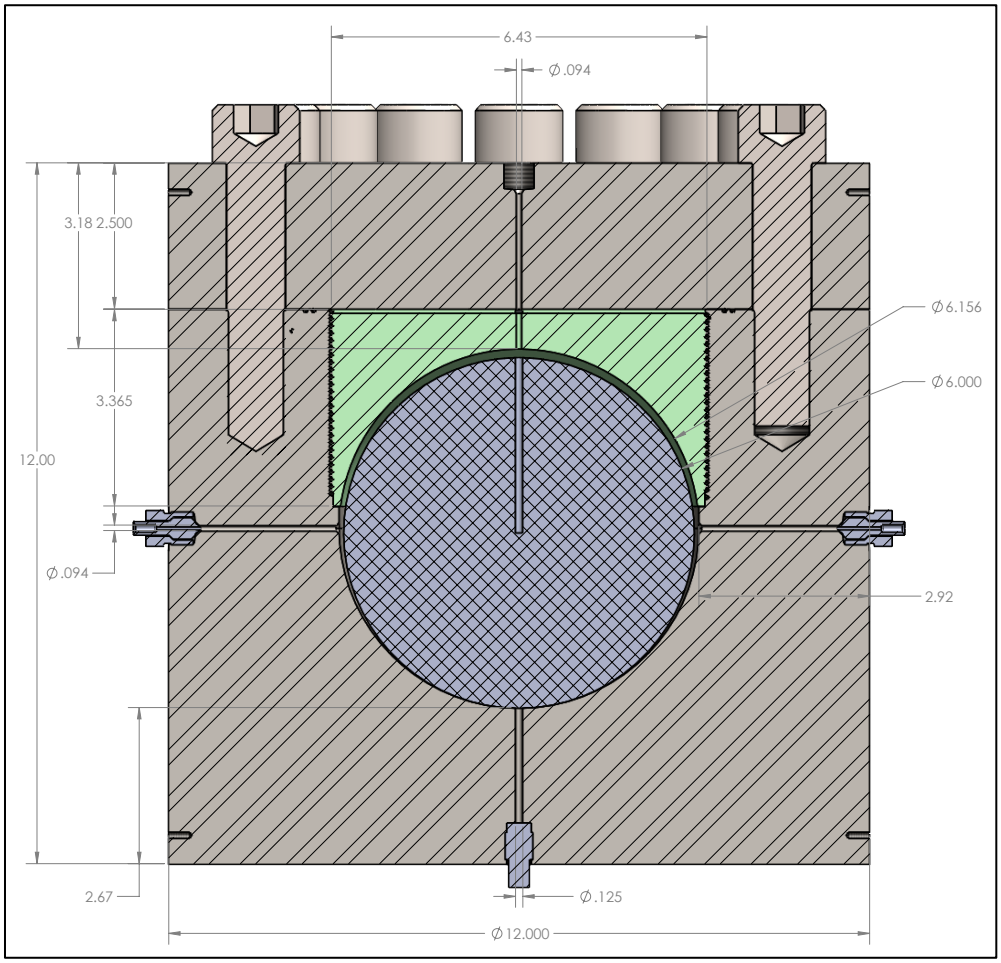

Figure 3. Cross-section view of vessel with dimensions.

2.3. Confinement Analysis

We divide the confinement into two rate regimes: quasi-static and dynamic. The quasi-static regime refers to the long, slow heating phase (over several hours) prior to self-ignition. During this phase, any pressure changes occur much slower than the acoustic speeds of materials; at any single moment, the assembly is amenable to a static analysis. The dynamic regime refers to the gas-production that occurs after self-ignition occurs. In this regime, gas evolves so rapidly that the materials involved (metal and explosive) experience stress gradients. In this regime, gas pressures inside the assembly may not have time to equalize (reaction rate exceeds the acoustic speed of the gas). Small gas vent/leak paths will experience choked flow, and will not act as vent paths on the time scale of the explosion.

Of the two confinement regimes—quasi-static and dynamic—the dynamic confinement is more relevant for the propensity to DDT. However, quasi-static conditions may contribute to the violence by preventing reaction potential from escaping the experiment. With the intent of *maximizing* confinement, the design incorporates features for both quasi-static and dynamic confinement.

In both regimes, it is quite challenging to predict a "pressure-rating" for vessel failure. We undertake a number of different methods to make this estimate.

2.3.1. Quasi-static Confinement

Quasi-static confinement consists of making the assembly gas-tight so that any gases produced during the long, slow heating phase are contained within the assembly. The quasi-static confinement can be characterized by its pressure rating and leak rate. On the Heavy assembly we use two silicone O-rings as a face seal (with operating temperature up to 230˚C). There are two feedthroughs for thermocouples for the heated tests; in unheated tests the feedthroughs are sealed with a solid plug. There is a feedthrough in the bottom of the vessel for a pressure transducer, and a feedthrough in the top of the vessel for the optical fiber. All feedthroughs are constructed from modified Autoclave Engineering HP-series fittings, with a working pressure rating of 50,000 psi. The weak point of the feedthrough itself is the method for potting the elements—e.g. a brazed potting in the case of the thermocouples and high-temperature epoxy for the laser fiber. The potting method is covered in more detail in the relevant diagnostic section of this report.

Sixteen 1-14 SHCS bolts (McMaster part#91251A322) are used to bolt the lid to the bucket. Each of these bolts is rated for a minimum tensile strength of 170,000 psi; each bolt has 0.636 in^2 area; this results in a simple estimate of strength for all 16 bolts of 1.73 Mlbs. This force acting on the exposed area of the inside of the lid (taking no credit for the reduced diameter of the insert) gives an estimate of the static pressure rating of the vessel to be 53 ksi.

An FEA structural static analysis of the assembly as a pressure vessel was performed with two pressure boundary conditions to provide a more rigorous estimate of the vessel's pressure rating. For the first simulation, pressure was applied to the surfaces identified with red dashed lines in Figure 4. This loading geometry is expected to accurately represent the conditions during the long, quasi-static heating phase, during which gas pressure can equalize through the insert both along the thread path and up through the center feedthrough hole. This is referred to as the "venting insert" version. In this scenario the threads of the insert are neglected. Estimating the yield strength of the steel as 103 ksi, the internal cavity pressure at which the steel yields is in the range of 40-50 ksi for this scenario. Figure 6 shows the false-color illustrations of the internal stress distribution for various cavity pressures.

A second pressure boundary scenario was modeled (Figure 5), in which the pressure was applied only to the spherical center cavity. This is the anticipated pressure loading during the dynamic event, when choked flow prevents the cavity pressure from being communicated effectively through the narrow vent paths. In this scenario the threads of the insert are given full credit; that is, the insert-bowl parts are treated as a single part monolithic part with no seam. We refer to this as the "sealed insert" scenario.

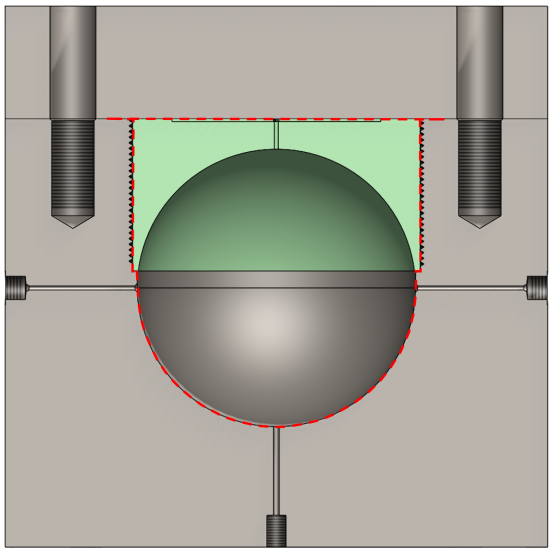

Figure 4. Cross-section diagram of vessel illustrating boundary condition for the first structural simulation—this is the "venting insert" version, which simulates the lowest strain-rate static loading regime. The red hashed line indicates the surfaces to which pressure is applied for this version.

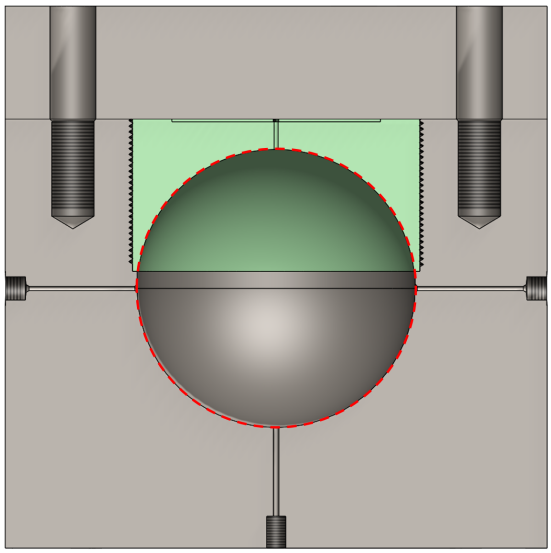

Figure 5. Cross-section diagram of vessel illustrating boundary condition for the second structural simulation—this is the "sealed insert" version, which simulates a slightly more dynamic loading regime. The red hashed line indicates the surfaces to which pressure is applied for this version.

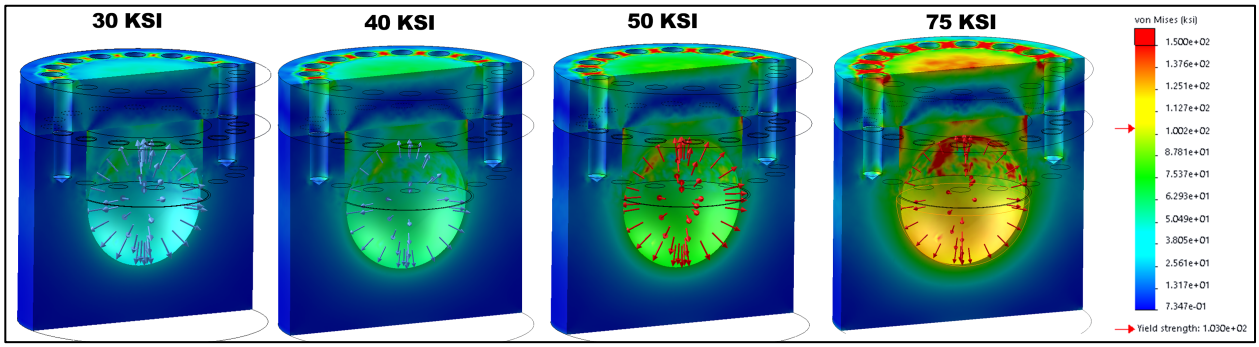

Figure 6. Illustration of internal stresses in the "venting insert" simulation, at various internal pressures. Considering the von mises stress and using a yield strength of 103 ksi, the simulation indicates failure in the range of 40-50 ksi of internal cavity pressure.

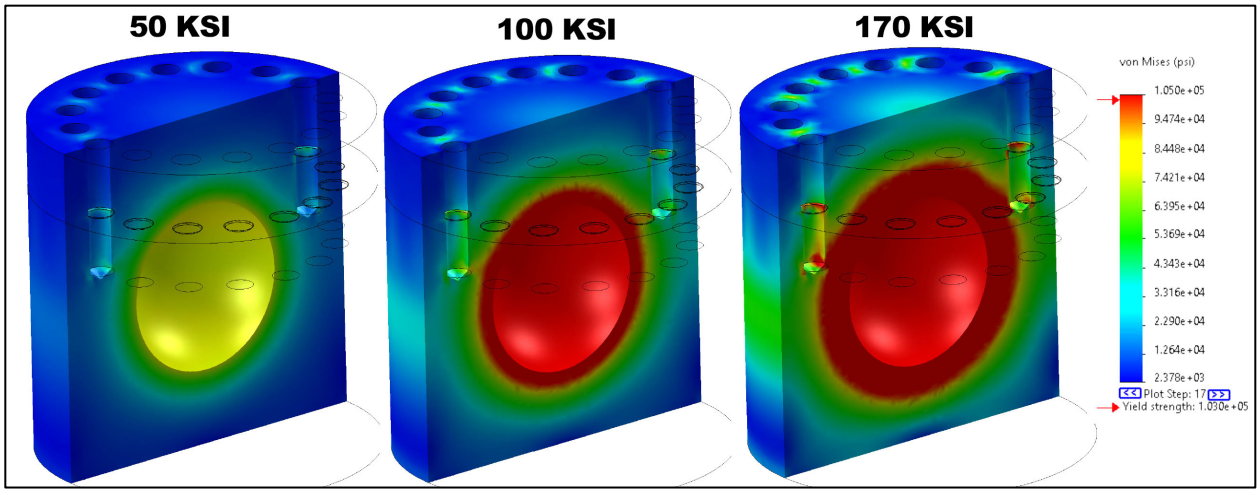

Figure 7. Illustration of internal stresses in "sealed insert" simulation, in which we take "credit" for the insert, at various internal pressures. In this model, the bucket is a single piece of steel with a hollow cavity. This simulation is useful only for visualizing the stress field.

The model is useful for visualizing the stress field, but is too unrealistic to extract a pressure rating. Figure 7 shows a false-color illustration of the internal stress distribution at three different pressures for this "credit for insert" scenario. In this figure we see the stresses exceeding the yield strength of the steel at the center, but without a fracture model the simulation cannot predict vessel rupture. This model is not much better than idealizing the vessel as a sphere with 2.5 inch-thick walls, which is calculated to fail in the vicinity of 170 ksi. We know that this static model doesn't accurately describe the dynamic event; during the dynamic event, the high strain-rates on the materials will result in considerably higher material strength, and the pressure attained will greatly exceed this static rating. During the dynamic event, this minimum pressure may be exceeded by orders of magnitude, and the final pressure in the vessel will depend primarily on the reaction rate.

The previous two methods for FEA simulations isolated the vessel characteristics and ignored the fastener strength. Sixteen 1-14 UNF bolts secured the lid. The tensile strength rating of the bolts was 170 ksi. A simple calculation of bolt area reveals that the collective bolt pattern of the assembly is rated to contain an internal pressure of 48 ksi; failure will occur at a pressure higher than this—how much higher depends on the actual strength of the bolts rather than the rated strength of course. Additionally, the strength of the threads on the insert will contribute to the final pressure that is achievable, to the extent that the pressurization rate outpaces the ability for pressure to equalize via leak paths through and around the insert.

2.3.2. Dynamic Confinement

Though it may be obvious, we reiterate that the dynamic pressure reached during the event will exceed any estimate for the quasi-static pressure rating of the vessel. Despite the best engineering efforts, it is not possible to contain reacting PBX 9501 inside a sealed cavity (lacking any ullage volume) without the vessel or pressure fittings failing (at least not with the strength of currently known materials). It is therefore *anticipated* that fittings and vessel will eventually fail, but the design of the vessel attempts to contain the reaction long enough to observe a DDT event prior to failure and subsequent venting of pressure and temperature in the cavity.

2.4. Diagnostics

2.4.1. Pressure

Pressure of the interior cavity was measured with a Kistler charge-mode piezoelectric transducer, model 6213BA with range 0-8000 bar (0-145,038 psi). The pressure transducer was mounted on the bottom face of the vessel, at the end of a 0.125-inch diameter hole. The cavity was filled with a high-temperature low-viscocity silicone fluid in order to more rapidly transmit the pressure experienced in the internal cavity through the small diameter hole to the pressure transducer (DPDM-400 dipenyl dimethyl silicone from Clearco Products with a viscosity of 400 cSt). This pressure transducer captures an intermediate rate regime; it does not record long-duration quasi-static pressurization (>10 s), and it is not sufficiently rapid response to capture the shock regime (<10 μs); it best characterizes the pressure in an intermediate, deflagration regime.

In previous experiments using this identical geometry with PBX 9502 explosive, the pressure recorded at the bottom pressure transducer exceeded the maximum range of the transducer, at 145 ksi. The transducer was located down a 2.5-inch long hole filled with silicone transfer fluid, and thus is not expected to have captured the maximum internal pressure of the internal cavity (the pressure would be attenuated by distance and time). Consequently the maximum pressure reached in those experiments may have been considerably higher than 145 ksi.

2.4.2. Velocimetry

Photon Doppler velocimetry (PDV) is used to record dynamic velocity profiles with sub-microsecond time resolution, such as occurs during a shock-accelerated event. Each PDV probe obtains velocity at a single special location on the outside of the Heavy vessel. In these experiments, between 4 and 7 probes were employed on each test. Primarily, PDV is used to determine the violence of the reaction and the likelihood that a DDT event occurred. Without PDV, the high-speed video record and post-shot fragment analysis are often inconclusive about the nature of the reaction inside—especially in cases near threshold. With PDV,

many possible deflagration, detonation, or partial reaction events can be distinguished from each other by a few features in the final record.

Namely, the shape and intensity of the initial jump-off, which indicates whether the reaction has transitioned into a detonation or not, and the final velocity achieved by the metal fragments, which indicates the efficiency of chemical energy conversion useful for driving the metal casing. PDV probes provide a seemingly continuous measurement (on these timescales) of the acceleration experienced at particular locations around the Heavy vessek–synchronized in time for symmetry comparisons.

All PDV records in this series were collected using an 8-channel homodyne PDV system designed in-house. The single laser (1550 nm IPG Photonics® 4 W max) is split evenly to all 8 channels. Reference/return beat frequencies are detected with Miteq 18 or 20 GHz photoreceivers and recorded with 2 each 4-channel Tektronix® 70,000 series oscilloscopes. At the Heavy vessel, the sample leg of each fiber optic interferometer is terminated with a 2.4 mm OD fiber collimator (AC Photonics®) mounted about 3 inches from the exterior surface. For this series, the fiber collimators (PDV probes) were mounted to a magnetic-base adjustable machinists' dial indicator holder (Clockwise Tools® model: MGBR-01).

PDV probes were aligned around the Heavy vessel, each measuring a particular location. The vessel was surface prepped with Scotch-Brite® scouring pads to remove the machining marks and make a more diffusely reflective surface, which proved very effective. The reflectivity of the metal surface—whether shocked or not— returned very high signal-to-noise data throughout its fly distance. The resulting data was processed using AnalyzeDataV1 (updated 3/31/2020) Java-based software package to perform the short-time Fast-Fourier transform (stFFT) analysis and extract velocities from the resulting spectrogram using a centroid image processing algorithm. Further data processing and visualizations were prepared using Python® version 3.7.4.

2.4.3. High-speed video

High-speed videography provides a redundant diagnostic for detonation, and also provides information on sub-detonative response. Two video cameras were employed. A Phantom® V2512 camera captured at a frame rate of 62,000, 200,000, and 30,000 fps for Tests 1, 2, and 3 respectively (frame rate was dependent on the illumination available in each test). On Test 2, a Shimadzu® HPV-X2 (400 px width by 250 px height) was used to record 256 frames at 200,000 fps (1.28 ms of total record time).

2.4.4. Postmortem

Fragments were collected and photographed after the test. The distribution of fragments, in size and quantity, correlates with the level of violence and is a useful metric for side-by-side comparisons between tests. This metric is often good for determining very low-order events from high-order detonations, but when DDT is near-threshold, the fragmentation is nearly identical between transitioned detonations and rapid deflagrations.

2.4.5. Triggering

In the event of a laser-ignited experiment (LIPX), the ignition and growth process may take several milliseconds before the vessel accelerates; depending on their memory buffer size, some diagnostics can record the entire process but others must be triggered after vessel wall motion to capture only the short acceleration (~150μs) of the vessel walls. The Phantom camera has sufficient buffer such that it was triggered simultaneously with the laser, allowing it to record the entire event, even if the vessel never burst apart. Conversely, the PDV oscilloscope and the Shimadzu camera were triggered by a piezoelectric pin positioned ≈3 mm from the cylindrical surface of the bowl which signals shortly after wall motion. Both the PDV oscilloscopes and the Shimadzu camera allow the experimenter to specify a pre-trigger buffer to ensure they record the initial jump-off moment even though the trigger comes after the wall traverses the 3 mm gap to strike the pin.

In the event of a self-ignited thermally-damaged explosive (SITX) experiment, the piezoelectric pin was used, as described for the LIPX test, for triggering all diagnostics, since the test heats for hours and may ignite at any time.

For the intentionally-detonated (DIPX) experiment, all triggers, including the high-voltage fireset, were handled through a master Stanford Research DG535 delay generator.

Consequently, Phantom video timestamps are relative to the laser trigger for LIPX (test 1), the firing signal for DIPX (test 2), and the piezo pin for SITX (test 3). The advantage of avoiding the piezo pin trigger where possible is to ensure that video data is captured regardless of whether the reaction violence is sufficient to actuate the piezo pin. Shimadzu video and PDV timestamps are relative to the piezo pin impact trigger for all tests. The interval between these triggers was captured on the oscilloscope.

3. Test 1 — LIPX — Laser-ignited pristine explosive

This test contained 9501 sphere serial number 19-183-01 and was executed on July 1, 2020. Charge mass was 3409.7 g and immersion density was measured to be 1.840 g (Appendix A).

3.1. Laser

Ignition was achieved by fiber-coupled, high-power laser (IPG Photonics® model YLR-300/3000-QCW-MM-AC-Y12). The laser operates at 1070 nm and is capable of ≤300 W continuous or ≤3000 W at a maximum pulse length of 10ms. The shape and power of the laser pulse are controlled using an analog pulse generator in conjunction with an SRS® DG-535 delay generator. Beam energy is calibrated using a with an Ophir® FPE80BF-DIF-C pyroelectric sensing head connected to an Ophir® StarBrite™ power/energy meter.

The nominal laser power used to ignite the thermite (described below) for this particular test was 5.37 W for 10.0 ms duration, a total energy of 53.7 mJ. The pulse energy was measured prior to assembly; over 10 pulses the standard deviation on the power measurement was 0.8 mJ. The optical pulse is intentionally ramped from zero to full power over 100 μs, and back to zero power at the end of the pulse over the same duration.

3.2. Igniter Design

A diagram of the igniter design is shown in Figure 8. The final segment of optical fiber is a 5 m length of Thorlabs® model FT400EMT; 400±8 μm diameter core, 425±10 μm diameter cladding, 1040±30 μm Tefzel™ coating outer diameter. The fiber optic is potted inside hypodermic tubing (McMaster® #8988K27, 304 stainless steel, 0.083 in. OD, 0.049 in. ID) using a high-temperature low-viscosity Duralco® 4461N epoxy. The furcation tubing was stripped off for the final portion of fiber that is potted (the Tefzel™ coating remains). The protruding tip of the optical fiber is mechanically cleaved by hand, approximately flush with the end of the hypodermic tubing.

A 0.125 in. diameter blind hole was drilled in the explosive charges by the J-8 explosive machining group at LANL (this diameter is the smallest they can safely drill to a depth of 3 inches). To assemble the igniter, thermite is first poured down the hole and lightly hand tamped with a plastic rod. The hypodermic tubing subassembly is inserted to the bottom of the hole, with the tip of the optical fiber touching the thermite. The subassembly is potted by injecting Duralco® 4461N epoxy using a long hypodermic needle affixed to a syringe until the hole is filled (the syringe permits the hole to be filled from the bottom up to avoid any air bubbles).

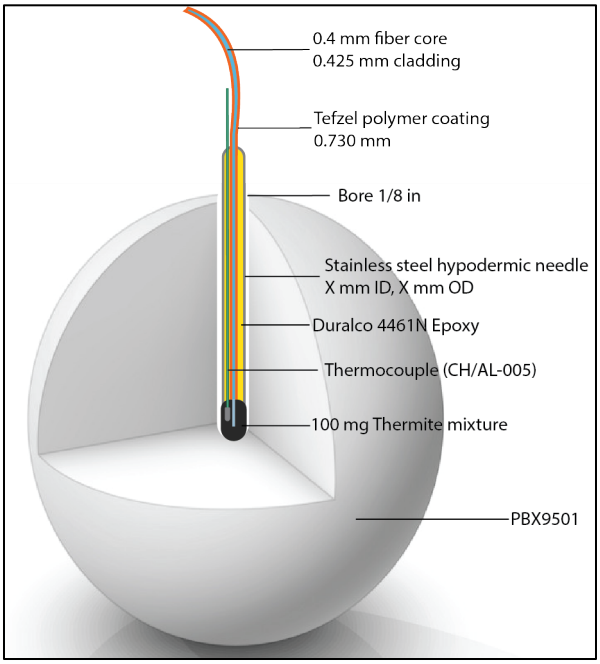

Figure 8. Diagram of igniter system.

3.3. Thermite Details

The thermite used in the experiments is a stoichiometric mixture of aluminum (Al) and iron II,III oxide Fe_3O_4. The aluminum is in powdered form, sourced from Valimet® as their H-5 product. The H-5 aluminum is characterized by Valimet using Microtrac equipment to have a particle distribution as follows: 90% <15 µm, 50% <8 µm, 10% <4 µm. The iron oxide is procured as powder from Alfa Aesar, product 12374-A7. This product is sieved through a No. 325 mesh (by the manufacturer) which yields a maximum particle size of 44 µm. These powders are mixed using a LabRAM™ acoustic mixer in a weight % ratio of 3.22:1 iron oxide to aluminum (this is the stoichiometric ratio). The chemical reaction is:

$$3Fe_3O_4(s)+8Al(s) \xrightarrow{\Delta H=-3.677\frac{kJ}{g}} 9Fe(s) + 4Al_2O_3(s)$$

Note when modeling the heat evolved from this reaction, that 3.298 kJ/g reaction heat is released from solid reactants to liquid products, and the last 0.379 kJ/g is released as the molten reactants solidify.

The explosive charge for this particular LIPX experiment was prepared with 112 mg of thermite lightly tamped into the bottom of the hole. The thermite depth after compaction was 0.286 in (a nominal density of 1.95 g/cc).

Table 1. Pre-test images of the firing site configuration.

Figure 9. Block house before explosion. Blocks and sandbags are mitigation to prevent hot fragments from escaping mound to potentially start fires in surrounding landscape.

Figure 10. View from behind porthole, showing the angle from which the high-speed video is viewing the shot. Both turning mirrors are visible in the photograph. Mirror in the foreground is directly over the porthole. Dark square visible in block house opening is the second turning mirror.

Figure 11. Wide-angle view of the shot situated in the block house.

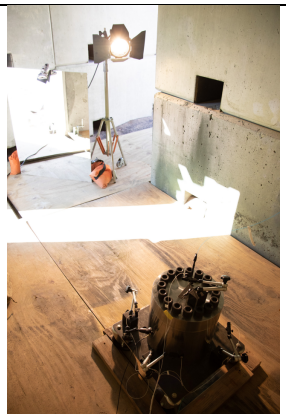

Figure 12. View from behind shot, looking towards the turning mirror.

3.4. Data

The pressure trace first indicated reaction at 34.260 ms after lasing commenced and reached a maximum pressure of 111 MPa before failure (Figure 13). The pressure record exhibits a precipitous decrease in pressure prior to a discontinuous increase that exceeded the maximum pressure capacity. We hypothesize that this decrease resulted from compressive waves transiting the steel more rapidly than through the cavity and accelerating the body of the transducer away from the diaphragm element, placing the piezo crystal into tension.

The piezo pin was impacted by the wall of the vessel at 34.667 ms after lasing (407 μs after first signs of pressurization were observed at the pressure transducer). The time at which the piezo pin trigger was actuated is depicted in frame 2 of Figure 18.

Stills from the Phantom video are shown in Figure 18.

Images of the fragments are shown in **Error! Reference source not found.**.

PDV probe velocities were extracted and are presented in section 6 alongside the PDV data from the other two tests.

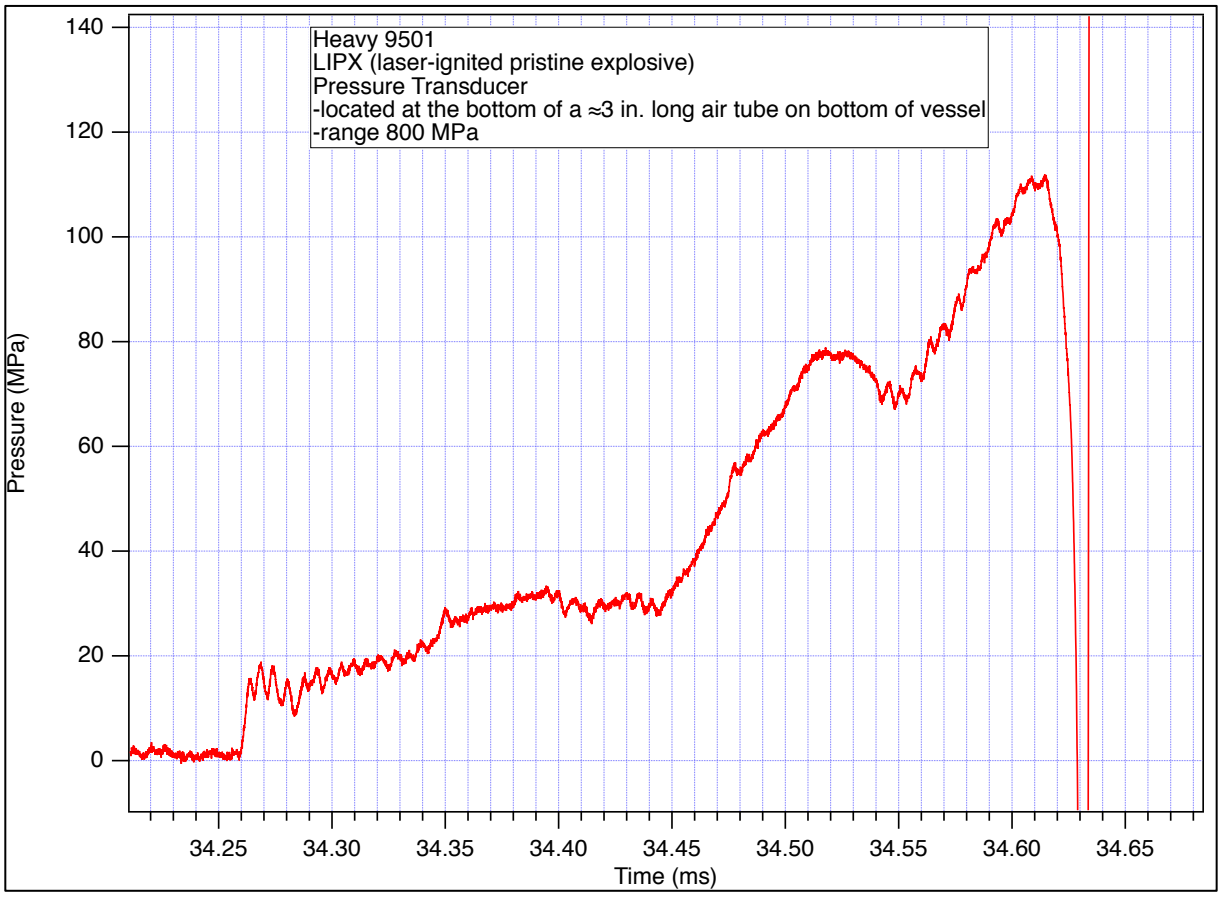

Figure 13. Pressure transducer record from LIPX. Note pressure rise begins 34.25 ms after laser is turned on, and shows ≈350 μs of data before failure.

Table 2. Post-test images from LIPX (Test 1).

Figure 14. Post-test view at entrance to block-house.

Figure 15. Post-test view of block-house interior.

Figure 16. Photograph of all the fragments that were collected from LIPX.

Figure 17. Fragments from lid.

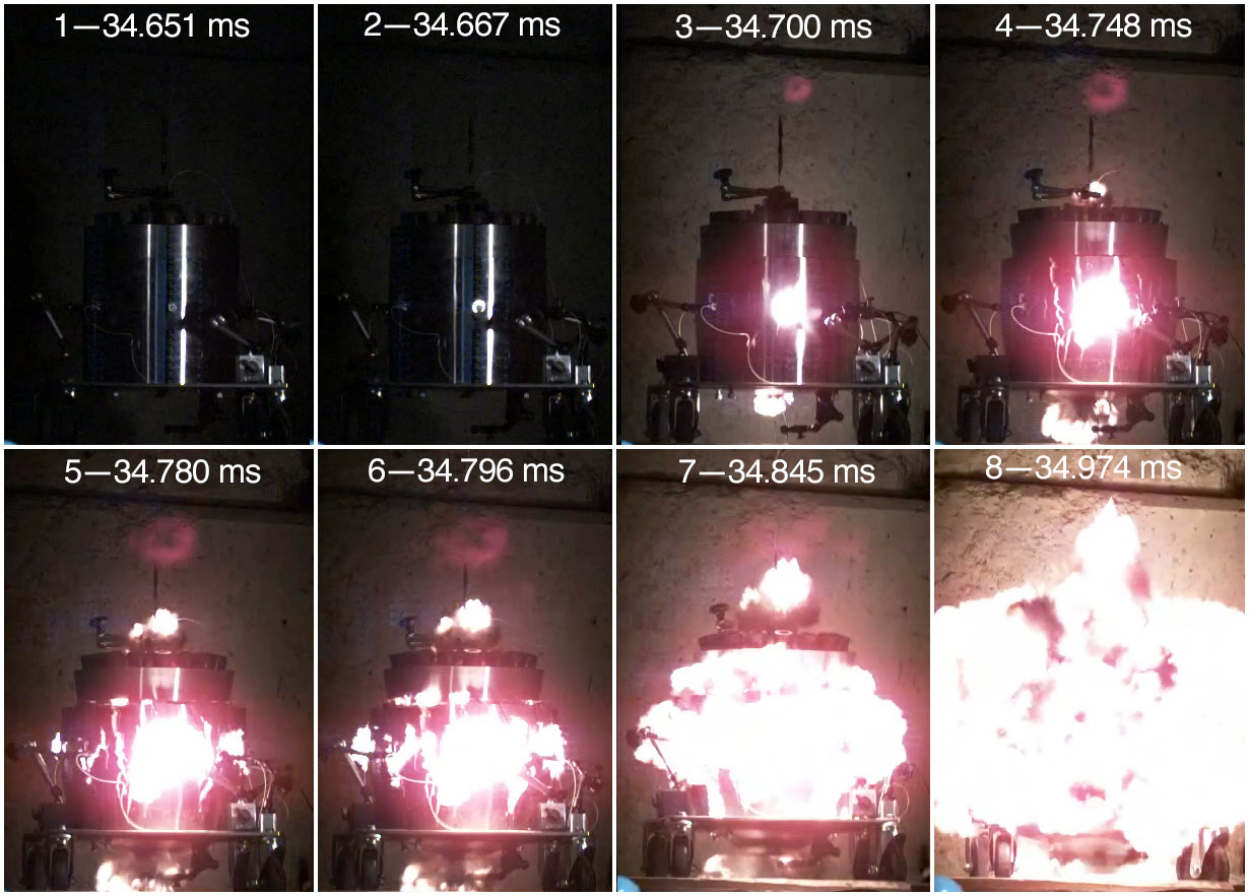

Figure 18. LIPX (Test 1), sequence from Phantom high-speed video. The first frame is the last frame that exhibited no evidence of reaction. On the second frame, light is first visible around the feedthrough.

4. Test 2 — DIPX — Detonator-initiated pristine explosive

This test contained 9501 sphere serial number 19-183-02 and was executed on September 1, 2020. Charge mass was 3407.8 g and immersion density was measured to be 1.839 g (Appendix A).

This test consisted of a deliberate, prompt center detonation accomplished with an RP-3 detonator into a small amount of Primasheet 1000 explosive (65% PETN, 8% nitrocellulose, and 27% acetyl tributyl citrate (ATBC) plasticizer[8]) booster (Appendix G), as the RP-3 detonator has insufficient output for reliable initiation of PBX 9501 directly. The depth of the Primasheet in the 0.125-inch diameter hole was ≈0.375-inch (mass of ≈110 mg).

The hole through the lid and insert for this test was enlarged from 0.094 inch to 0.200 inch in order to provide room for the detonator cables to exit the vessel.

The pressure transducer first shows data at 12.1 μs after the trigger signal was sent to the fireset.

PDV oscilloscopes for this test were triggered coincident with sending the trigger signal to the fireset. For this test only, all diagnostics were triggered simultaneously and share a time zero.

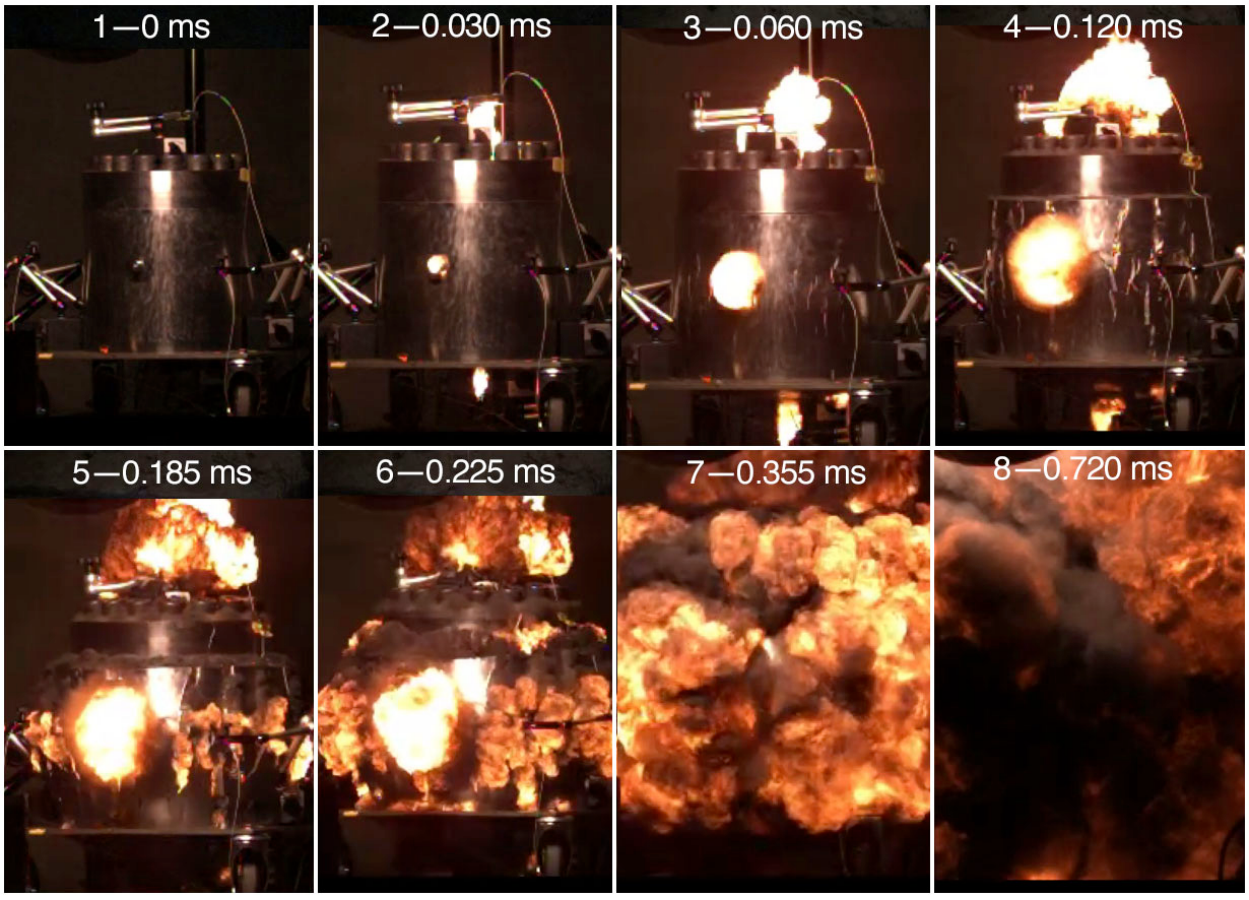

Figure 19. DIPX (Test 2), sequence from Phantom high-speed video. Time zero is coincident with the firing signal sent to the CDU. Visually, there is no noticeable distinction between this test and the first LIPX test (the color differences are an irrelevant artifact of the image processing).

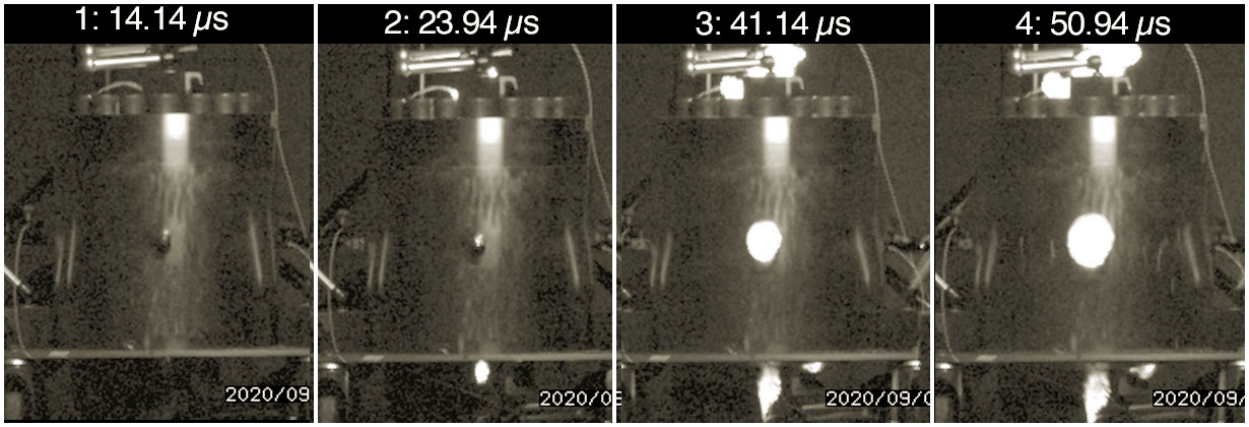

Figure 20. Sequence of selected frames from the Shimadzu high-speed video record. The firing signal is sent at time zero. Light is first visible at 14.14 μs below the bottom feedthrough; fracture is first visible sometime between frames 3 and 4 (between 41.14 and 50.94 μs after trigger signal). Frame 4 was the last frame captured in the 256-frame buffer, by which point the initial fracture pattern is just becoming evident.

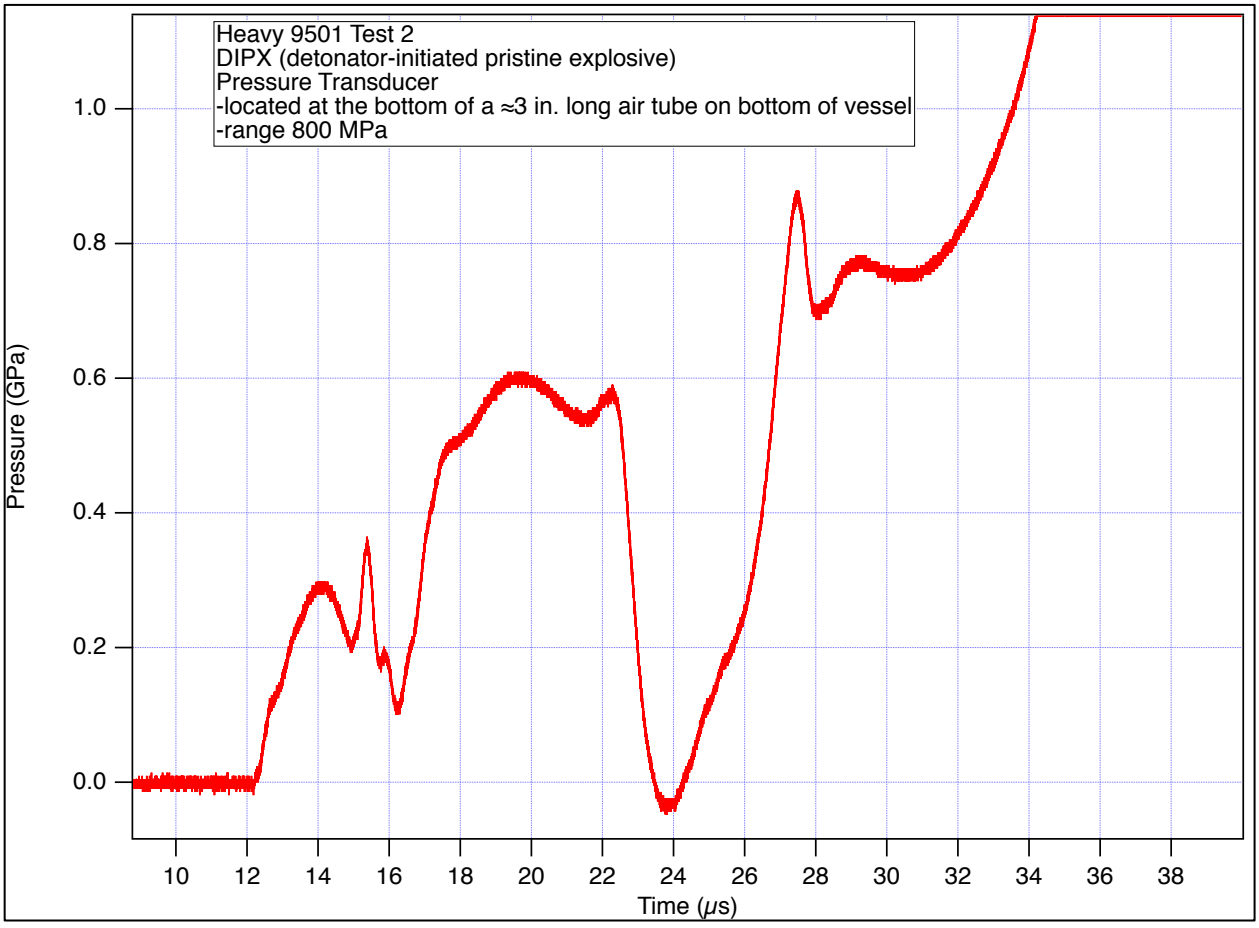

Figure 21. Pressure data for DIPX (Test 2). Response time of the pressure transducer is too long compared to the dynamic phenomena experienced in this test for the data to be very useful.

5. Test 3 — "SITX" — self-ignited thermally-damaged explosive

This test contained 9501 sphere serial number 19-183-03 and was executed on September 9, 2020. Charge mass was 3407.0 g and immersion density was measured to be 1.839 g (Appendix A).

5.1. Heating System

The facility power available at the firing site is 480V three-phase. An off-the-shelf UL-listed commercially available transformer (Larson® model MPD-480-75K-200BE-120-208-C-W with 75 KVA capacity) is used to supply 208Y to a power distribution unit (Motion Laboratories® model 1300-200A-09-2-01), the output of which is nine separate channels of three-phase 208 V. A single channel of three-phase 208 V from the PDU was used to supply a custom-built relay box. Custom-written software (a Labview VI) implemented a PID control algorithm. The heating controller (and all diagnostics) were remotely operated via a fiber-optic network from outside the clearance area of the firing mound.

The assembly is wrapped in heating tape, the Duo-Tape™ product from HTS/Amptek®, model AWH-052-160D. Each assembly uses four heating tapes. The tapes are wired across the poles of the 208V three-phase power. The center two heating tapes are wired in parallel across one phase; the top and bottom are wired individually across the other two phases (Figure 22). The total nominal heating power was 5313 W.

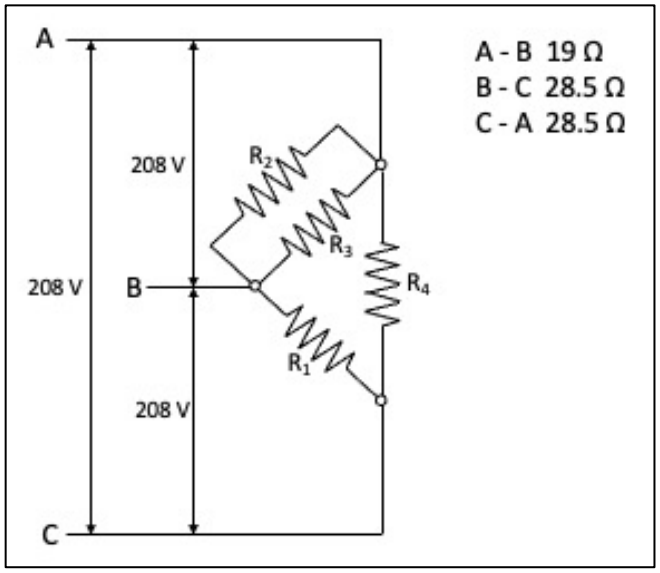

Figure 22. Wiring diagram for the four heating tapes. Resistances R2 and R3 represent the heating tapes wrapped closest to the midplane.

5.2. Temperature Diagnostics

Temperatures internal to the explosive charge were obtained by potting thermocouples (Omega® model 5SRTC-TT-K-30-72) down the blind hole at varying depths (Figure 28). Figure 23 documents the locations of the thermocouples interior to the explosive. The wires for these TCs were led out the top of the vessel, through the holes in the insert and lid. High-temperature epoxy (JB Weld®) was used to pot the wires where they exit the lid. During testing it was observed that this feedthrough seal failed, allowing black, partially-burned, syrupy binder to leak out and spread across the top surface of the lid (this was observed with surveillance video, Figure 24).

Temperatures at the outside surface of the explosive sphere and inside metal surface of the bowl cavity, were obtained with thermocouples routed through the two feedthroughs on the midplane (Figure 29-Figure 32). These internal thermocouples were metal-sheathed for high-temperature resistance, and so that they can be sealed into the feedthrough via brazing. The thermocouples are an Omega® product, model number KMTXL-020U-48, which specifies a type K thermocouple with a sheath outer diameter of 0.020 inches, ungrounded

tip, 48 in. long, with a miniature plug. The small diameter and potential strain-hardening of the metal sheath on these probes makes them quite fragile. They must be handled carefully, and even so failures due to broken probe wires are not uncommon.

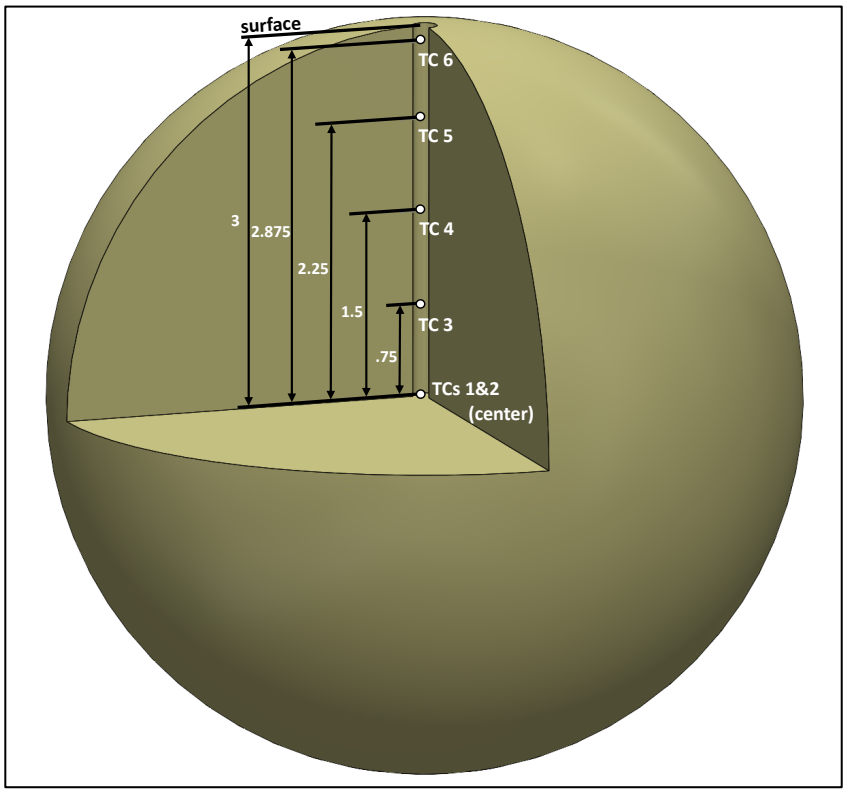

Figure 23. Diagram showing locations of thermocouples potted in the hole inside the explosive charge.

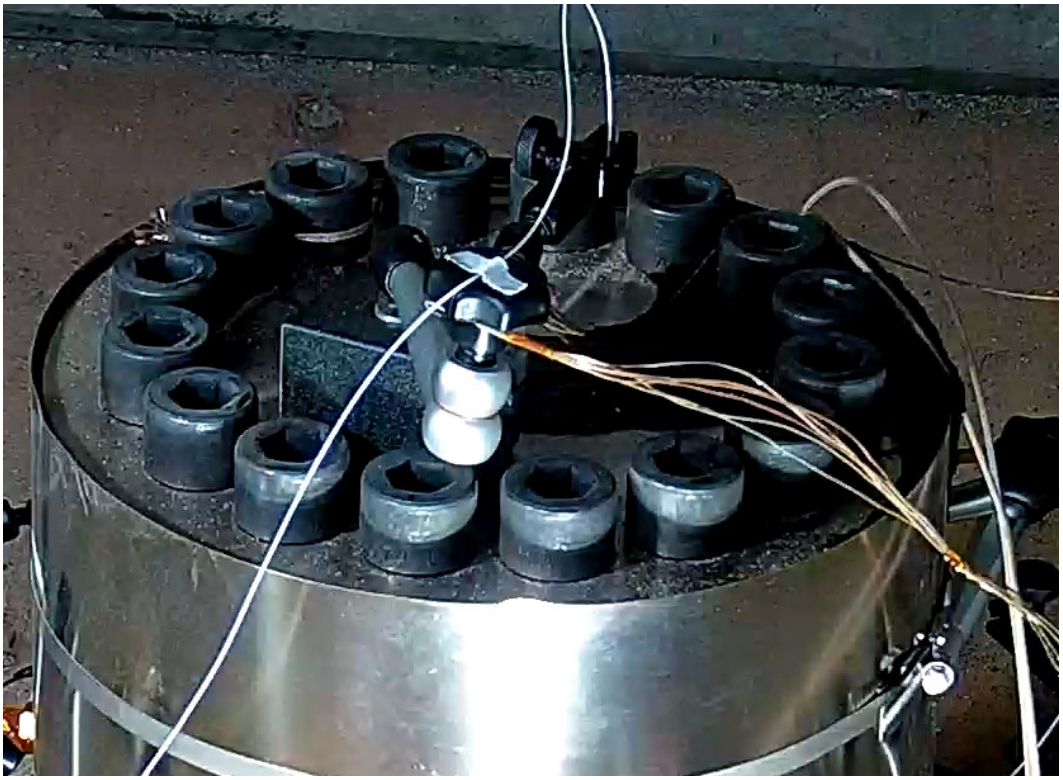

Figure 24. Binder expelled from top feedthrough is visible on lid in this still frame from surveillance video during the test.

To seal the feedthrough, an Autoclave Engineers model AP40 is drilled with a small-diameter through hole, and a larger diameter counterbore on the outside to act as a "cup" for holding braze material (Figure 29 and Figure 30). Thermocouples are inserted through the fitting, to the proper pre-determined depths on the probe, and then the fitting is filled with high-strength braze alloy (56% silver/22% copper/17% zinc/5% tin with melt temperature of 1140-1200 ˚F). This brazing is performed on the benchtop, away from the vessel, before any explosive is introduced.

On the inside of the vessel, thermocouples for the lower half of the charge are taped to the metal surface of the bowl (Figure 33). The charge is inserted, and then the thermocouples for the upper half of the charge are taped to the explosive (Figure 34). Until the charge thermally expands to fully fill the cavity, it is anticipated that the bottom thermocouples will measure a temperature of the metal and charge, while the top thermocouples will only measure the metal temperature due to the air gap; this is a necessary design compromise since there is no feasible assembly method to allow taping the upper thermocouples to the inside of the metal insert. Figure 25 documents the locations of the thermocouples on the exterior surface of the explosive.

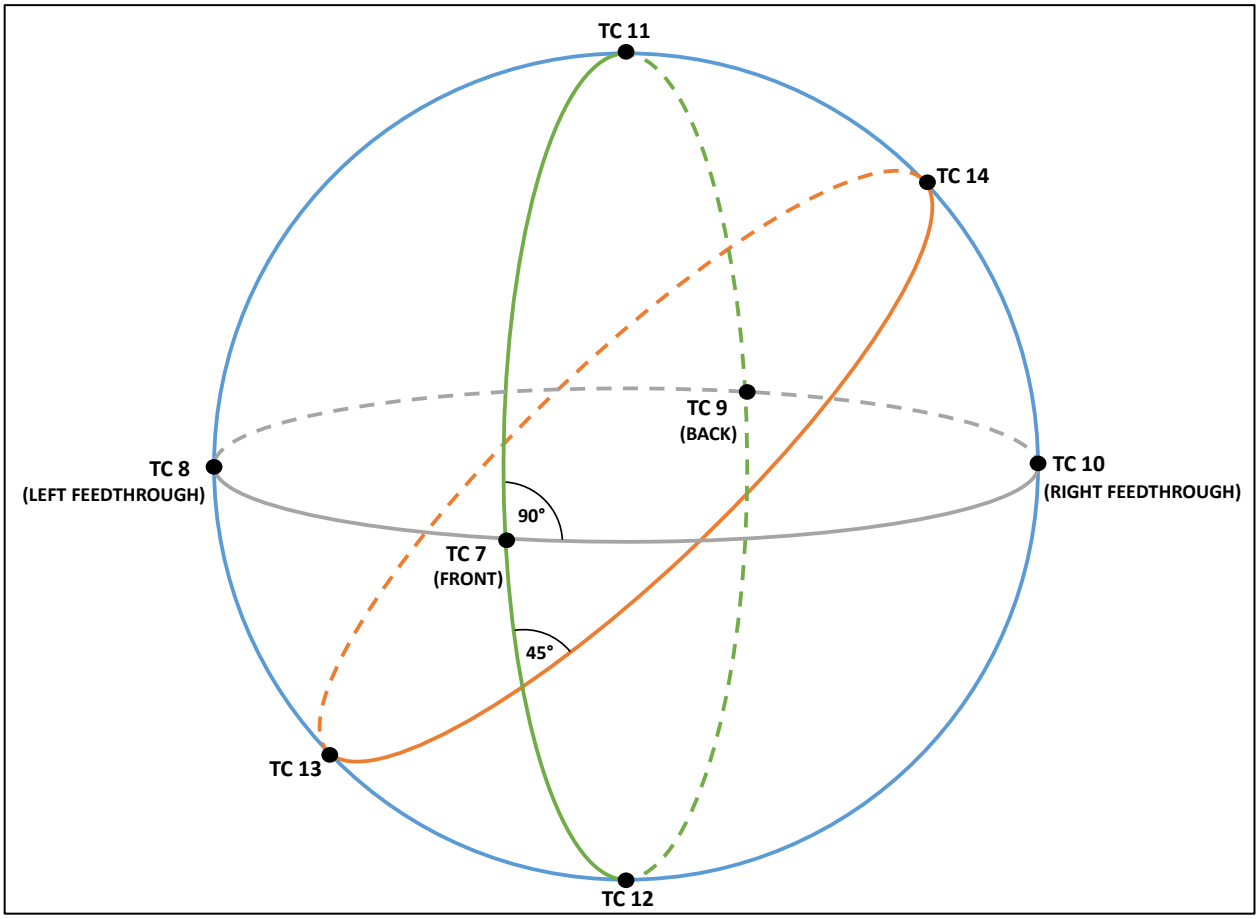

Figure 25. Diagram showing locations of thermocouples on surface of explosive (inside surface of steel bowl).

To record temperatures of the exterior surface of the vessel, thermocouples were taped with Kapton to the surface and covered with a layer of foil-backed fiberglass insulation to minimize errors caused by convective air currents. Figure 26 shows the layers of adhesive tape and insulation that were used for each thermocouple. The thermocouples at the mid-plane were used as the process input value for the PID heating control system. Figure 27 documents the locations of the thermocouples on the exterior surface of the vessel.

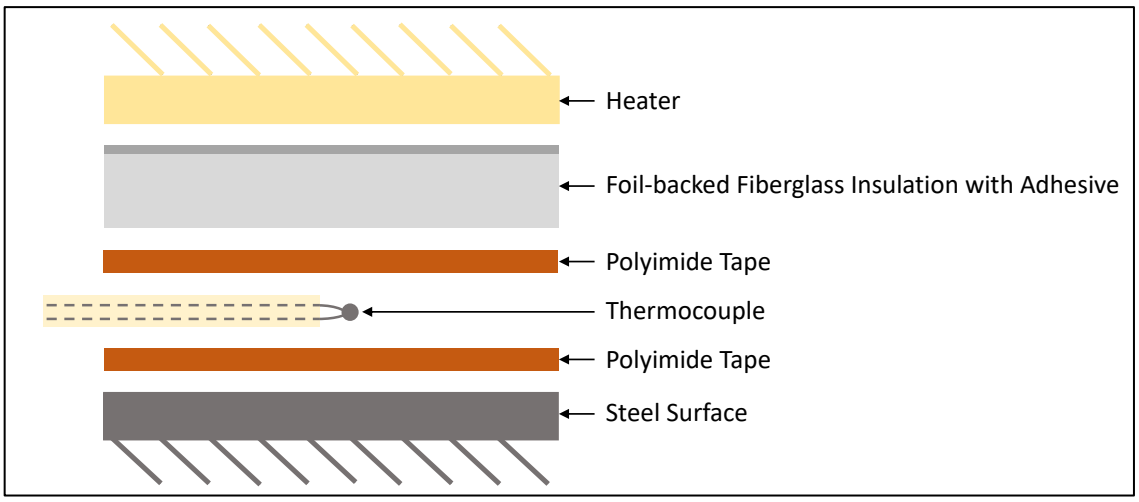

Figure 26. Diagram of stack-up of thermocouple layers, including polyimide tape and insulation

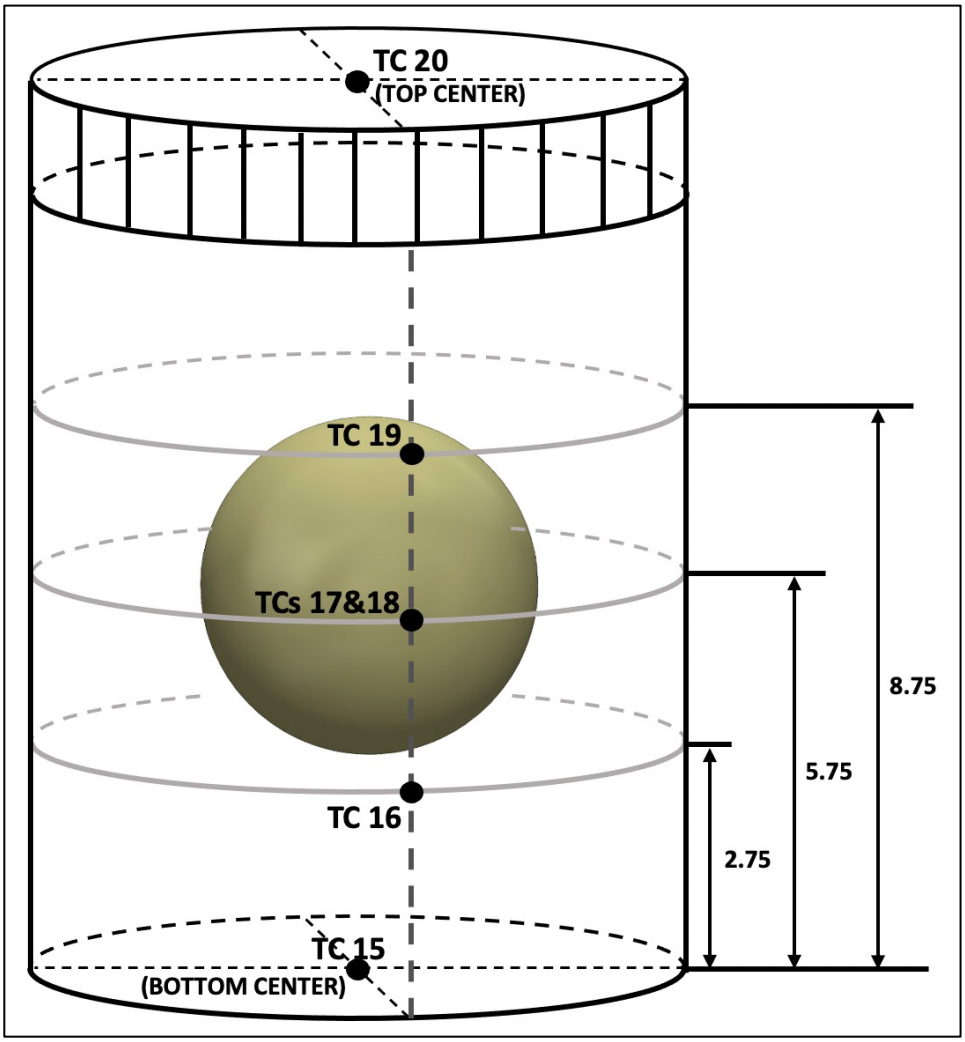

Figure 27. Diagram showing locations of exterior thermocouples. Charge location is indicated for reference.

Table 3. Assembly images from SITX (Test 3).

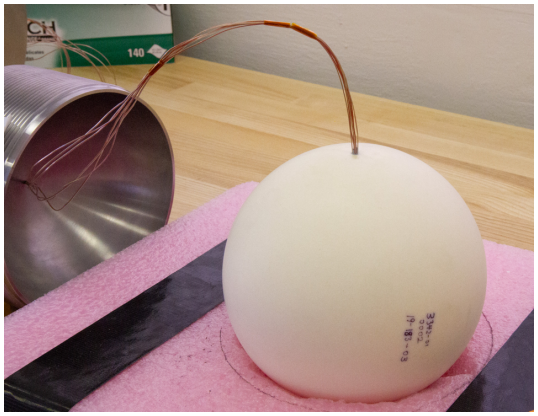

Figure 28. Interior thermocouples potted into charge.

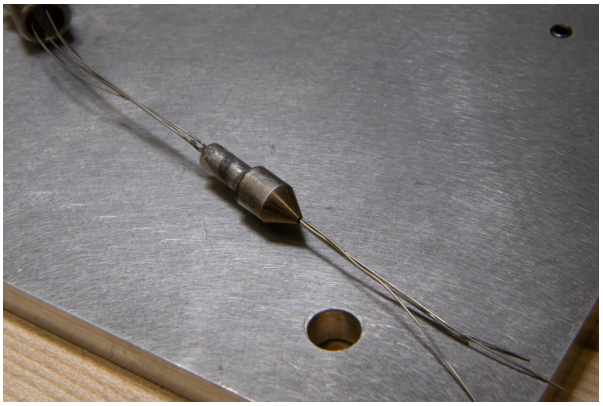

Figure 29. Thermocouples brazed into feedthrough fitting.

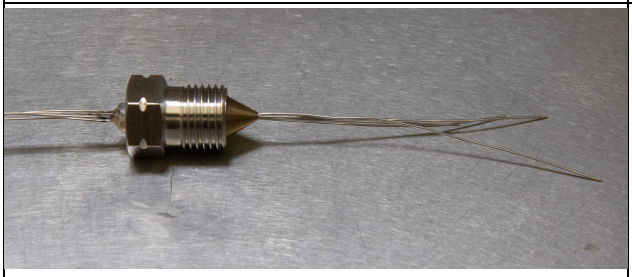

Figure 30. Fitting with the clamping nut in position, as it is mounted in the shot.

Figure 31. Feedthrough mounted in vessel; heating tapes partially wrapped.

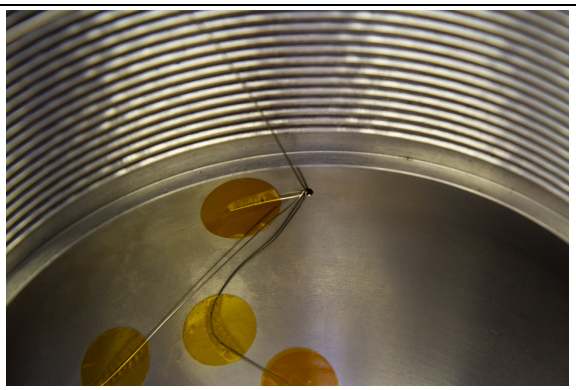

Figure 32. Thermocouples entering the bowl from the feedthrough.

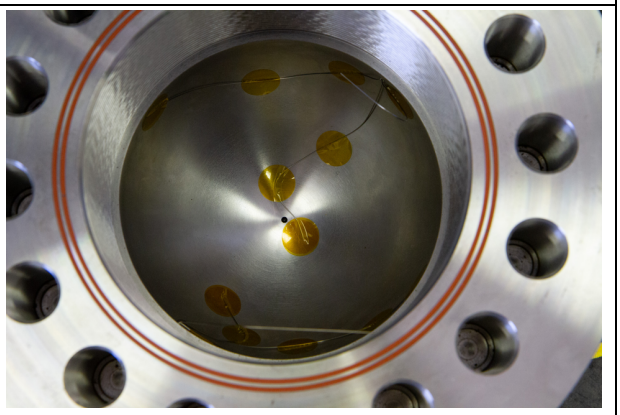

Figure 33. View of interior TCs taped to bottom of bowl.

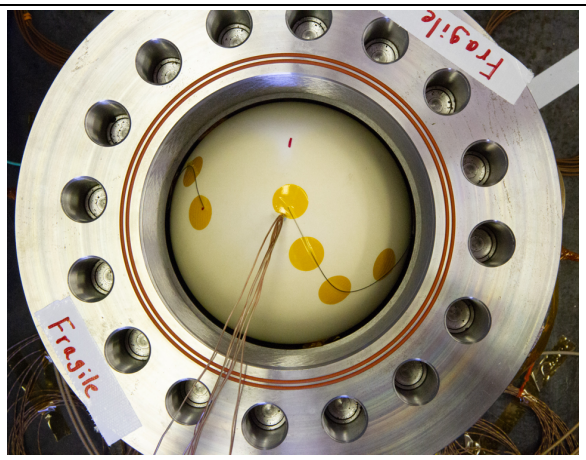

Figure 34. View of charge inserted into bowl, with TCs taped to top surface.

Figure 35. Charge situated in block house, ready for testing.

5.3. Thermal profile

In a heated explosive experiment, numerous design aspects must be carefully optimized in order to contrive a conservative, worst-case scenario. In this section we discuss thermochemistry considerations for HMX, details of a kinetics model, details of a porosity and volumetric expansion model, and the resulting design choices motivated by the model predictions.

Thermal damage is a crucial aspect when considering the DDT in plastic bonded explosives. For example, to the best of the author's knowledge, without thermal damage, pristine PBX 9501 has never undergone DDT. The exposure of PBXs to thermal insults results in several chemical and morphological changes to the explosive which increases the likelihood of DDT.

The most obvious effect of thermal damage is the thermal decomposition of HMX and binders in PBX 9501. This decomposition creates porosity due to two main effects. First, both HMX and binder decomposition turns them to gaseous products, leaving a pore where the solid material used to be. Secondly, the binder in PBX 9501 softens at higher temperatures which allows the crystals of HMX to mechanically rearrange when exposed to decomposition gas pressure in the newly formed pores. This causes the PBX to 'puff up' and introduces extra porosity.

Another important aspect of thermal damage is the $\beta \rightarrow \delta$ (beta-to-delta) phase change in HMX that occurs in the range of 150-190 ˚C[9]. δ-phase HMX is worse—from a DDT perspective—than β-phase for two reasons: a) δ-phase is intrinsically more shock sensitive, and b) the PBX properties change since the phase transition to delta phase is accompanied by volumetric expansion, comminution of average particle size from HMX crystallite fracturing and correspondingly increased porosity and surface area[10].

The $\beta \rightarrow \delta$ phase transition does not occur instantaneously, but is characterized by a kinetic process that is a function of temperature and time. The kinetics of the phase transition are an integral part of the Dickson four-step cookoff kinetics model[11-13]. We implement these Dickson four-step kinetics in an FEA simulation.

We iterated simulation runs, altering heating ramp rate, soak temperature, and soak duration, to choose a choice of thermal profile for the SITX heated experiment according to the following considerations:

1. Maximize the fraction of PBX 9501 that undergoes the $\beta \rightarrow \delta$ phase transition, thus striving for a uniform material state at the time of ignition.

2. Avoid inadvertent early self-ignition of the PBX 9501.

3. Bound heating times such that we can execute the experiment in a reasonable period of time (ideally a single work shift).

5.4. Data

The temperature data are presented in Figure 36. The experiment was ramped at an average of 1.95 ˚C/min to a soak temperature of 175 ˚C. The ramp rate was limited by maximum power available from heating elements[2]. The temperature referenced is the boundary temperature on the exterior surface of the bowl. This boundary soak temperature of 175 ˚C was maintained for a duration of 9.7 hours to induce thermal damage. At that point, the available locations of interior thermocouple measurements were showing negligible evidence for self-heating, and were below the model predictions. The decision was then made to increase the boundary control temperature to 185 ˚C in order to encourage additional chemistry.

The experiment cooked off at 14.43 hours after heating was first started. Cookoff occurred 211 minutes after the exterior of the vessel reached the setpoint of 185 ˚C. Significant signs of self-heating were observed, but the highest internal temperature observed at the moment of cookoff was 185.2 ˚C on TC6, which was at the

[2] If the experiment was better insulated, higher ramp rates would have been possible. However, it was desirable to use the minimum insulation possible in order to minimally obstruct the view of the high-speed video cameras. The only effect of the limitation on ramp rate is to extend the duration of the initial heating period.

outside edge of the charge. This implies that the highest temperatures were occurring elsewhere in the charge and that our thermocouples were not positioned to capture the highest temperatures at the ignition location. This is not surprising, as we only had internal temperatures along one radius.

On this experiment, the piezo pin served as master trigger; data from PDV oscilloscopes, high-speed cameras, and force transducer share a common time zero. The pressure transducer recorded a nearly discontinuous (at the temporal response limit and beyond the maximum pressure range of 1 GPa) rise at 70 μs prior to the piezo pin trigger.

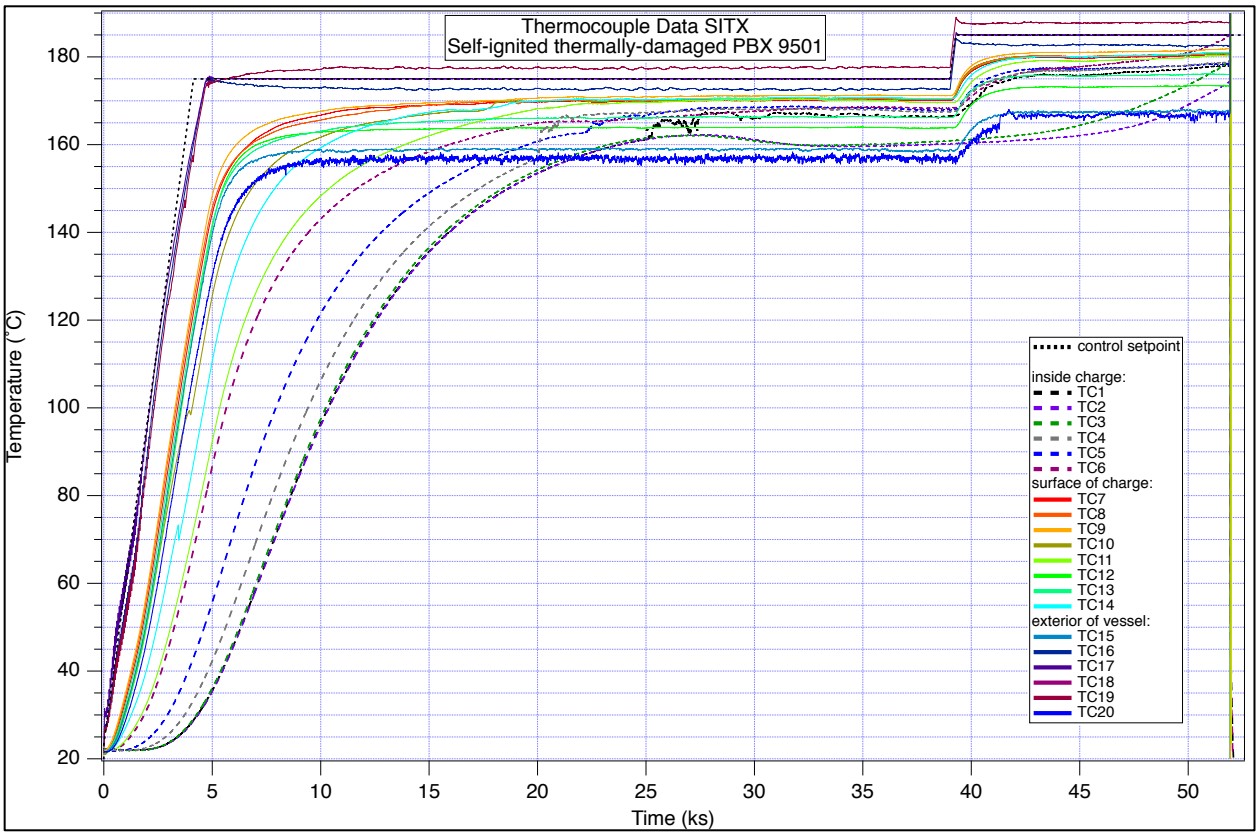

Figure 36. Temperature data from SITX. TC1 and TC5 become erratic and abandon their internal peers to join the group measuring the charge surface temperature. This suggests that they became shorted where they enter the hole in the insert, developing a new voltage junction away from the bead which gives erroneous readings.

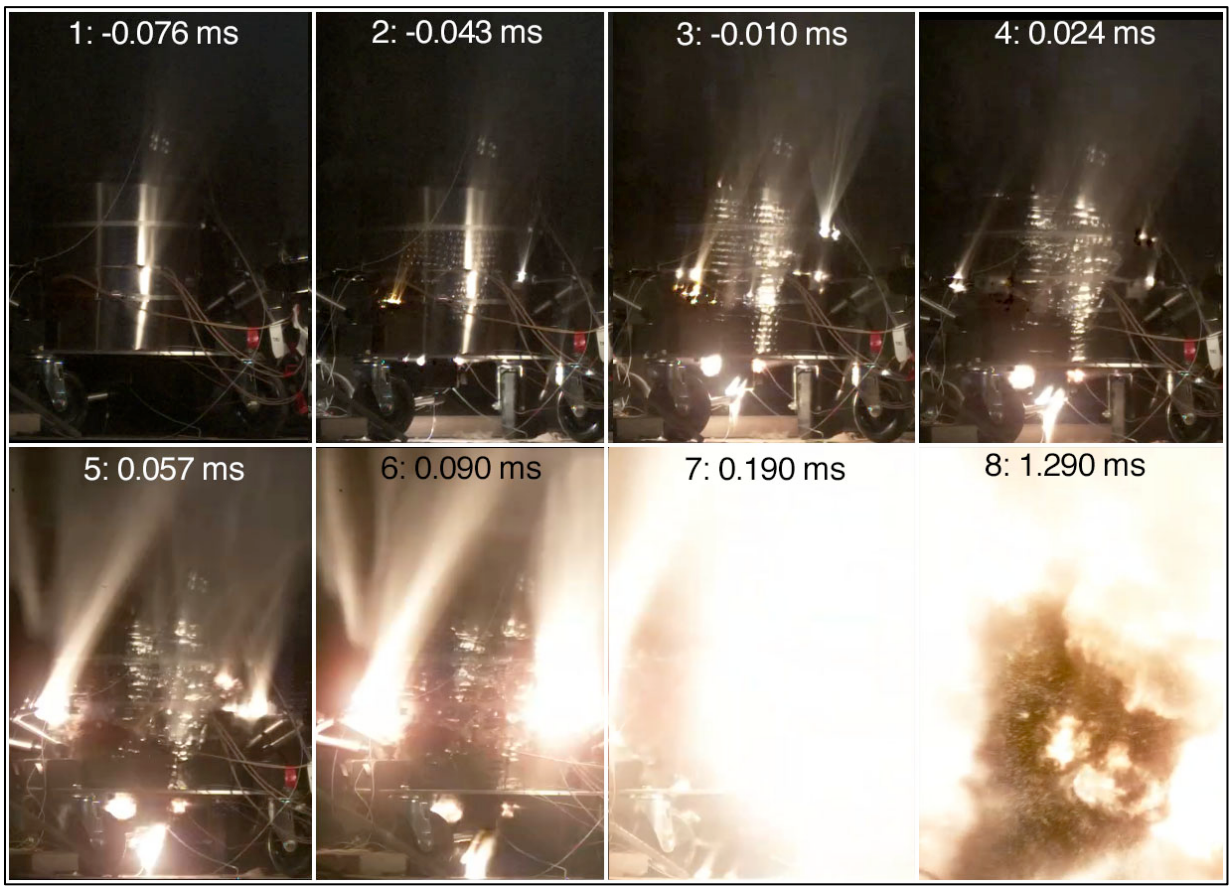

Figure 37. SITX (Test 3) still sequence from high-speed video record. Video was captured as 20,000 fps. Insulation and metal flashing is wrapped around the shot and obstructs the view of the fracturing metal surface that is visible in the first two experiments. The view is blurry because rain collected on the glass porthole in the middle of the night; the camera was looking through a puddle of water.

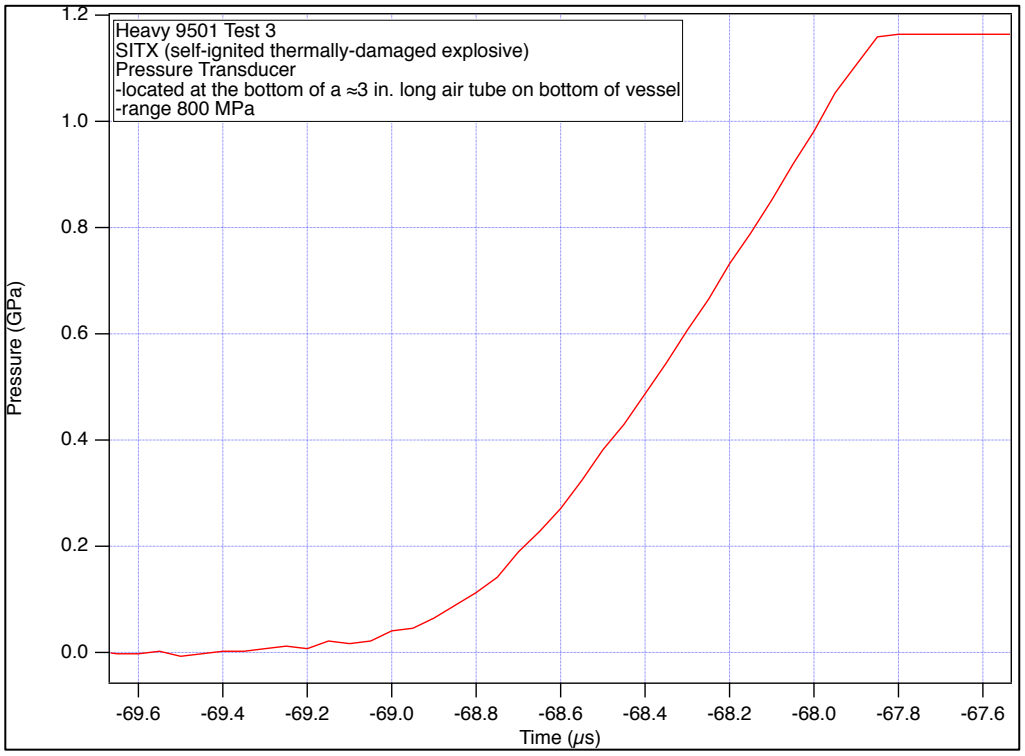

Figure 38. SITX (Test 3) pressure data. Pressure rise is remarkably smooth. The top pressure attained is not physical; that indicates that the pressure exceeded the range of the sensor.

6. Analysis and Discussion of all three experiments using PDV Data

Figure 39 contains diagrams indicating PDV probe locations. The six PDV probe locations will be identified in the text as 45deg, 135deg, 225deg, 315deg, Top, and Bottom.

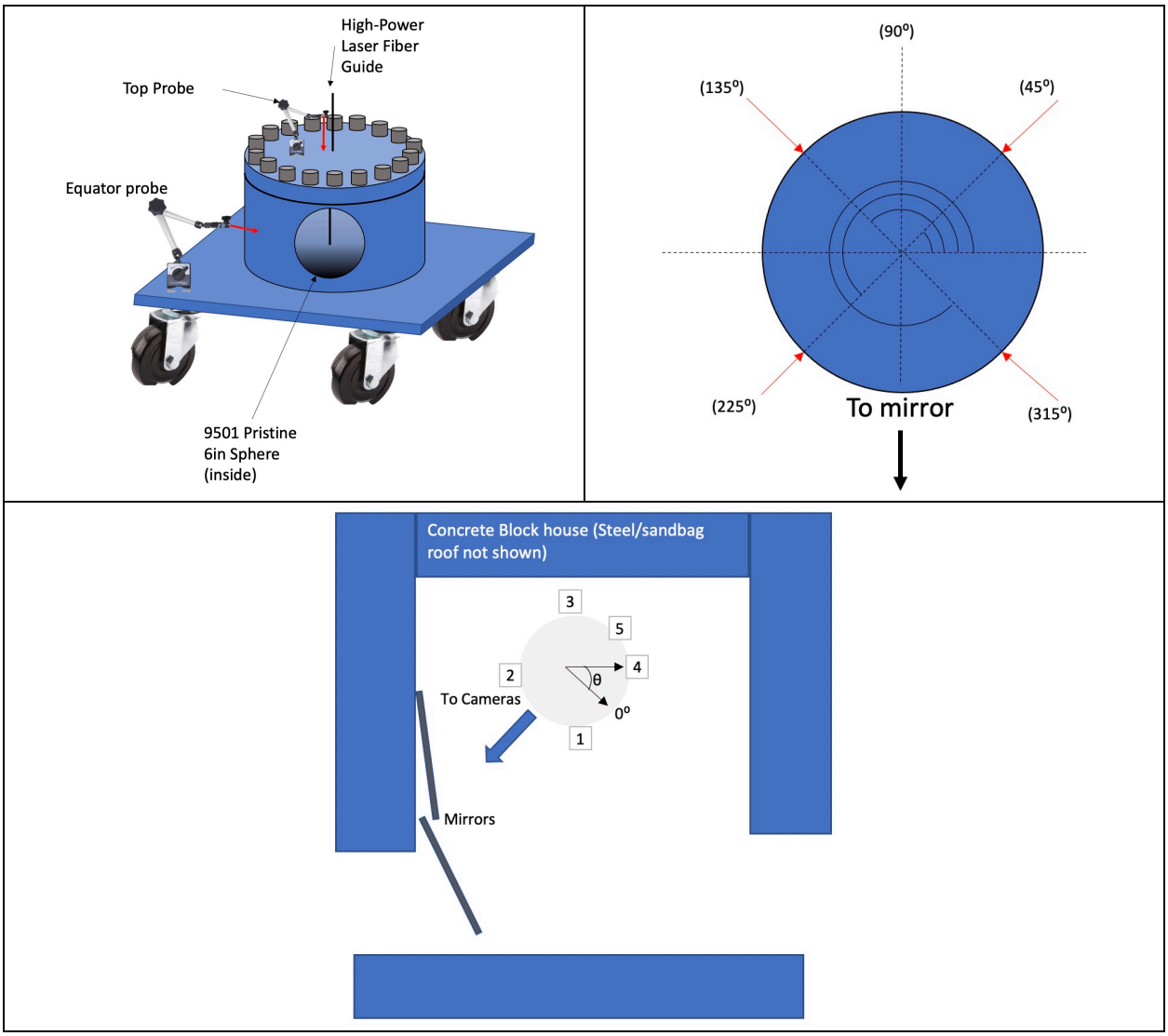

Figure 39. Diagrams of PDV probe locations.

6.1. DIPX Velocimetry Discussion

The DIPX experiment (Figure 40) serves primarily to identify the characteristics of the PDV record from an experiment that fully detonated; by observing the features in the velocimetry records for the DIPX experiment, the thermally-ignited experiments can be compared to see if full detonation had occurred. This experiment is also the most likely to match the hydrodynamic modeling simulations to which the other experiments will also be compared.

Figure 40 shows all PDV probes recorded for the DIPX shot. A few predictable features are observed. Firstly, the sharpness of the shock jump from total rest—a feature that is visible in all DIPX probes—indicates the super-sonic nature of the pressure wave in the steel. Secondly, the shock jump from each position is relatively close in time; e.g. with the exception of one outlier (Top), the equatorial probes all jumped off within 60 ns of each other. This indicates that the initiation point was concentric to the vessel cavity to

within ~500 µm. Together, these features also indicate that the vessel failed simultaneously at all locations, and that the supported disturbance moving through the steel was a plastically-failing shockwave.

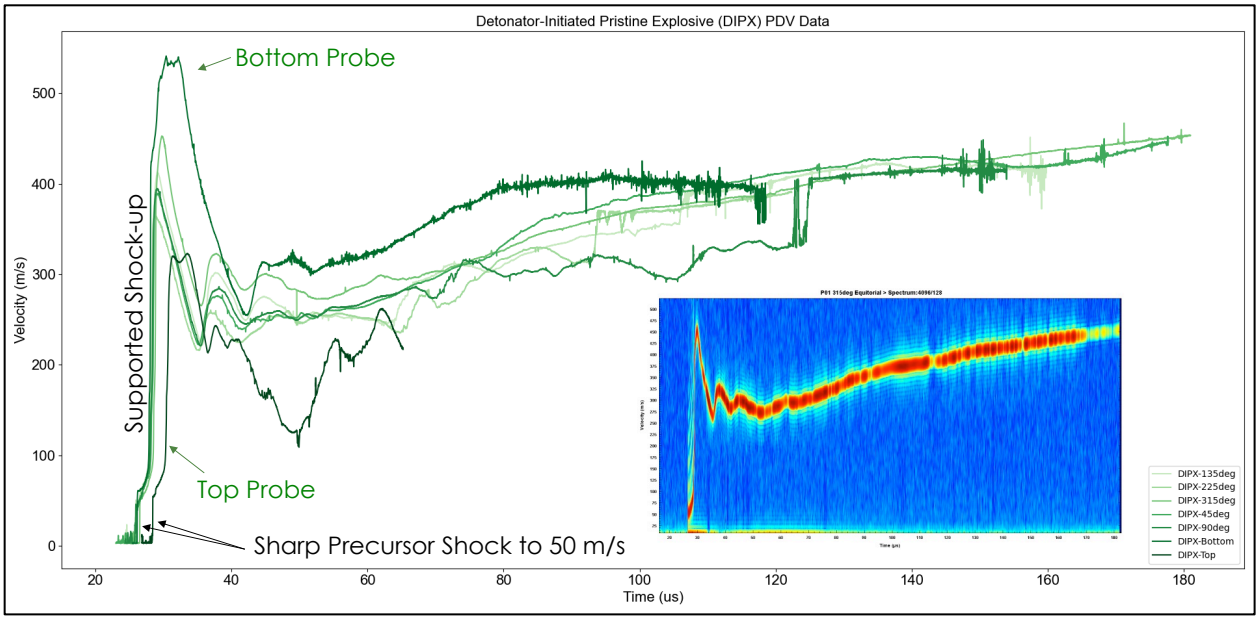

Figure 40. DIPX, all 7 probes that were fielded. (Inset: stFFT spectrogram of DIPX-315deg)

The third notable feature is the variability in acceleration profiles at different probe locations. If the equator probes (DIPX-135deg, DIPX-225deg, DIPX-315deg and DIPX-90deg) are considered baseline, the top probe (DIPX-Top) shows lower velocities throughout the time record. This is anticipated, because accelerating the vessel in this direction—where there's more metal mass through the insert and lid—provides more tamping. Conversely, the bottom probe (DIPX-Bottom) always records faster velocities than any of the equator or bottom probes. Although the bottom probe and the equator probes have a very similar cross-sectional metal mass, the equator probes measure a cylindrical surface while the bottom probe measures a flat surface. Additionally, the explosive charge rests on the bottom of a slightly oversized cavity, which leads to minimal attenuation between explosive and steel at the base of the charge, and some amount of attenuation at the sides of the charge where there's a slight air gap. Either/both of these reasons may be responsible for the higher velocity profile of the Bottom probe as compared to the equator probes.

The appearance of the elastic precursor wave is worth noting. This is the first detectable wall motion, and very consistent at every DIPX location. The high sound-speed in the stiff alloy of the vessel exhibits an elastic wave that is faster than the strong, sustained, detonation-supported shock (although significantly lower in amplitude). This is more an artifact of the vessel's material properties than an indication of the reaction in PBX 9501; the elastic precursor will be a common attribute for this type and thickness of steel when subjected to a strong shock.

The last feature to note is that the final velocity of the metal fragments was nearly identical for all locations (except DIPX-top, for which the PDV beam path was smoked out by escaping detonation products much earlier than the others and truncated the record). Velocity continued to increase throughout the PDV record, indicating that some of the explosive's energy was still being deposited into accelerating the vessel fragments even at late time (150 µs after jump-off). The end of the PDV record approximately coincides with the observation of gas blowby commencing through fractures in the high-speed video record. (Figure 19). The lack of ductility in the vessel alloy causes early fracture compared to a softer metal, and as such the final velocities are likely decremented from simple predictions by some fraction because the working fluid blows-by before terminal velocity is reached.

6.2. SITX Velocimetry Discussion

In Figure 41, the PDV velocities for all SITX probes recorded are shown. Comparing this experiment to the DIPX experiment, we can see many indications of DDT. In all locations we observe a no-velocity vibration for

approximately 85 μs prior to jump-off (visible in the spectrograms inset to Figure 41). This vibration is attributed to the turbulence of the burning reaction in 9501 while the vessel is still perfectly intact. The jump-off profiles of each individual probe in the SITX experiment are shown in Figure 42 (overlaid in scope-time) and Figure 43 (stacked, time-adjusted to 200 m/s threshold). These profiles show one of two types of behavior. Probes at 135deg and 45deg on the equator and the bottom all look very similar to the DIPX probes, i.e. jumping sharply to a 50 m/s elastic precursor shock, followed promptly by a supported detonation-supported shock. Neither of the two remaining probes jumped-off with a sharp shock, but rather a slow-moving constant-pressure type acceleration like would be expected in a quasi-static failure of the vessel. In the record from the 225 deg probe on the equator, the ramp-up is promptly interrupted by what appears to be an elastic precursor shockwave, but the probe at 315 deg is interrupted much later into the ramp, by what looks more like the detonation-supported shock seen in the DIPX experiment.

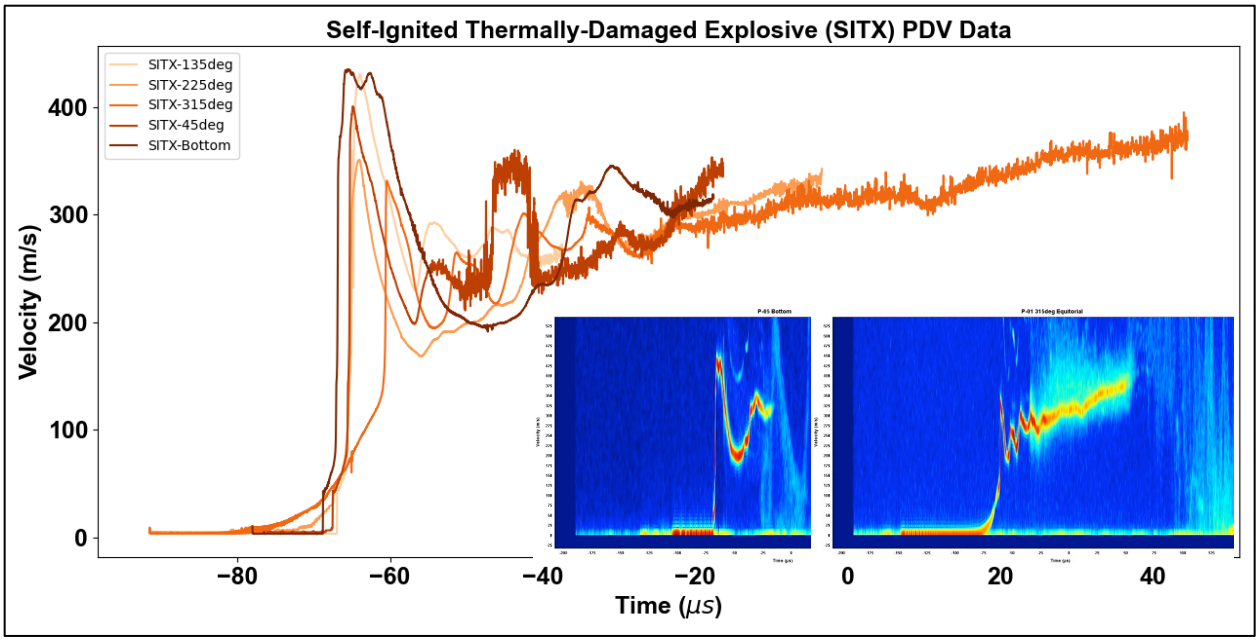

Figure 41. SITX experiment PDV Data, all 5 probes that returned data. Inset Left: SITX Bottom probe, which shows a DIPX-like sharp shock at first breakout. Inset Right: SITX-315deg, which shows a slow ramp, eventually overtaken by a discontinuous shock.

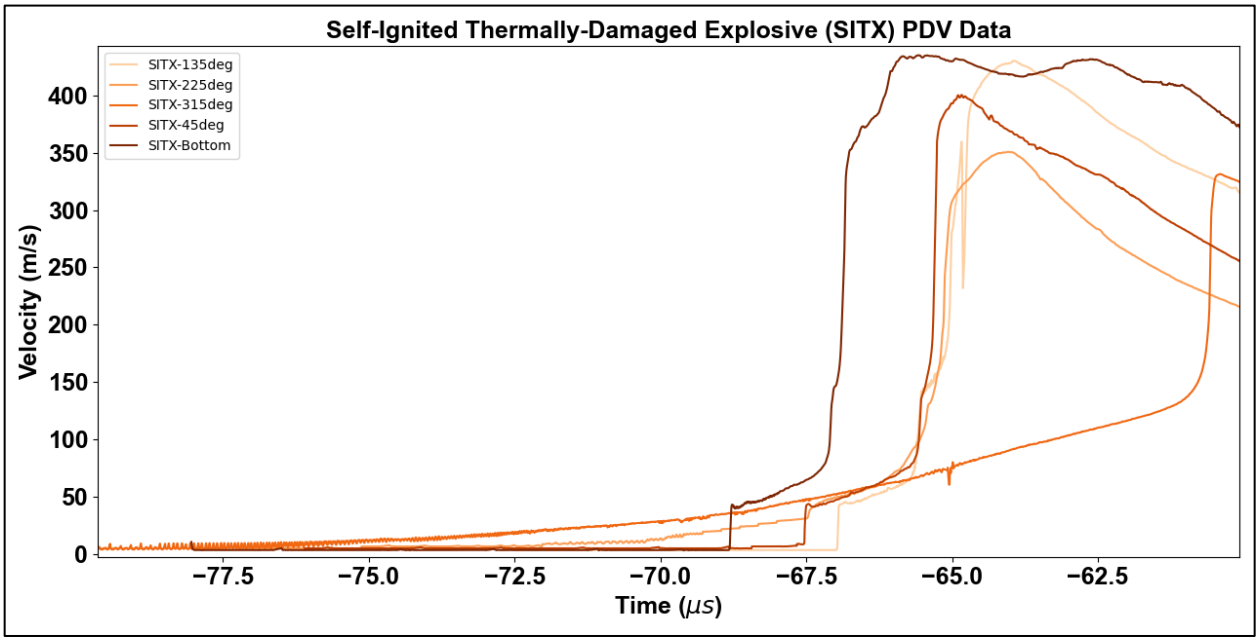

Figure 42. SITX. Detail view of arrival times. A basic threshold analysis of the probes indicate an ignition point below and towards 135deg on equator.

Motion breaks out at very different times in this experiment, as much as 10 μs between the earliest and latest jump-off times. This, and the fact that motion begins slowly for the earliest jump-off times, and shocks up for later times, indicates that the vessel initially failed by quasi-static pressure rupture at certain locations, rather than the uniform shock disturbance in the DIPX experiment.

Figure 43 gives a closer look at all the SITX probes adjusted in time to a threshold of about 200 m/s. Here, it's easy to see how much time the slow-ramping velocity profiles at 225deg and 315deg accelerate prior to shock breakout. The evidence suggest that the vessel contained the pressurizing reaction until it eventually failed at a single weak point between probe SITX-315deg and SITX-225deg (these probes show the earliest wall motion). This rupture relieves the pressure at that location, reducing the violence of reaction nearby. We also observe lower jump-off velocities of these "early-rupture" probes, compared to a direct detonation-driven shock. Opposite these locations, where the vessel walls were still intact (there was no early wall motion at these locations), the records imply that the DDT turnover point was lower than center, and radially favoring 135deg. The 135deg and 45deg probes, closer to the proposed DDT turnover point, show the highest jump-off velocities.

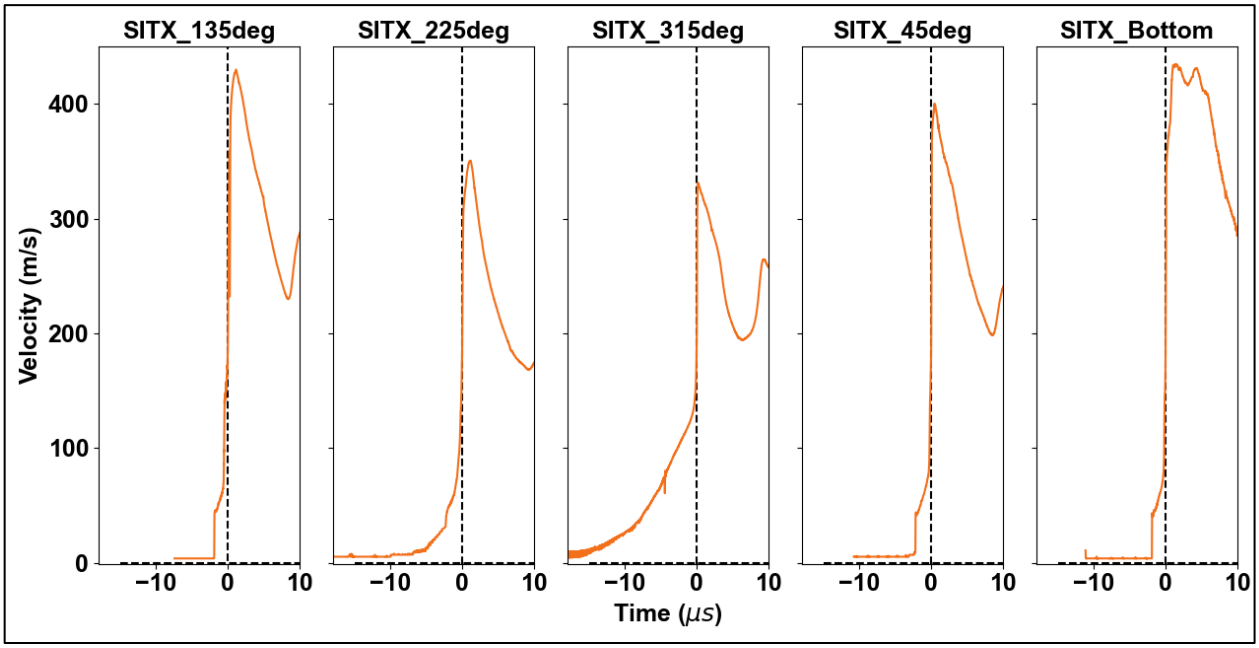

Figure 43. Detail view of breakout comparisons in SITX. In 135deg, 45deg, and Bottom probes the elastic precursor is the first sign of reaction, followed by the shock transit. In 225deg there is slow acceleration before the elastic precursor arrives, followed by the shock transit. In 315deg there is a long period of smooth acceleration before the shock transit, without obvious signs of an elastic precursor.

In the DIPX experiment, the bottom probe was observed to travel the fastest because of the geometric design of the vessel, but in the SITX experiment we believe the bottom probe and 135deg probes record higher velocities because the DDT turnover point is closest to those locations and furthest from the quenching effect of early rupture we suspect happened between 225deg and 315 deg.

In the SITX experiment, at locations where shock broke out immediately (45deg, 135deg, bottom), the elastic precursor looks nearly identical in structure to the elastic precursor in the DIPX experiment. The 225deg probe record shows the tail end of an elastic precursor wave overtaking the ramp wave, but no elastic precursor structure is identifiable in the 315deg probe record.

The final velocity of records in the SITX experiment were somewhat difficult to distinguish from each other, because only two of the probes continued to collect data to later travel times. Both the 315deg location and the bottom location, which were shocked the hardest (but not as hard as any probe in the DIPX experiment), were smoked out or otherwise rendered useless after 50 μs of fly time. For comparison, all but one of the DIPX probes continued to collect data through 120 μs of fly time. From what we can tell, the final velocities of the 225deg, 315deg and Bottom locations would have likely been slightly higher than the 315deg location which survived the longest (~110 μs of fly time).

6.3. Laser-Ignited Pristine Explosive (LIPX)

The LIPX experiment was initiated by a high-power laser and small thermite reaction; its velocity records share many of the features from both of the other two experiments. Figure 44 below plots all five records returned for this experiment.

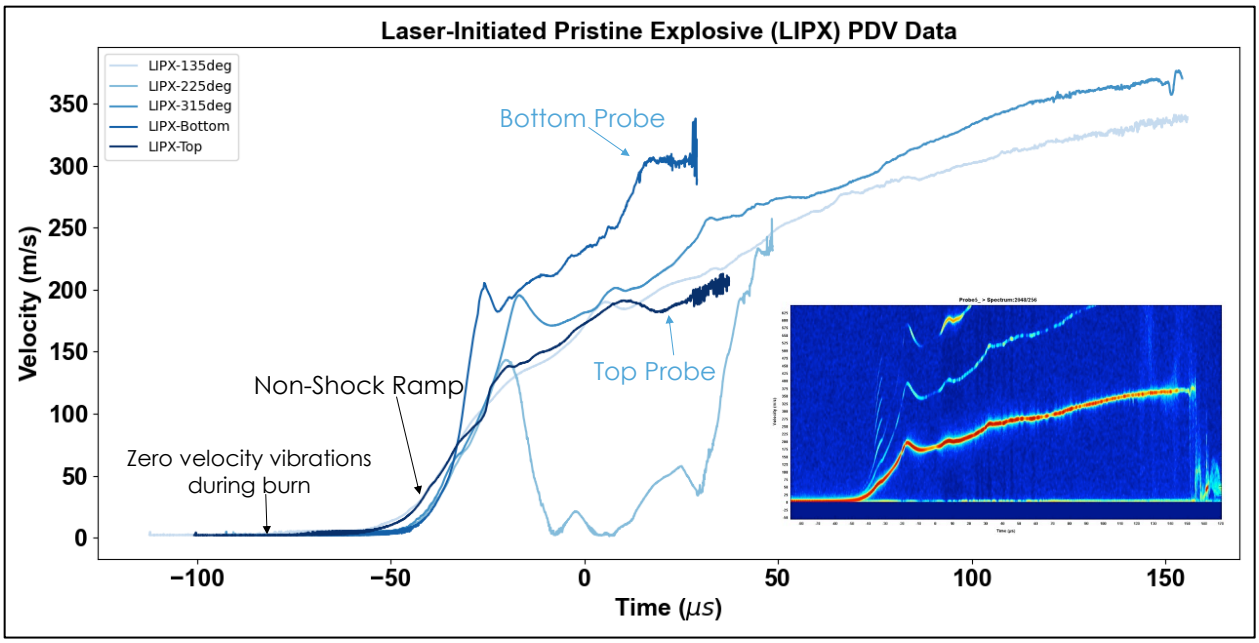

Figure 44. LIPX, all five probes that were fielded.

The first noticeable quality of this experiment's results is the slow, gentle ramping nature of the accelerations at every location. The overall impression of this experiment to the authors is that the 9501 in the LIPX experiment underwent a very rapid deflagration, but that a DDT shock likely never occurred or occurred in a nearly undetectable fashion. The jump-off times indicate that the vessel failed in a quasi-static fashion like in the SITX cookoff, but unlike SITX, no observable shock discontinuity is observed within the first 60 μs at any location.

Like the SITX experiment where we suggest the vessel quasi-statically ruptured at a particular location, we conclude that the vessel in the LIPX experiment ruptured similarly; the jump-off times were again spanned across 10 μs. Also, the locations that seem to jump-off earliest are not in logical order, further implicating a rapid pressure growth that exceeded the failure stress of the vessel at only a few particular defects before the vessel broke up in bulk. A strong shock, as discussed in the DIPX results, would have exhibited a jump-off at each surface according to the distance that surface was from the ignition point. With a strong shock, all equator, top, and bottom probes are predicted (by simple assumptions of the transit through 9501 and vessel to each location) to arrive within 2.0 μs of each other (DIPX probes arrived within 2.5 μs).

LIPX probes show no evidence of an elastic precursor, which suggests an absence of sharp pressure gradients that would have propagated a wave-like disturbance. LIPX probes display behavior more consistent with a constant pressure acceleration (e.g. a propellant burn accelerating a projectile). The absence of the elastic precursor is not itself evidence of the absence of detonation in 9501. However, in comparison with the DIPX experiment—in which the elastic precursor was stable and measurable—we can conclude that in the LIPX experiment there existed no strong detonation wave supporting a discontinuous pressure gradient in the steel vessel.

Two of the probes from the LIPX experiment survived through 200 μs of acceleration—this was the longest survival time of any probe in any of the experiments. The final velocities achieved at these late times are much lower than from the other two experiments, but still sufficient to indicate that the 9501 released most of its energy during the deflagration event. It's unclear exactly how efficient the 9501 chemistry was without an experiment designed to take such a measurement. The comparatively thick, brittle steel and Heavy vessel

geometry make an estimate of energy release difficult, but a Gurney analysis of relevant theoretical shapes have been undertaken to provide perspective on the energy release in the three different experiments (Section 8).

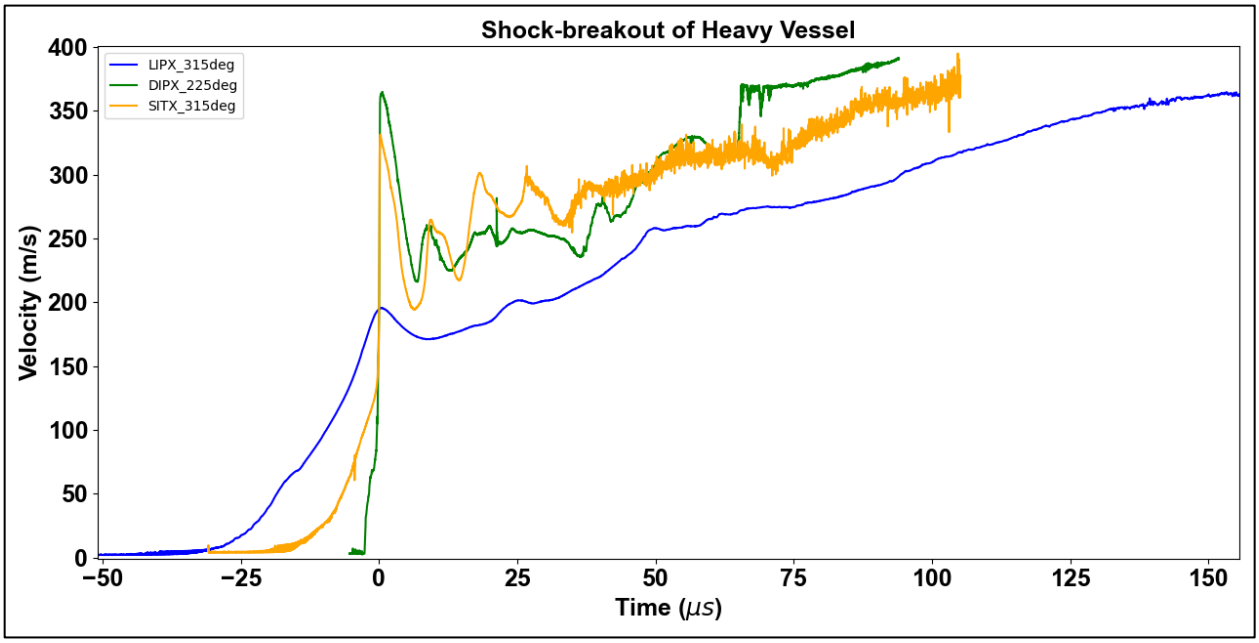

Figure 45. Experiment comparisons, using a single representative probe from each.

7. Simulations

7.1. Two models of One Experiment

Hydrodynamic modeling codes are used to virtually simulate an experimental geometry by representing the components and nearby environment as a mesh grid of finite elements, and allows the modeler to specify very specific material properties and high explosive detonation parameters. These codes apply finite difference iterations that naturally propagate the expected dynamic conditions through the modeled problem using natural physical laws, capturing the thermodynamic conditions of each cell through time. The accuracy of the resulting simulation is largely dependent on the accuracy of the material equation of state (EOS) and plasticity model (for the steel) in the pressure-temperature ranges being modeled and whether the mesh is highly-resolved enough to capture the behavior in all the geometric complexities of the problem. The more complex the material model and the finer-resolved the mesh grid, the more computational time is required, even when these problems are computed on multi-thousand core supercomputers. These models allow for virtual, non-interacting pressure/temperature/velocimetry sensors (called tracer particles) to be placed at will inside the mesh that record the state variables and material velocities, providing a time-resolved record to compare PDV data. All simulations reported here were conducted on the M6 cluster (1216-core Intel Xeon). Existing materials and fracture models in each codes' material libraries were used to model the steel. In CTH a model for 4340 with a hardness of RC40 was used, while in ALE3D a model for 4340 with a hardness of RC53 was used. Engineering judgment was used to tweak the fracture and element erosion parameters in ALE3D to improve agreement with the experimental fragmentation of the vessel. Variations between the nominal hardness of the experimental vessel and the nominal hardness of each material model are acknowledged. Full characterization of the steel vessel and improved material models were beyond the scope of the project.

Two different hydrodynamic modeling efforts were pursued independently. These simulations were performed after the first LIPX experiment, prior to the subsequent baseline tests. The purpose of these models was to ascertain what the predicted external wall velocities would be from an intentional detonation, and how they compare to those observed in the LIPX laser-ignited experiment. Both modeling efforts assumed perfect CJ detonation in the 9501 charge; these models were used for comparison to a detonation

scenario and are specifically optimized to provide good agreement with the intentional detonation (DIPX) experiment. No attempt was made to model the thermal ignition of laser/thermite reaction in LIPX or self-heating cookoff conditions of SITX. Such would require numerous unfounded assumptions of the thermally-damaged equation of state and combustion parameters, which are considerably more complicated and cannot currently be captured by any extant model.

These two simulations were conducted in separate modeling environments with different degrees of simplifications of the geometry; each was chosen to more accurately model a particular aspect of the DIPX experiment. Because highly-resolved 3-D simulations of complex geometries like the Heavy vessel are computationally intensive to conduct, reducing the problem into two separate, strategically-different (but more solvable) virtual representations can be an effective way to bound the expected real behavior. Or, as is the case here, accurately describe only particular features of the real experiment with each model. Each simulation is expected to match certain features of the experiment very well and other features somewhat poorly, but both simulations can be reasonably performed in a few days' time rather than the months of computational burden it would require to run a single highly-resolved model that better captures the entire experiment. In this way, each simulation can easily be performed and tweaked several times as needed. The specific nature of each simulation is discussed below.

7.2. 2D Cylindrical Symmetry (DIPX_2DC)

The first model used the Sandia National Laboratory (SNL) code CTH[14], approximating the Heavy vessel's intrinsic two dimensional cylindrical (2DC) symmetry. As a result, the mesh could be very refined spatially—a resolution of 0.25 mm/element. This model will be nicknamed the DIPX_2DC in future plots.

This framework will be particularly effective at capturing the shockwave structure (shape, intensity, etc) as the detonation shock transits the steel vessel. This finer resolution model is also expected to observe an elastic precursor wave- a rather subtle phenomena. Although the virtual vessel material model references a strength and failure parameter (the model's ability to fracture the material at high strains), in 2D cylindrical symmetry the vessel will be incapable of fracturing properly (the symmetry constraint requires uniformity along the angular "θ" dimension). This model still fractures, but only along the cross-sectional corners. This leads to inaccuracies in the fragment velocities after fracture. The model's representation of the fracture pattern is very different than what was observed in the experiment, and as such, the fragment velocities will likely mismatch at late times. The extent to which hot detonation products "blow-by" fragments at late times is the largest contributor to matching PDV data at late times, and is intrinsically impossible with the 2DC assumption.

7.3. 3-Dimensional Cylindrical Symmetry (DIPX_3DR)

A second, three-dimensional modeling effort was undertaken using the Lawrence Livermore National Laboratory (LLNL) code ALE3D [15] in an attempt to better capture the fracturing behavior of the thick steel walls (and thus the energy that is dissipated into fracture) using embedded mesh coupling and quarter symmetry. This model will be nicknamed the 3DR—three-dimensional rectangular—for simplicity (more precisely ALE3D allows for arbitrary hexahedral element geometries in 3D that may or may not be rectangular). For this model, a fully-Lagrangian model for the pressure vessel was coupled to an Arbitrary Lagrangian Eulerian (ALE) model containing the explosive and air to allow for fracture and venting of the vessel without advection of the vessel material and associated state properties, e.g. damage, plastic strain, etcetera. This model had significantly lower spatial resolution (≈3 mm), owing to computing limitations. This model will be nicknamed DIPX_3DR. ALE3D was also run in 2DC geometry, without using embedded meshes, and produced similar results to CTH, not shown here for the sake of brevity.

The coarse resolution of the 3DR simulation was unable to capture the fine structure of the shock transiting through the steel vessel. This means the high temporally-resolved PDV record will express features (i.e. the elastic precursor, spallation, etc.) that will not be visible in the 3DR simulation. The third dimension added in this mesh allows the material to fail with higher fidelity, since the fragments are not constrained to be axisymmetric, i.e. rings, and gas "blow-by" phenomena is much better simulated. Therefore, we expect this simulation to be optimized for simulating the late-time velocity record rather than the jump-off features.

7.4. Model/Experiment Comparison

The DIPX experiment was executed after the modeling efforts. Here we will compare the modeling with the DIPX experiment. This exercise seemed perfectly arranged to highlight the strengths of each modelling approach. In Figure 46 the models are compared with DIPX data at the initial wall jump-off; in Figure 47 (same plot as Figure 45 with different time limits) the models are compared with the longer duration record that occurs as the vessel is fracturing.

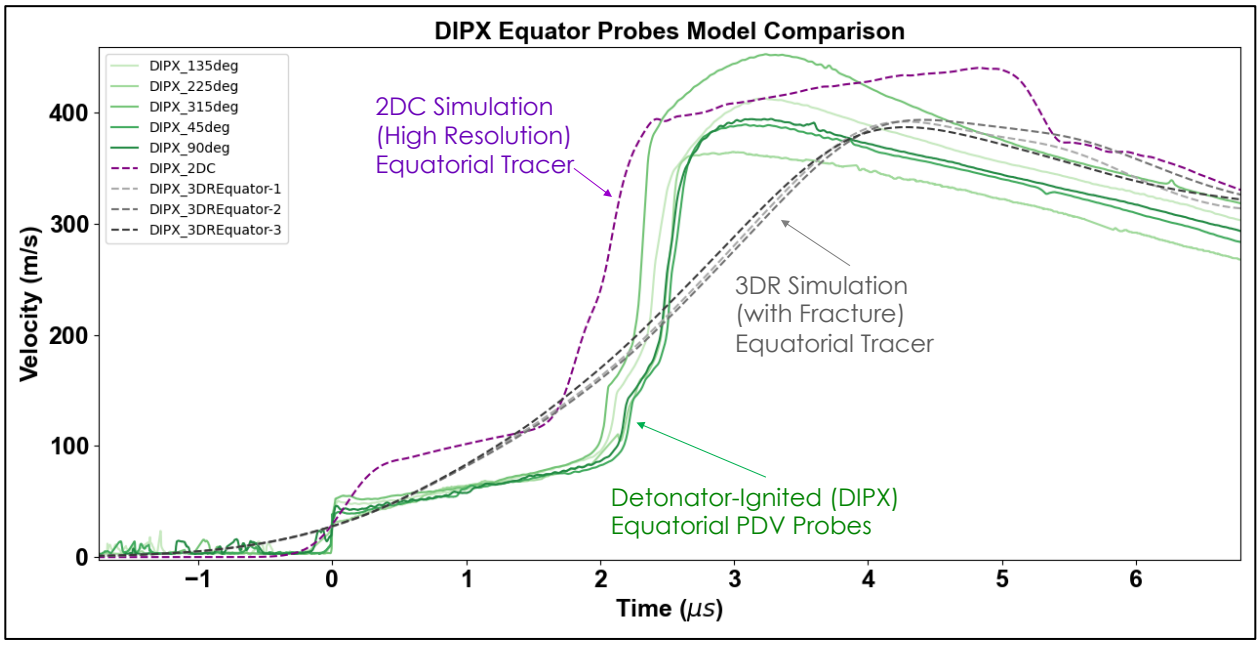

Figure 46. Comparison of models with experimental data at jump-off (time adjusted to 40 m/s threshold). Note the inability of the coarse 3DR model to capture the elastic precursor compared to the 2DC simulation. Also, only DIPX experimental probes on the equator are plotted.

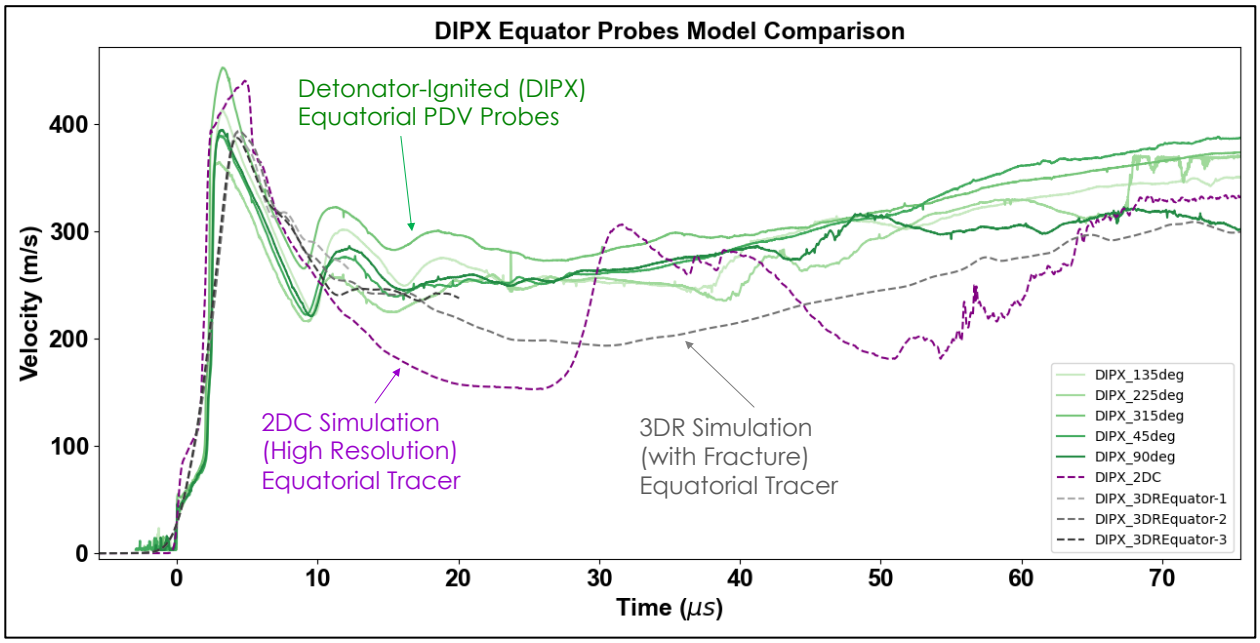

Figure 47. Comparison of models with experimental data over longer duration. Note how the fragmentation in the 3DR simulation smooths the record at late times, where the fractured fragments cannot support ringing shockwaves; the experiment is seemingly bounded by the two behaviors. Two of the 3D tracers failed to continue after 50μs due to being on a fracture plane; the third survived to late times and is used in subsequent comparisons.

The 2DC model was designed to specifically capture the initial shock transit through the steel and the steel response prior to fracture at a very high resolution, and successfully captures the features and timing of the experiment behavior during the first 4 μs. It captures the elastic precursor shape and the detonation-supported shock arrival, with good agreement in both timing and magnitude. However the axisymmetric constraint results in significant oscillations and variation from the PDV traces after about 10 μs.

The 3DR model was specifically designed to allow fragmentation behavior and effects of venting that occur at later times to contribute to the final velocity of the vessel fragments. The 3DR model successfully captures the longer duration behavior after fracture, in the 10-80 μs interval.

The 2DC model is superior for the short duration features owing to the much better spatial resolution that was achievable by reducing symmetry to two-dimensions, while the 3DR model is superior for capturing long duration features due to more realistic fragmentation behavior due to the lack of an axisymmetric constraint. Both models are useful for different portions of the PDV traces. Figure 48 shows a sequence of predicted wave shapes from the 2DC simulation, as the pressure wave transits through the steel. Note that the 2DC simulation successfully captures the development of an elastic precursor that transits the steel faster than the shock, which proceeds at a slower velocity. In this figure, the dashed traces are predictions, while the solid green trace shows the measured jump-off velocity at one of the PDV probes.

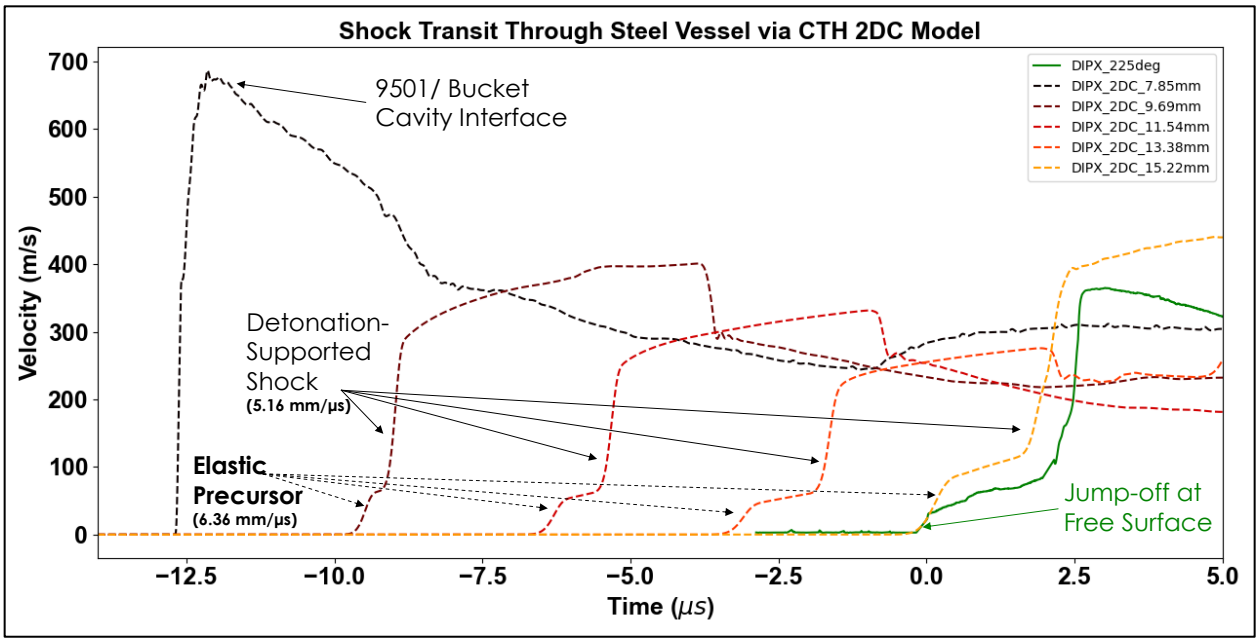

Figure 48. 2DC CTH simulation showing predicted evolution of wave shape through steel. The DIPX_2DC tracers are placed uniformly through the steel vessel (7.85, 9.69, 11.54, 13.38, and 15.22mm from the vessel axis) and capture the elastic precursor and detonation-supported shock evolution prior to jump-off. The last tracer particle (DIPX_2DC_15.22mm) is located on the outer wall, and is used to compare with the PDV trace (DIPX_225). The (x2) increase in velocity at the last tracer particle is expected when the shockwave interacts with a free surface. The 2D simulation predicted an 83.7 m/s elastic precursor velocity compared to 47 ± 6 m/s measured on DIPX equator probes.

8. Initiation Location Analysis via Breakout Times

The outside surface of the steel commences expansion at different times in different locations. The relative timing of this wall jump-off can be used to infer the symmetry and spatial origin of initiation.

We use the 2-dimensional DIPX_2DC CTH model to predict jump-off times (t_{jump}) of a perfectly center-initiated experiment. In such a situation, the bottom probe location should jump-off earliest and we choose that as the reference location.

We then extract from the experimental PDV data the time-shifted moment that each probe record overcomes a particular velocity threshold and compare that to the theoretical predictions. The velocity threshold was chosen specific to each test: for DIPX 180 m/s, SITX 160 m/s, LIPX 8 m/s, DIPX_3DR 180 m/s.

The DIPX and SITX experiments and the DIPX_3DR simulation all showed a detonation-supported shock at each probe location, and the thresholds for these experiments—180 m/s, 160 m/s, and 180 m/s, respectively—were chosen to synchronize a comparable section of the shock transit for each of the probe locations in the records.

No shock was observed in the LIPX experiment, so a low threshold of 8 m/s was chosen to identify the first motion. This choice of a particularly low velocity will reveal the location of origin of the quasi-static vessel failure rather than any shock arrival (since there was no shock arrival in the LIPX experiment).

The SITX experiment may have also failed quasi-statically as in LIPX, but each location—whether its record showed early rupture-like motion or not—eventually presented a detonation-supported shock at some time that could be used as a synchronization feature. Quasi-static vessel rupture behavior correlates with low velocity features in the velocity records; higher-velocity shock arrival correlates with detonation initiation location. Therefore, when this analysis method is applied to the SITX experiment using a low-velocity threshold (such as 11 m/s for example), the arrival analysis would identify the vessel rupture location as being nearest the 315˚ probe. However, this finding is no more useful than viewing the raw velocity data for the SITX experiment (Figure 42) and noting that the velocity for the 315˚ probe increases first amongst the probes. In order to use this analysis to identify detonation initiation location, we therefore choose a higher threshold of 160 m/s for the SITX experiment.

The time each probe crosses its threshold is recorded as the raw jump-off time t_{jump}. First, each t_{jump} picked for every velocity record was time-shifted to make the arrival of that experiment's bottom probe equal 0.0 μs. Then equatorial and top probes were shifted further by the predicted difference between DIPX_2DC $(t_{jump\ Bottom} - t_{jump\ Equator}) = 426\ ns$ and $(t_{jump\ Bottom} - t_{jump\ Top}) = 759\ ns$. The t_{jump} of the bottom probe will always be 0.0 μs in this analysis, and the other locations are showing both sign and magnitude of the deviation from a predicted center-ignited detonation. The times shown in Figure 49 are such that if an experiment initiated at the perfect center, and the detonation propagates just like in the DIPX_2DC simulation, then the numbers in the figure would all equal zero, indicating no spatial discrepancy between locations. For example: according to the 2DC simulation, the shock breakout at the equator should lag 426 ns from the breakout at the bottom. If an equatorial probe were to break out at exactly this predicted delay of 426 ns, the shifted t_{jump} shown in the table would be zero, indicating a perfectly-centered initiation point. Any equatorial probes that break out earlier than 426 ns relative to the bottom probe in that experiment will display that discrepancy as a negative value, and t_{jump} times delayed from its analogous bottom probe breakout at the bottom greater than 426 ns will appear positive, indicating a longer time between bottom and that location.

To interpret the figure, note that negative time values (e.g. DIPX-135deg probe is reported as -0.25 μs) imply that the arrival of shock at that probe (compared to the bottom) was earlier than it would have been if the detonation originated at the center. This implies that the detonation initiation location occurred physically closer to the probes reporting negative t_{jump} values. Positive values (e.g. SITX-315deg = 5.8 μs) indicate the detonation broke out off-center, and closer to the bottom. Figure 49 displays the adjusted t_{jump} values onto a top-down projection in the spatially-located box for one of 7 locations (45˚, 90 ˚, 135 ˚, 225 ˚, 315 ˚, Top, and Bottom). Note: not all probe locations were measured for each experiment. The figure is also formatted to display a sliding scale of color: darker color to represent earlier t_{jump}, lighter color for later t_{jump} to visualize the effect.

This simple analysis has limitations. For example, it doesn't take into account the possibility of multiple initiation points (this was possible in both the LIPX and SITX). It can, however, be implied from Figure 49 that the deliberate detonation in the DIPX experiment was very well axially centered, slightly favoring 135˚, but somewhat lower-than-center (i.e. off center away from the Top probe). It can also be implied that the DDT point in the SITX experiment is off-axis—initiated away from the 315˚ direction and slightly above center (this is because all equator probes exhibit slightly delayed arrival times). The LIPX experiment shows large discrepancies between probes. It appears the vessel fails nearest the 135˚ probe location, off-axis and closer to the top by almost 10 μs. However, while this analysis shows that *vessel rupture* was asymmetric, the long delay times for the LIPX test require caution with attributing that rupture asymmetry to internal reaction asymmetry (a symmetric reaction can cause asymmetric vessel failure when we are in a non-hydrodynamic regime in which the stochastic nature of metal fracture plays an important role).

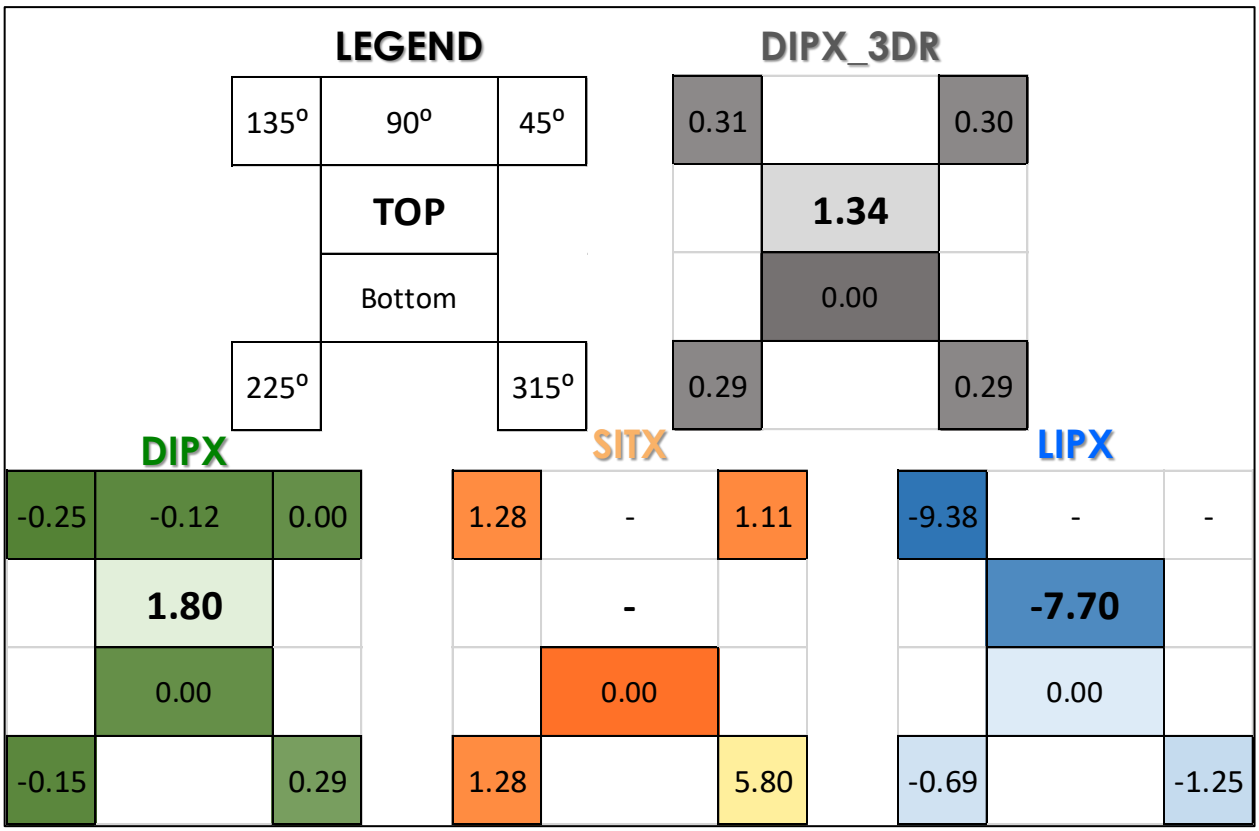

Figure 49. Spatial representation of arrival times (in μs) of detonation shock normalized to the "Bottom" location of each record and shifted according to DIPX_2DC results. Colors are linearly scaled from darkest-to-lightest arrival time in each experiment. The top left diagram provides a template for identifying probe locations for the rest of the figures. Note: if arrival times for DIPX_2DC were displayed in one of these diagrams, all entries would be zero.

9. Gurney Analysis

The acceleration of the vessel was slower in the LIPX experiment than either DIPX or SITX; however the ultimate fragment velocity that was recorded indicates a large fraction of the explosive energy was released. To estimate the relative energies that were transferred from the explosive's potential to the fragments, we use a simplified Gurney analysis[16].

The terminal velocity for a spherical casing accelerated by a spherical charge is given by:

$$v_m = \sqrt{2E_G}\left(\frac{m}{c}+\frac{1}{2}\right)^{-\frac{1}{2}} \quad (1)$$

Where v_m is the terminal velocity of the metal casing, m is the mass of the metal fragments, c is the explosive charge mass, $\sqrt{2E_G}$ is the Gurney velocity, and E_G is the Gurney Energy. For the Gurney velocity of PBX 9501, we use we use the assumption[16] that generally the Gurney velocity is ~D_v/2.97 where D_v is the detonation velocity of an explosive charge—in this case 8.9 mm/μs—yielding the Gurney velocity of 3.0 mm/μs.

When approximating the Heavy apparatus as a sphere, we have choices regarding the mass of metal to use for the calculation. Figure 50 shows two different approximations. Using the entire mass of the vessel, converted to a spherical geometry, provides the larger radius option. This larger amount of metal at the radius would result in a lower terminal fragment velocity. In actuality, some of the vessel mass is located at the "corners" where less velocity will be imparted, and so approximating it as the larger radius sphere will result in a

"minimum fragment velocity" result. Alternatively, we use a reduced metal mass for the gurney calculation, chosen such that the outer radius of the sphere matches the minimum vessel wall thickness. This provides a "maximum Gurney energy" result.

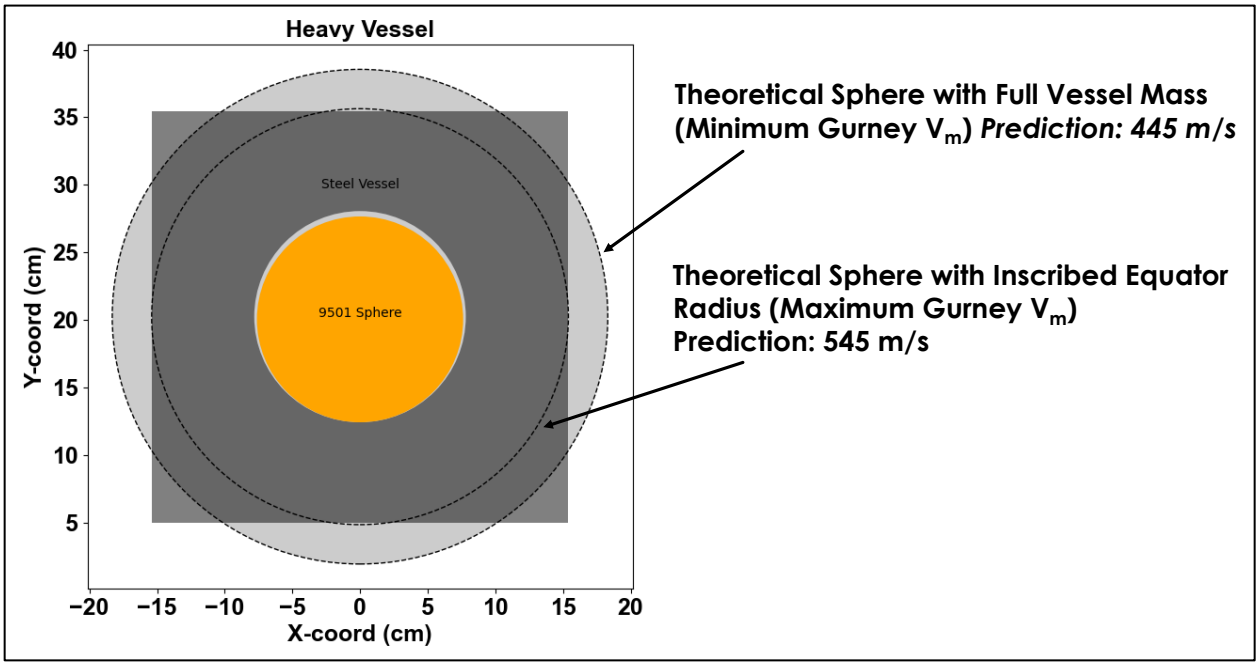

Figure 50. Two different choices for Gurney simplification: take the entire vessel mass and convert it into a larger sphere, or use a reduced metal mass such that the sphere radius matches the minimum wall thickness.

The maximum-m/minimum-V_m calculation results in a Gurney velocity of 445 m/s; the minimum-m/maximum-V_m calculation gives a Gurney velocity of 545 m/s. For comparison to the experiments, the minimum Gurney velocity of 445 m/s is displayed alongside the PDV data in Figure 51. Unfortunately the PDV record is truncated before acceleration has fully completed, but the trend from the PDV data suggests that fragments would ultimately have attained a terminal velocity somewhere bounded by the two Gurney predictions (445-545 m/s).

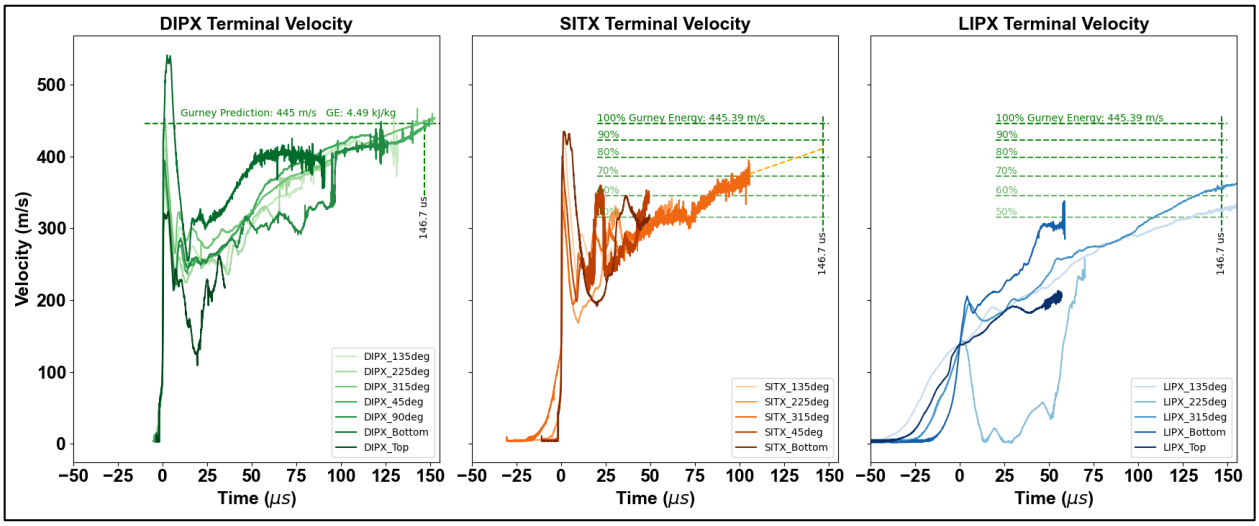

Figure 51. Comparison of Gurney energy estimates for DIPX and SITX. Traces are time-adjusted to a threshold of 125m/s.

The Gurney approach allows us to quantify what fraction of the total energy available in the explosive was converted to fragment motion, and provides useful side-by-side comparisons of these experiments. The DIPX experiment fragment velocity reached the lower Gurney prediction of 445 m/s after approximately 125 μs (146.7 μs labeled in Figure 51)) when signals were adjusted to set the time when the velocity record reached

a threshold of about 125 m/s to be time zero. The Fragment velocities in the SITX experiment attained the 80% Gurney energy velocity prediction after 100 μs. A rough extrapolation predicts that 80-90% of the energy may have eventually been converted to velocity after approximately the same 150 μs duration observed in the DIPX experiment. The LIPX indicates conversion of 55-65% of the Gurney energy to fragment velocity after the same 150 μs. This indicates that a considerable fraction of the explosive energy is delivered to the metal fragments, but over a longer duration than the shock driven behavior observed in DIPX and SITX.

10. Conclusions

The purpose of this project was to investigate the ultimate violence attained when heavily confined, pristine (i.e. mechanically and thermally undamaged) PBX 9501 is thermally ignited in the center of a 6-inch spherical charge using an infrared laser. Three experiments were successfully completed: LIPX (laser-ignited pristine explosive), DIPX (detonator-initiated pristine explosive), and SITX (self-ignited thermally damaged explosive).

LIPX was the first, primary experiment. The velocimetry data obtained from the outer metal surface of the LIPX vessel indicated no discontinuous wave phenomena. This suggested the possibility that a classical detonation of the PBX 9501—in which a discontinuous >10 GPa shock front passes through the material—did not occur. However, the extreme thickness of the confinement (>2.5 inches) and the choice of hardened chromoly steel that may absorb considerable energy into fracture behavior, warranted additional investigations to support these observations (it was considered possible—though improbable—that a weakened detonation front in the 9501 could be sufficiently attenuated while passing through the steel to produce the velocimetry observations, and further work was necessary to rule out this possibility).

Two additional experiments were executed to provide baseline comparison data. The DIPX (detonator-initiated pristine explosive) experiment deliberately detonated the pristine PBX 9501 sphere at its center. The SITX (self-ignited thermally-damaged explosive) was a cookoff experiment in which DDT was anticipated.

Hydrocode modeling was performed, of two independent flavors—one with two-dimensional, high-spatial resolution using CTH™ and one with three-dimensional fracture parameters using ALE3D™. The 2D modeling nicely captured the initial shock jump-off behavior of the DIPX experiment, including both the elastic precursor and detonation-supported shock, but deviated from the DIPX experiment at late times. The 3D model smeared the elastic precursor over its larger cell size, but nicely captured the longer-duration fragment acceleration where fracture mechanics of the steel play a more important role.

Comparison of the LIPX experiment to the baseline DIPX and SITX experiments supports the claim that a classical detonation did not occur in the LIPX experiment. However, the ultimate violence observed in the LIPX experiment was still quite high—fragments were accelerated with approximately 55-65% of the Gurney energy before the PDV record was truncated. Fragments were still accelerating at the end of the PDV record, so ultimate energy conversion and terminal fragment velocity would have been even higher.

To restate this primary finding: the LIPX experiment did not exhibit a traditional DDT event. Here we define "traditional DDT event" as a discontinuous shock front of sufficient pressure in the explosive to push the metal such that most of the available energy is converted to kinetic motion of the fragments in a short duration (<5 μs). In comparison, energy conversion to fragment motion in the LIPX experiment occurred over ~100 μs. Nevertheless, the ultimate fragment velocity achieved at late times was still high—a significant percentage of the terminal velocity. This raises the question: does the lack of a shock front (and associated rapid fragment acceleration) make a difference? Or does the lack of a shock front not matter as much as the terminal fragment velocity? The answer will naturally depend on the relevant time-scales of the individual application. Does it matter that the fragments took ten times longer to reach terminal velocity, or is 100 μs is still short relative to the application? It is beyond the scope of this investigation to determine the lack of a traditional DDT shock event is relevant when applied to high-fidelity scenarios.

It is also worth noting that fragment analysis and high-speed videography diagnostics did not distinguish between the LIPX, DIPX, and SITX experiments. Considering only these diagnostics, the LIPX experiment would likely have been deemed a classical detonation. Only in the velocimetry data is a difference observed.

This may have implications for historical experiments—for which PDV did not exist—that reported classical detonation as the outcome.

11. Acknowledgments

We gratefully acknowledge Debra Johnson from the W88 Alt and Refresh Program for motivating and funding this work. We also thank Darren Hanson and his explosive machining team for fabricating the explosive spheres, particularly for overcoming the challenges inherent to drilling a deep and narrow blind hole into energetic material. We thank the firing leaders that responded flexibly to a constantly changing schedule and worked hard in extreme summer heat to complete these experiments despite the additional obstacles imposed by COVID-19, including Dennis Jaramillo, Dennis Herrerra, Eva Baca, and Angelo Cartelli.

12. Data Requests

Videos of the tests as well as various other raw data can be made available on request. Please contact Matt Holmes at mholmes@lanl.gov or 505-665-4107.

13. References

[1] Cuauhtemoc, A.-R., Parker, G. R. and Holmes, M. D., "Simulations of Two Heavily Confined PBX 9502 Cook-off Tests" *Los Alamos National Laboratory Report: LA-UR-18-21834*, 2015.
[2] Maienschein, J. L., Leininger, L. D. and Hooks, D. E., "IHE Material and IHE Subassembly Qualification Test; Description and Criteria; DRAFT" *Los Alamos National Laboratory Report: LA-UR-15-29238*, 2016.
[3] Parker, G. R., Heatwole, E. M., Holmes, M. D., Asay, B. W., Dickson, P. M., et al., "Deflagration-to-detonation transition in hot HMX and HMX-based polymer-bonded explosives" *Combustion and Flame,* Vol. 215, pp. 295-308, https://doi.org/10.1016/j.combustflame.2020.01.040, 2020.
[4] Gurule, J., "Quick Look Report for Heavily Confined HE Investigation", Memorandum, *Los Alamos National Laboratory*,
[5] Parker, G. R., "Quick Look Report for Local Test-55-1 & -2: The Heavily Confined PBX 9502 Cookoff Tests" *Los Alamos National Laboratory* 2015.
[6] Holmes, M. D., Parker, G. R., Heatwole, E. M., Feagin, T. A., Broilo, R. M., et al., "Center-Ignited Spherical-Mass Explosion (CISME); FY 2018 Report" *Los Alamos National Laboratory Report: LA-UR-18-29651*, 2018.
[7] Harmony, S. C., Hatler, L. E. and Fletcher, M. A., "Hazards and vulnerability tests on PBX 9501, PBX 9502, X-0298, and various HMX/TATB mixtures" *Los Alamos National Laboratory Report: LA-CP-84-57*, 1984.
[8] Cooper, P. W., *Explosives Engineering*, Wiley-VCH, 1996.
[9] Cady, H. H. and Smith, L. C., "Studies on the polymorphs of HMX" *Los Alamos Scientific Laboratory Report: LAMS-2652*, 1961.
[10] Parker, G. R. and Rae, P. J., "Mechanical and Thermal Damage" in *Non-Shock Initiation of Explosives*, *Shock Wave Science and Technology Reference Library*, edited by B. W. Asay, pp. 293-401, Vol. 4, Springer-Verlag, 2010.
[11] Smilowitz, L. B., Henson, B. F., Asay, B. W. and Dickson, P. M., "A Model of the b-d Phase Transition in PBX 9501" *Proceedings of the 12th International Detonation Symposium*, pp. 103-110, San Diego, CA, 2002.
[12] Dickson, P., Asay, B. W., Henson, B. F., Fugard, C. S. and Wong, J., "Measurement of phase change and thermal decomposition kinetics during cookoff of PBX 9501" *Proceedings of the AIP, Shock Compression of Condensed Matter*, p. 837, 1999.
[13] Henson, B. F., Asay, B. W., Sander, R. K., Son, S. F., Robinson, J. M., et al., "Dynamic Measurement of the HMX b-d Phase Transition by Second Harmonic Generation" *Physical Review Letters,* Vol. 82, pp. 1213-1216, 1999.
[14] CTH Hydrocode, Sandia National Laboratory, https://www.sandia.gov/CTH/.
[15] ALE3D, Lawrence Livermore National Laboratory, https://wci.llnl.gov/simulation/computer-codes/ale3d.
[16] Zukas, J. A. and Walters, W. P., *Explosive Effects and Applications*, Springer, 1998.

Appendix A Explosive density report from HE machining

Task Order: 3342-01 Cal File # 006863
Exp. Date 6/5/2020

Date: 8/12/2019

Description: 6" Hemi

2.32907

1.836 +/- .006

	Dry	Dry	Average	Std Dev	Water	Water	Wet	Wet	Average	Std Dev	Std Wet	Density
	Weight	Weight	Dry	Dry	Temp	Density	Weight	Weight	Wet	Wet	Weight	at 20 °C
Material	#1	#2	Weight	Weight			#1	#2	Weight	Weight	Correction	Temp
Silicone Standard	1839.500	1839.500	1839.500	0.000	18.42	0.99852	1051.100	1051.100	1051.100	0.000	1.00018	2.32907

Part SN#	Material	Dry	Dry	Average	Std Dev	Water	Water	Wet	Wet	Average	Std Dev	Std Wet	Density
		Weight	Weight	Dry	Dry	Temp	Density	Weight	Weight	Wet	Wet	Weight	at 20 °C
		#1	#2	Weight	Weight			#1	#2	Weight	Weight	Correction	Temp
19-183-01	9501	3409.700	3409.700	3409.700	0.000	18.42	0.99852	1560.500	1560.500	1560.500	0.000	1.00018	1.840
	80348												
19-183-02	9501	3407.800	3407.800	3407.800	0.000	18.42	0.99852	1558.900	1558.900	1558.900	0.000	1.00018	1.839
	80349												
19-183-03	9501	3407.000	3407.000	3407.000	0.000	18.42	0.99852	1558.200	1558.200	1558.200	0.000	1.00018	1.839
	80350												

Appendix B Design Drawings

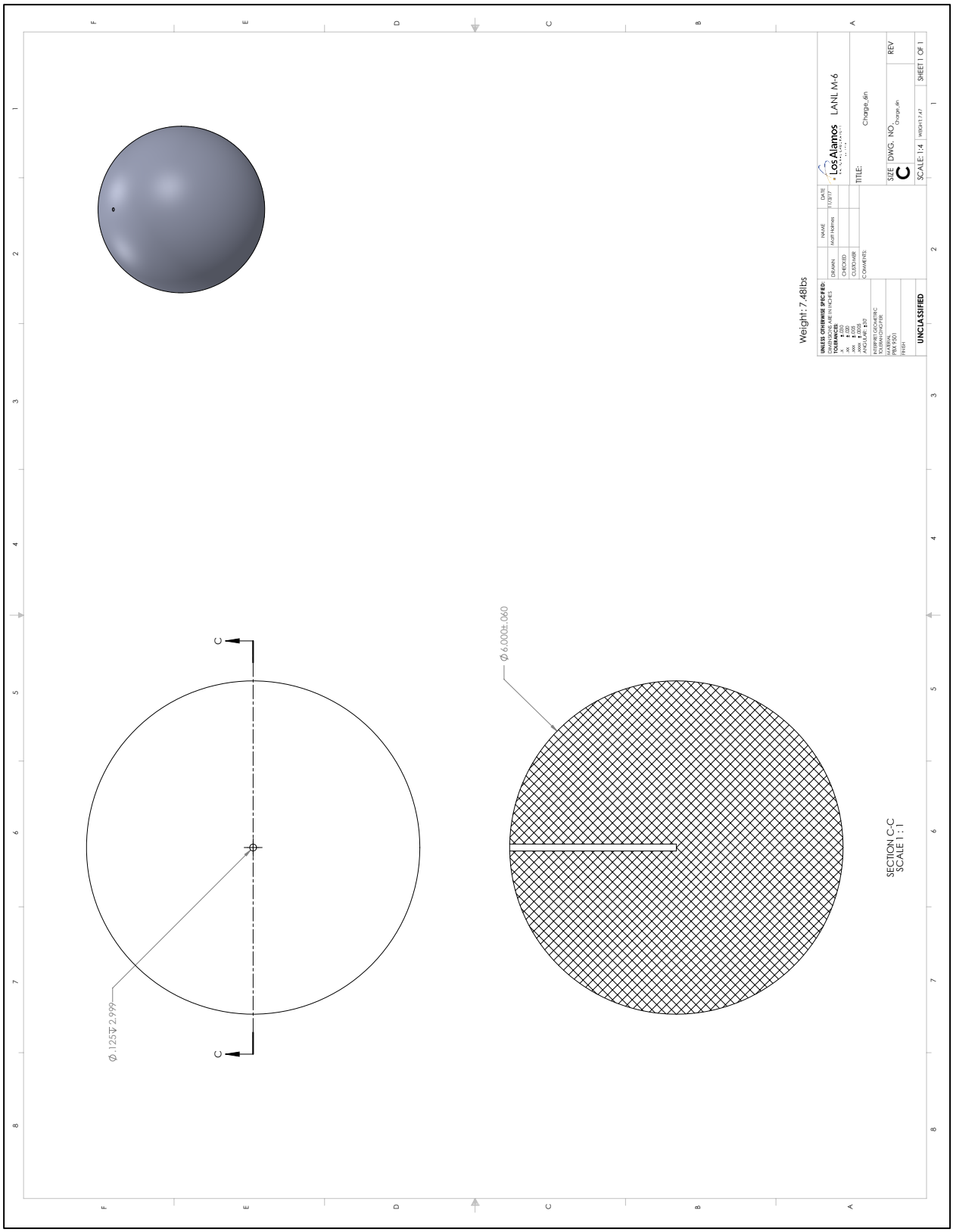

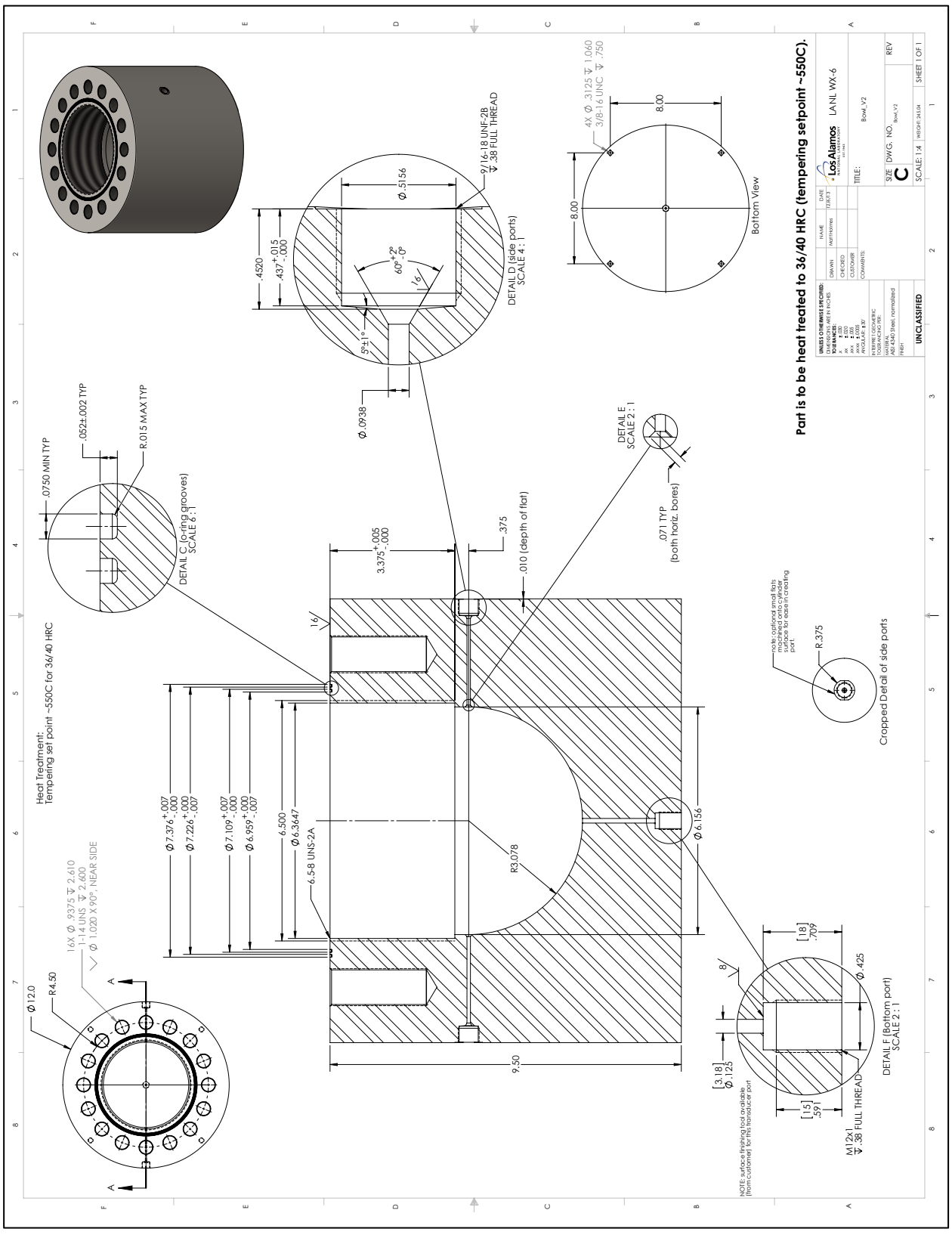
Part is to be heat treated to 36/40 HRC (tempering setpoint ~550C).
Heat Treatment:
Tempering set point ~550C for 36/40 HRC
Bottom View
Cropped Detail of side ports
DETAIL C (o-ring grooves)
SCALE 6 : 1
DETAIL D (side ports)
SCALE 4 : 1
DETAIL E
SCALE 2 : 1
DETAIL F (Bottom port)
SCALE 2 : 1
.0750 MIN TYP
.052±.002 TYP
R.015 MAX TYP
.071 TYP
(both horiz. bores)
.375
.010 (depth of flat)
9/16-18 UNF-2B
↧.38 FULL THREAD
M112x1
↧.38 FULL THREAD
6.5-8 UNS-2A
R3.078
R.375
9.50
8.00
8.00
UNCLASSIFIED
LA-NL WX-6
Bowl_V2
SCALE: 1:4
SHEET 1 OF 1

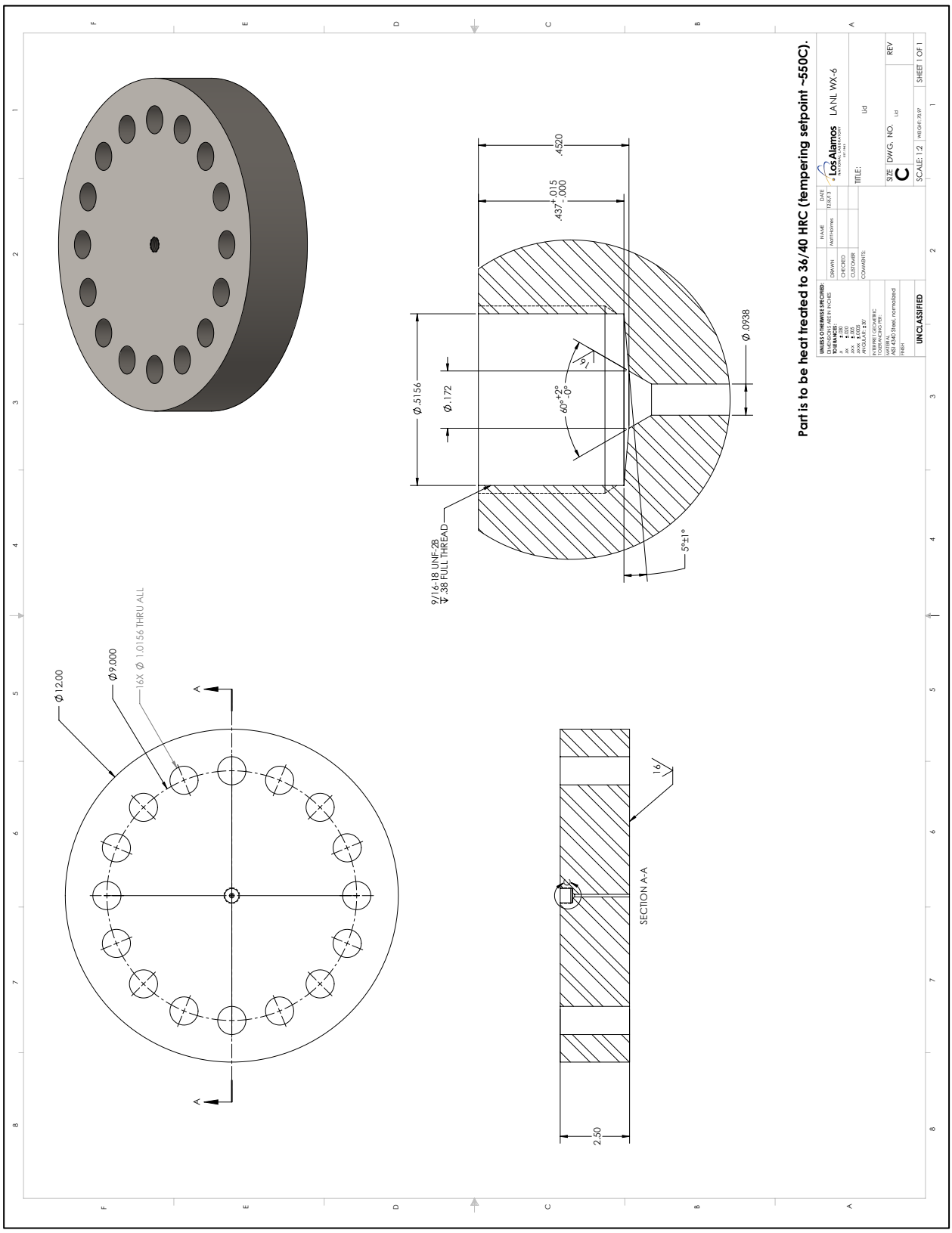
Part is to be heat treated to 36/40 HRC (tempering setpoint ~550C).
.4520
.437 +.015 -.000
Ø.5156
Ø.172
60° +2° -0°
Ø.0938
9/16-18 UNF-2B
↧.38 FULL THREAD
5°±1°
Ø12.00
Ø9.000
16X Ø 1.0156 THRU ALL
A
A
16
SECTION A-A
2.50
Los Alamos
LANL WX-6
TITLE:
lid
SIZE C
DWG. NO. lid
REV
SCALE: 1:2
WEIGHT: 0.197
SHEET 1 OF 1
UNCLASSIFIED

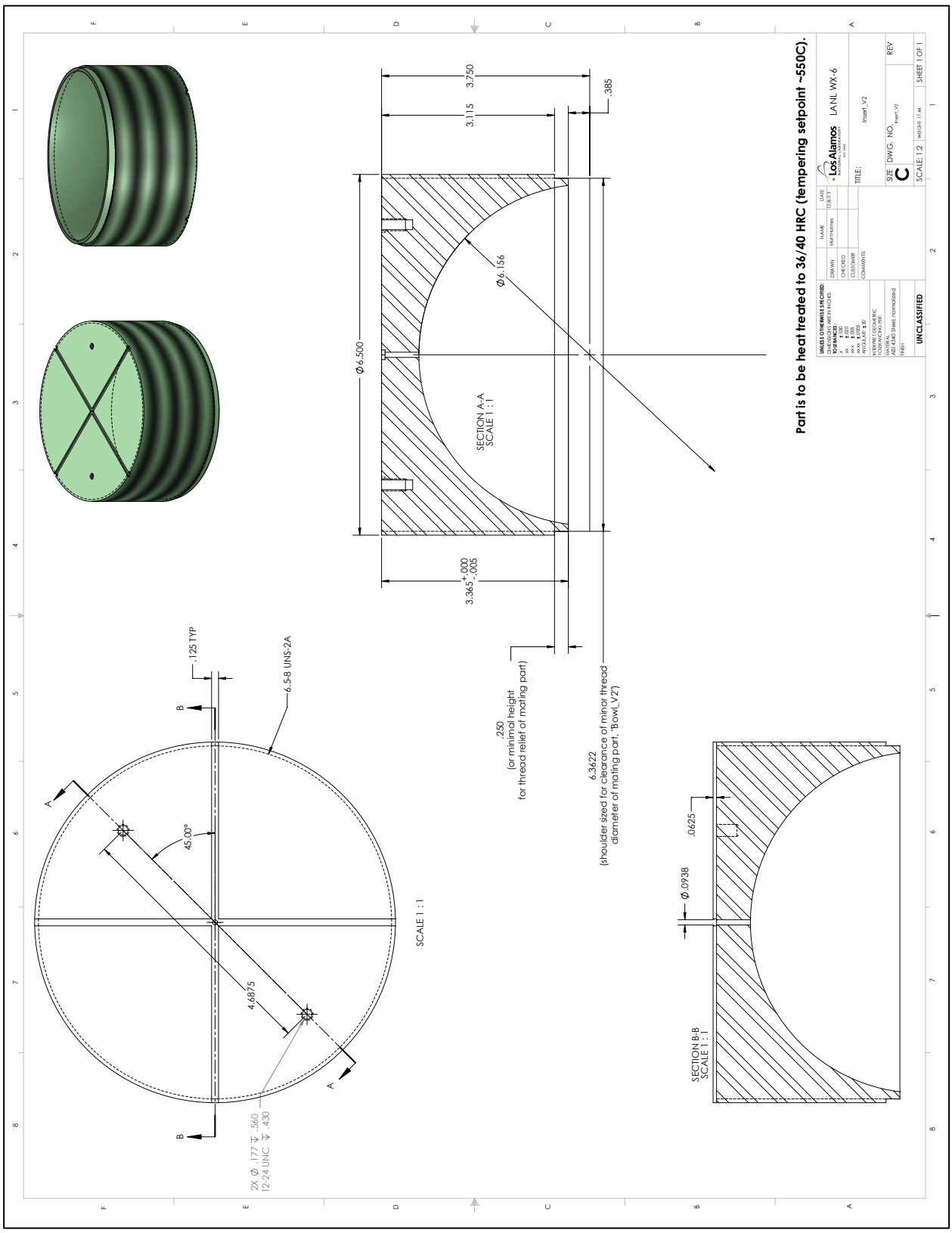
Part is to be heat treated to 36/40 HRC (tempering setpoint ~550C).
3.750
3.115
.385
Ø6.500
Ø6.156
SECTION A-A
SCALE 1 : 1
3.365 +.000 -.005
.250
(or minimal height
for thread relief of mating part)
6.3622
(shoulder sized for clearance of minor thread
diameter of mating part, "Bowl_V2")
.125 TYP
6.5-8 UNS-2A
45.00°
4.6875
2X Ø .177 ↧ .560
12-24 UNC ↧ .430
SCALE 1 : 1
Ø.0938
.0625
SECTION B-B
SCALE 1 : 1
UNCLASSIFIED
TITLE:
Insert_V2
SIZE C
DWG. NO. Insert_V2
REV
SCALE: 1:2
WEIGHT: 17.44
SHEET 1 OF 1
LA-NL WX-6

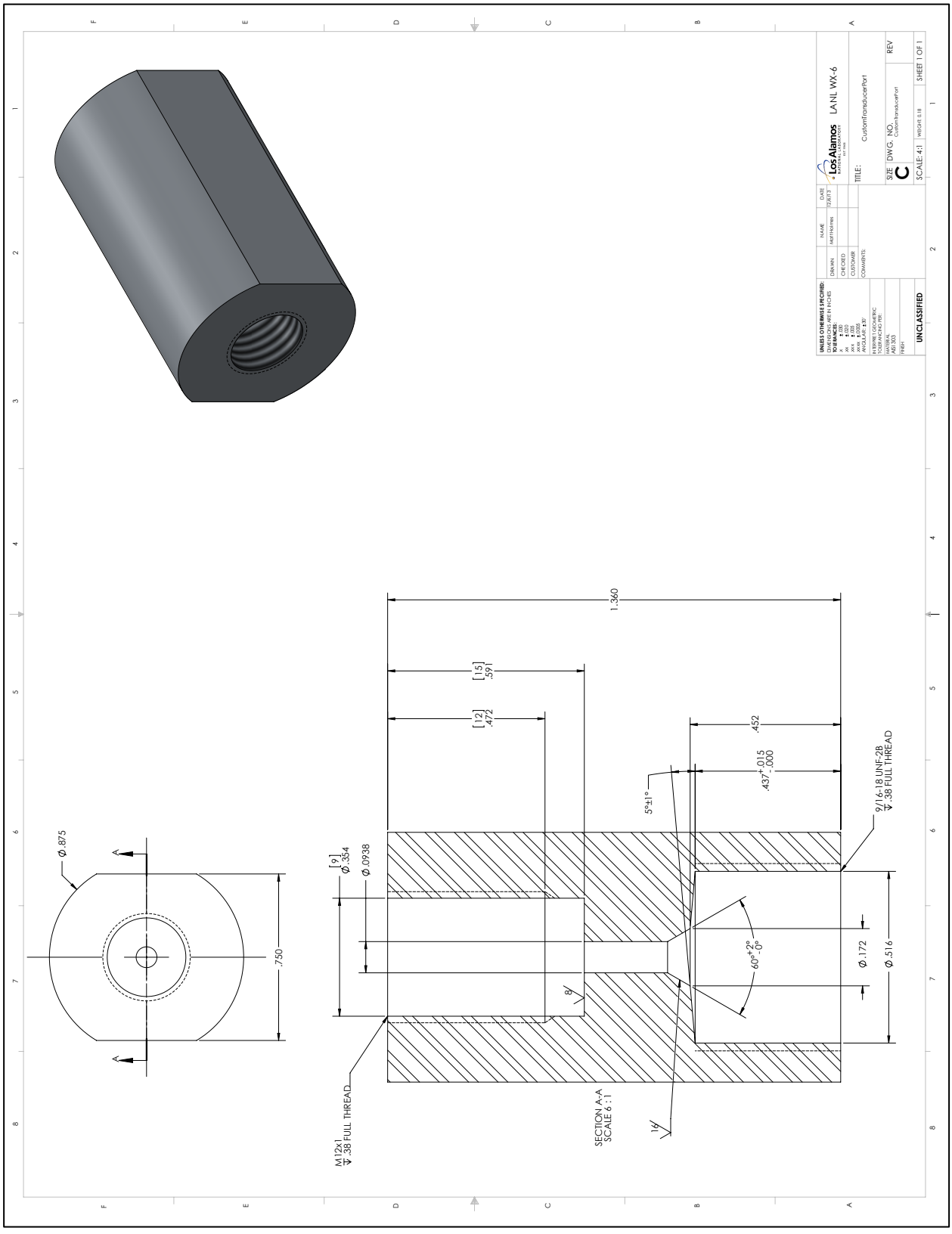
LANL WX-6
TITLE: CustomTransducerPort
SIZE C
DWG. NO. CustomTransducerPort
REV
SCALE: 4:1
WEIGHT: 0.1 lb
SHEET 1 OF 1
UNCLASSIFIED
1.360
[15] .59
[12] .472
.452
.437 +.015 -.000
5°±1°
9/16-18 UNF-2B ↧.38 FULL THREAD
Ø.516
Ø.172
60° +2° -0°
[9] Ø.354
Ø.0938
8
16
M12x1 ↧.38 FULL THREAD
SECTION A-A SCALE 6 : 1
Ø.875
.750

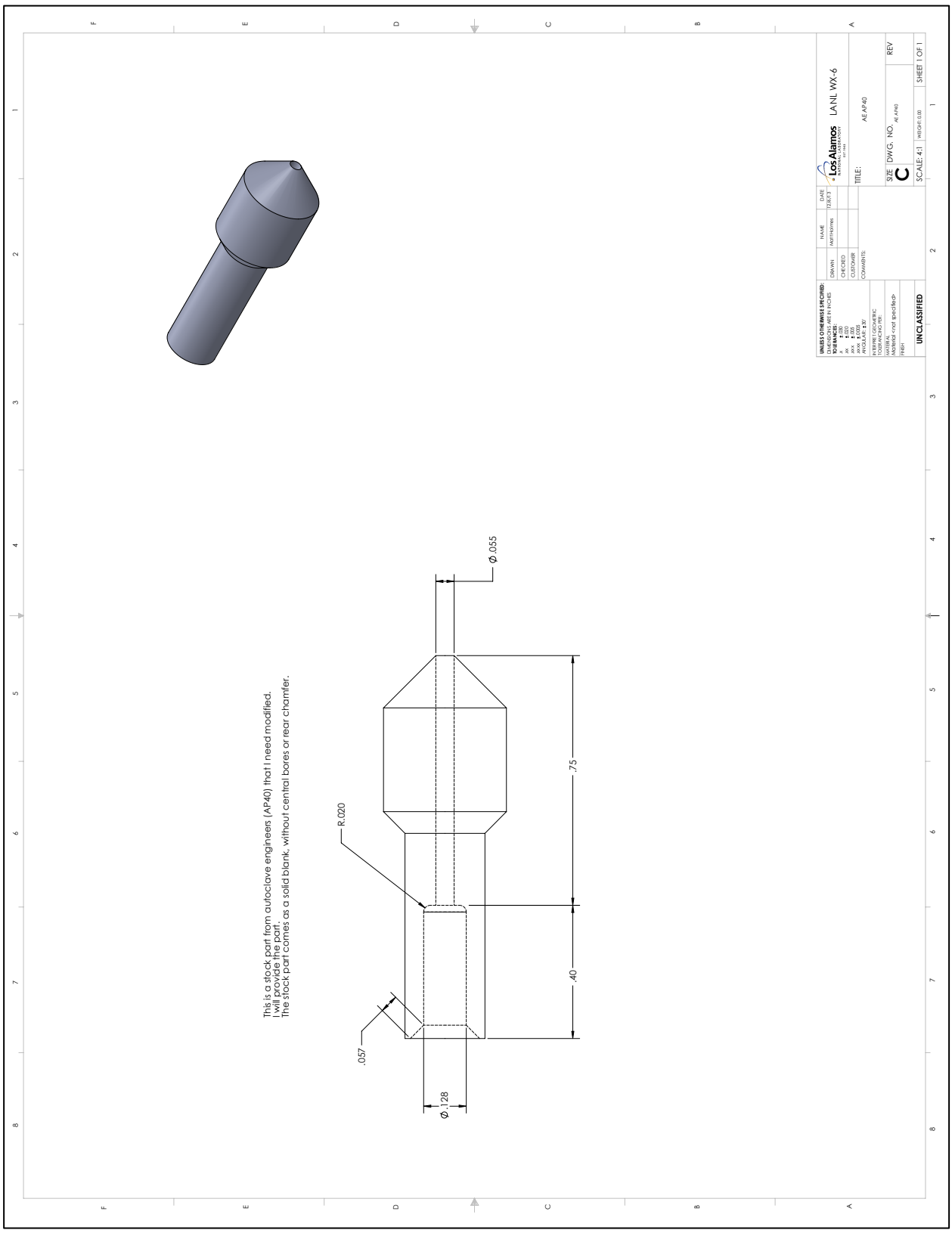
Ø.055
R.020
.75
.40
.057
Ø.128
This is a stock part from autoclave engineers (AP40) that I need modified.
I will provide the part.
The stock part comes as a solid blank, without central bores or rear chamfer.
LANL WX-6
TITLE:
AE AP40
SIZE
C
DWG. NO.
AE AP40
REV
SCALE: 4:1
SHEET 1 OF 1
UNCLASSIFIED

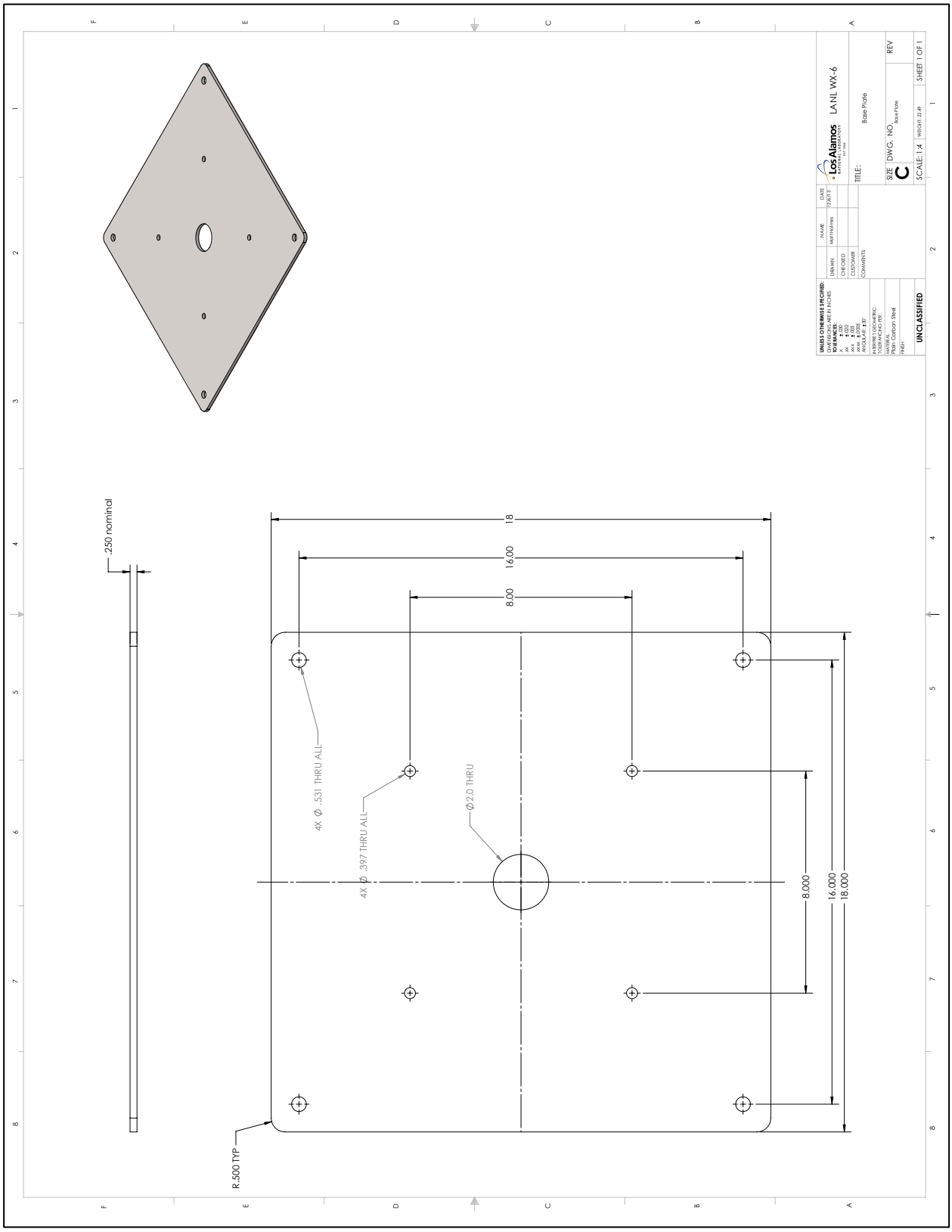
.250 nominal
18
16.00
8.00
4X Ø .531 THRU ALL
4X Ø .397 THRU ALL
Ø2.0 THRU
8.000
16.000
18.000
R.500 TYP
LANL WX-6
Base Plate
SIZE C
DWG. NO. Base Plate
REV
SCALE: 1:4
SHEET 1 OF 1
UNCLASSIFIED

Appendix C Assembly Procedures

Experiment Procedure: Heavy Bucket PBX 9501 — LIPX 1
M-6 Los Alamos National Laboratory Revision C (issued 10/12/20)

There are three versions of the Heavy Bucket PBX 9501 experiment:

- **LIPX (laser-ignited pristine explosive)**
- **DIPX (detonator-initiated pristine explosive)**
- **SITX (self-ignited pristine explosive)**

This procedure is specific to the LIPX version of the experiment.

This procedure is divided into three sections:

A. Assembly
B. Pre-test Preparations at the Firing Site
C. Test Execution
D. Post-test

Notes:

- **Steps in red are particularly relevant for safety**
- **Steps in hot pink are particularly important (either hard to forget and/or consequential)**
- **Steps in orange include a task to be photographed or notes/measurements recorded.**
- **(text cannot be two colors at once; priority is given as per the list order above)**

A. ASSEMBLY

1. Mount caster wheels to baseplate
2. Clean discoloration off bucket with combination of brass wire brush, ScotchBrite pads, paper towels, and solvent, with particular attention to the interior of the cavity and insert
3. Carefully clean bottom port for dynamic transducer
4. Bolt bucket to base plate with 4 3/8-16 hex head bolts, 1.5" long
5. Insert solid blank plugs into two side feedthrough ports
6. Install teflon spacers at designated locations in the bottom cavity, using kapton tape (document locations in notebook)
7. Install teflon spacers inside cavity of insert
8. Install bottom transducer
   - 8.1. Apply lube to threads of transducer
   - 8.2. Install fresh sealing ring, being careful of orientation, and hold in place with dabs of vacuum grease
   - 8.3. Torque to 40 Nm (30 ft-lbs)
9. Use syringe to fill bottom feedthrough hole with silicone fluid
10. Use solvent to clean any silicone fluid spills from the bottom of cavity as necessary
11. Prepare explosive charge
    - 11.1. Arrange top lid, insert, and explosive charge in a line, as they will be installed into the bucket, so that the optical fiber/thermocouples can be passed through the first two and potted into explosive charge. These three components will become inextricably connected via fragile thermocouple wiring. It would be best to do this on a table that is at the same level at the bucket, to aid the independent transfer of each of these parts into the bucket. Locate components close enough to bucket so that explosive charge can be inserted into bucket without having to move the insert or top lid (this depends on the amount of slack available in the optical and thermocouple cables).
    - 11.2. Cut the tip of optical fiber.
    - 11.3. Pass tip of optical fiber through top lid, from outside-in (pass it through the side with the mounting location for the pressure feedthrough)
    - 11.4. Pass tip of optical fiber through the insert, from outside-in.
    - 11.5. Pass optical fiber through hypodermic tubing.
      - 11.5.1. Note: the hypodermic tubing for potting must be long enough to reach from bottom of blind hole in explosive all the way up through the insert and top lid, to protrude from the top lid. Check this before installation.
    - 11.6. Repeat the same process for the thermocouple wire(s) that will be potted alongside the fiber optic.
    - 11.7. Build potted tubing assembly
      - 11.7.1. Leave optical fiber protruding slightly from tip of hypodermic tubing (it will be freshly cleaved after potting).
      - 11.7.2. Locate bead of thermocouple barely proud of hypodermic tubing.
      - 11.7.3. Pot optical fiber and thermocouple into hypodermic tubing using thin epoxy.
      - 11.7.4. After epoxy cures, cleave optical fiber just proud of thermocouple bead (to avoid accidentally cutting off thermocouple bead)
    - 11.8. Pot tubing assy in explosive charge
      - 11.8.1. Use thin wooden dowel to measure (record) depth of blind hole in explosive charge.
      - 11.8.2. Carefully measure (record) quantity of thermite
      - 11.8.3. Pour thermite into bottom of blind hole in explosive
      - 11.8.4. Bottom tubing assembly into the thermite.
      - 11.8.5. Mark tubing level at the surface of charge with a sharpie line

Experiment Procedure: Heavy Bucket PBX 9501 — LIPX 2
M-6 Los Alamos National Laboratory Revision C (issued 10/12/20)

- 11.8.6. Briefly remove tubing assembly to measure (and record) depth of penetration of tubing assembly
- 11.8.7. Reinsert tubing assembly into thermite, confirming that same depth is achieved
- 11.8.8. Epoxy tubing assembly into explosive charge
  - 11.8.8.1. Use a syringe with a hypodermic needle tip to carefully inject epoxy into hole to pot tubing assembly into explosive charge
  - 11.8.8.2. Endeavor to fill hole from bottom upward, to minimize trapped air
  - 11.8.8.3. Endeavor to minimize puddling/beading on explosive charge (any epoxy out of the hole will impinge on the ability for the charge to rest tangentially in the cavity
- 11.8.9. Photograph the results after epoxy cures

12. Carefully arrange remaining loose upper TCs alongside fiber optic in preparation for inserting HE charge.
13. Ensure that charge, insert, and lid are close enough to bucket that charge can be inserted without disturbing insert or lid.
14. Place o-rings in grooves PRIOR TO INSERTING EXPLOSIVE INTO BUCKET
15. Lower explosive charge into cavity of bucket. Use gaff-tape straps to accomplish this.
16. Clean the mating surface where the insert will meet the bucket
17. THE STEPS WHICH FOLLOW—THOSE THAT INVOLVE HEAVY METAL PARTS—MUST BE EXECUTED WITH EXTREME CARE TO AVOID BREAKING CABLING
18. Install insert into bucket
    - 18.1. Two people will be required for this step
      - 18.1.1. One person protects and guides the hypodermic tubing through the hole in the insert, managing the optical and thermocouple wires
      - 18.1.2. Second person manipulates the insert, with two hands, guided and directed by the first person.
    - 18.2. Position z-axis stages at full extension on top of bucket
    - 18.3. Confirm that insert will rest on stages such that top level of hypodermic tubing is lower than z-axis platform (so that lid does not impact hypodermic when resting on stages); use blocks as necessary
    - 18.4. Lower insert, guiding fiber optic through hole, until insert is resting on z-stages
    - 18.5. Use z-stages to lower insert over the fiber/tubing junction
    - 18.6. After tubing is well into the insert, one person suspends insert while another person removes the z-stages
    - 18.7. Lower insert onto top of bowl, guiding fiber optic through
    - 18.8. After insert is positioned with hypodermic tubing protruding:
      - 18.8.1. Screw insert into vessel until bottomed out
      - 18.8.2. One person maintains secure hold on protruding hypodermic tubing to prevent excessive rotation
    - 18.9. Confirm depth of insert below mating face (measure & record)
    - 18.10. PHOTOGRAPH
19. Thoroughly clean top mating surface of bucket, especially o-ring grooves
20. Clean mating surface of lid (the underside)
21. Lower lid flat onto top surface
    - 21.1. Install guide rod jigs, one each on opposite sides of the bucket.
    - 21.2. Position z-axis stages at full extension on top of bucket
    - 21.3. Confirm that lid will rest on stages such that top level of hypodermic tubing is lower than z-axis platform (so that lid does not impact hypodermic when resting on stages
    - 21.4. THREE people are required for this step
      - 21.4.1. One person to protect and guide hypodermic tubing up through the hole in the insert, managing the optical and thermocouple wires
      - 21.4.2. Second and third person lift and lower the lid into position, onto guide rails and to rest atop z-axis stages, guided and directed by the first person
      - 21.4.3. Lower lid until it rests on stages
    - 21.5. Use stages to lower lid until junction of optical fiber with hypodermic tubing is guided into the lid (this is to avoid pinching & breaking the fiber optic where it exits the hypodermic tubing)
    - 21.6. Install wedges
      - 21.6.1. Ensure that o-rings remain properly positioned.
      - 21.6.2. Purpose of the wedges is to allow lid to be lowered straight down over hypodermic tubing, without damaging hypodermic tubing, and without pinching workers fingers between lid and bucket.
      - 21.6.3. Thickness of wedges at edge of bucket where fingers will be removed should be 9/16 inch
      - 21.6.4. Tape wedges to bucket with tape at outer edge where it can be easily removed after lid is resting atop wedges.
    - 21.7. Two workers take weight of lid while third worker removes z-stages.
    - 21.8. Lower lid straight down until it rests on the wedges.
    - 21.9. Carefully work wedges out, monitoring the hypodermic tubing in the vanishing gap, until lid rests on vessel and wedges are removed entirely.
22. Insert and tighten bolts (as much as possible—do not use impact wrench however—the chance of disturbing the position of the explosive charge is too great).
23. Prep bucket for transport
    - 23.1. Arrange and secure fiber optic and TC wiring

B. Pre-Test Preparations at the Firing Site

1. Check scope settings, phantom settings, delay generator, etc
2. Check dynamic transducer
   - 2.1. Examine dynamic transducer trace while on long-time mode, should observe slow drift—this confirms connection
   - 2.2. Switch dynamic transducer amp to short time mode
   - 2.3. Make sure it is in "operate" mode
   - 2.4. Confirm zeroed trace on scope
3. Weather-protect
   - 3.1. place cover on both pelican boxes
4. Confirm all network connections
5. Install shot on mound
   - 5.1. Drive shot to mound and roll into block house
   - 5.2. Wire up dynamic transducer
6. Position bounce mirrors, cameras, lighting

C. Test Execution

1. Start data capture
   - 1.1. check settings
2. Depart Mound
3. Fire the laser

D. Post-Test

4. Save Data Files
   - 4.1. High-speed cameras
   - 4.2. Surveillance cameras
   - 4.3. Scope traces
5. Turn off facility power to all devices that are located on the mound
6. May now ascend mound to assess safety

Experiment Procedure: Heavy Bucket PBX 9501 — DIPX 1
M-6 Los Alamos National Laboratory Revision C (issued 10/12/20)

There are three versions of the Heavy Bucket PBX 9501 experiment:

- **LIPX (laser-ignited pristine explosive)**
- **DIPX (detonator-initiated pristine explosive)**
- **SITX (self-ignited pristine explosive)**

This procedure is specific to the DIPX version of the experiment.

This procedure is divided into three sections:

A. Assembly
B. Pre-test Preparations at the Firing Site
C. Test Execution
D. Post-test

Notes:

- **Steps in red are particularly relevant for safety**
- **Steps in hot pink are particularly important (either hard to forget and/or consequential)**
- **Steps in orange include a task to be photographed or notes/measurements recorded.**
- **(text cannot be two colors at once; priority is given as per the list order above)**

A. ASSEMBLY

1. Mount caster wheels to baseplate
2. Clean discoloration off bucket with combination of brass wire brush, ScotchBrite pads, paper towels, and solvent, with particular attention to the interior of the cavity and insert
3. Carefully clean bottom port for dynamic transducer
4. Bolt bucket to base plate with 4 3/8-16 hex head bolts, 1.5" long
5. Insert solid blank plugs into two side feedthrough ports
6. Install teflon spacers at designated locations in the bottom cavity, using kapton tape (document locations in notebook)
7. Install teflon spacers inside cavity of insert
8. Install bottom transducer
   - 8.1. Apply lube to threads of transducer
   - 8.2. Install fresh sealing ring, being careful of orientation, and hold in place with dabs of vacuum grease
   - 8.3. Torque to 40 Nm (30 ft-lbs)
9. Use syringe to fill bottom feedthrough hole with silicone fluid
10. Use solvent to clean any silicone fluid spills from the bottom of cavity as necessary
11. Prepare explosive charge
    - 11.1. Arrange top lid, insert, and explosive charge in a line, as they will be installed into the bucket, so that the detonator cabling can be passed through the first two and potted into explosive charge. These three components will become inextricably connected via fragile detonator wiring. It would be best to do this on a table that is at the same level at the bucket, to aid the independent transfer of each of these parts into the bucket. Locate components close enough to bucket so that explosive charge can be inserted into bucket without having to move the insert or top lid (this depends on the amount of slack available in the optical and thermocouple cables).
    - 11.2. Pot detonator in explosive charge
      - 11.2.1. Use thin wooden dowel to measure (record) depth of blind hole in explosive charge.
      - 11.2.2. Cut small pieces of primasheet, roll into tiny balls.
      - 11.2.3. Weigh out ≈100 mg worth of primasheet "bbs".
      - 11.2.4. Insert primasheet bbs into the hole in the charge, using wooden dowel to pack it in.
      - 11.2.5. Use thin wooden dowel to measure (record) depth of blind hole in explosive charge.
      - 11.2.6. Mark detonator wiring level at the surface of charge with a sharpie line
      - 11.2.7. Insert detonator into charge, confirming that proper depth is achieved. Use detonator cabling to firmly bottom the detonator into the primasheet booster material.
      - 11.2.8. Epoxy detonator cabling into explosive charge
        - 11.2.8.1. Use a syringe with a hypodermic needle tip to carefully inject epoxy into hole to pot tubing assembly into explosive charge
        - 11.2.8.2. Endeavor to fill hole from bottom upward, to minimize trapped air
        - 11.2.8.3. Endeavor to minimize puddling/beading on explosive charge (any epoxy out of the hole will impinge on the ability for the charge to rest tangentially in the cavity
      - 11.2.9. Photograph the results after epoxy cures
12. Carefully arrange remaining detonator cable in preparation for inserting HE charge.
13. Ensure that charge, insert, and lid are close enough to bucket that charge can be inserted without disturbing insert or lid.
14. Place o-rings in grooves PRIOR TO INSERTING EXPLOSIVE INTO BUCKET
15. Lower explosive charge into cavity of bucket. Use gaff-tape straps to accomplish this.

16. Clean the mating surface where the insert will meet the bucket
17. THE STEPS WHICH FOLLOW—THOSE THAT INVOLVE HEAVY METAL PARTS—MUST BE EXECUTED WITH EXTREME CARE TO AVOID BREAKING CABLING
18. Install insert into bucket
    - 18.1. Two people will be required for this step
      - 18.1.1. One person protects and guides the hypodermic tubing through the hole in the insert, managing the optical and thermocouple wires
      - 18.1.2. Second person manipulates the insert, with two hands, guided and directed by the first person.
    - 18.2. Position z-axis stages at full extension on top of bucket
    - 18.3. Confirm that insert will rest on stages such that top level of hypodermic tubing is lower than z-axis platform (so that lid does not impact hypodermic when resting on stages); use blocks as necessary
    - 18.4. Lower insert, guiding fiber optic through hole, until insert is resting on z-stages
    - 18.5. Use z-stages to lower insert over the fiber/tubing junction
    - 18.6. After tubing is well into the insert, one person suspends insert while another person removes the z-stages
    - 18.7. Lower insert onto top of bowl, guiding fiber optic through
    - 18.8. After insert is positioned with hypodermic tubing protruding:
      - 18.8.1. Screw insert into vessel until bottomed out
      - 18.8.2. One person maintains secure hold on protruding hypodermic tubing to prevent excessive rotation
    - 18.9. Confirm depth of insert below mating face (measure & record)
    - 18.10. PHOTOGRAPH
19. Thoroughly clean top mating surface of bucket, especially o-ring grooves
20. Clean mating surface of lid (the underside)
21. Lower lid flat onto top surface
    - 21.1. Install guide rod jigs, one each on opposite sides of the bucket.
    - 21.2. Position z-axis stages at full extension on top of bucket
    - 21.3. Confirm that lid will rest on stages such that top level of hypodermic tubing is lower than z-axis platform (so that lid does not impact hypodermic when resting on stages
    - 21.4. THREE people are required for this step
      - 21.4.1. One person to protect and guide hypodermic tubing up through the hole in the insert, managing the optical and thermocouple wires
      - 21.4.2. Second and third person lift and lower the lid into position, onto guide rails and to rest atop z-axis stages, guided and directed by the first person
      - 21.4.3. Lower lid until it rests on stages
    - 21.5. Use stages to lower lid until junction of optical fiber with hypodermic tubing is guided into the lid (this is to avoid pinching & breaking the fiber optic where it exits the hypodermic tubing)
    - 21.6. Install wedges
      - 21.6.1. Ensure that o-rings remain properly positioned.
      - 21.6.2. Purpose of the wedges is to allow lid to be lowered straight down over hypodermic tubing, without damaging hypodermic tubing, and without pinching workers fingers between lid and bucket.
      - 21.6.3. Thickness of wedges at edge of bucket where fingers will be removed should be 9/16 inch
      - 21.6.4. Tape wedges to bucket with tape at outer edge where it can be easily removed after lid is resting atop wedges.
    - 21.7. Two workers take weight of lid while third worker removes z-stages.
    - 21.8. Lower lid straight down until it rests on the wedges.
    - 21.9. Carefully work wedges out, monitoring the hypodermic tubing in the vanishing gap, until lid rests on vessel and wedges are removed entirely.
22. Insert and tighten bolts (as much as possible—do not use impact wrench however—the chance of disturbing the position of the explosive charge is too great).
23. Prep bucket for transport
    - 23.1. Arrange and secure fiber optic and TC wiring

B. Pre-Test Preparations at the Firing Site

1. Check scope settings, phantom settings, delay generator, etc
2. Check dynamic transducer
   - 2.1. Examine dynamic transducer trace while on long-time mode, should observe slow drift—this confirms connection
   - 2.2. Switch dynamic transducer amp to short time mode
   - 2.3. Make sure it is in “operate” mode
   - 2.4. Confirm zeroed trace on scope
3. Weather-protect
   - 3.1. place cover on both pelican boxes
4. Confirm all network connections
5. Install shot on mound
   - 5.1. Drive shot to mound and roll into block house

5.2. Wire up dynamic transducer
6. Position bounce mirrors, cameras, lighting

C. Test Execution

1. Start data capture
   1.1. check settings
2. Depart Mound
3. Fire the laser

D. Post-Test

4. Save Data Files
   4.1. High-speed cameras
   4.2. Surveillance cameras
   4.3. Scope traces
5. Turn off facility power to all devices that are located on the mound
6. May now ascend mound to assess safety

Experiment Procedure: Heavy Bucket PBX 9501 — SITX 1
M-6 Los Alamos National Laboratory Revision C (issued 10/12/20)

There are three versions of the Heavy Bucket PBX 9501 experiment:

- **LIPX (laser-ignited pristine explosive)**
- **DIPX (detonator-initiated pristine explosive)**
- **SITX (self-ignited pristine explosive)**

This procedure is specific to the SITX version of the experiment.

This procedure is divided into three sections:

A. Assembly
B. Pre-test Preparations at the Firing Site
C. Test Execution
D. Post-test

Notes:

- **Steps in red are particularly relevant for safety**
- **Steps in hot pink are particularly important (either hard to forget and/or consequential)**
- **Steps in orange include a task to be photographed or notes/measurements recorded.**
- **(text cannot be two colors at once; priority is given as per the list order above)**

A. ASSEMBLY

1. Mount caster wheels to baseplate
2. Place 8 layers of .125" fiberglass fabric between bucket and baseplate
3. Clean discoloration off bucket with combination of brass wire brush, ScotchBrite pads, paper towels, and solvent, with particular attention to the interior of the cavity and insert
4. Carefully clean bottom port for dynamic transducer
5. Bolt bucket to base plate with 4 3/8-16 hex head bolts, 1.5" long
6. Mark locations of thermocouples in cavity using flexible ruler
7. Mark TC locations on mock
8. Install teflon spacers at designated locations in the bottom cavity, using kapton tape (document locations in notebook)
9. Install teflon spacers inside cavity of insert
10. Build side-port TC feedthrough assembly
    10.1. Use design drawings to calculate required length of TC probes to protrude from feedthrough fitting.
    10.2. Insert TC probes through AE nut and feedthrough to the required length.
    10.3. Record locations
    10.4. Photograph
    10.5. Braze TCs into feedthrough while they are installed in the correct spots with mock (NO HE)
    10.6. Carefully organize external TC wires for maximum protection
11. Test all TC probes, make note of inoperable ones
12. Tape side-port TCs to surface of explosive charge.
13. Install bottom transducer
    13.1. Apply lube to threads of transducer
    13.2. Install fresh sealing ring, being careful of orientation, and hold in place with dabs of vacuum grease
    13.3. Torque to 40 Nm (30 ft-lbs)
14. Use syringe to fill bottom feedthrough hole with silicone fluid
15. Use solvent to clean any silicone fluid spills from the bottom of cavity as necessary
16. Prepare explosive charge
    16.1. Mark TC locations on top half of explosive
    16.2. Arrange top lid, insert, and explosive charge in a line, as they will be installed into the bucket, so that the top feedthrough port thermocouples can be passed through the first two and potted into explosive charge. These three components will become inextricably connected via fragile thermocouple wiring. It would be best to do this on a table that is at the same level at the bucket, to aid the independent transfer of each of these parts into the bucket. Locate components close enough to bucket so that explosive charge can be inserted into bucket without having to move the insert or top lid (this depends on the amount of slack available in the optical and thermocouple cables).
    16.3. Pot interior thermocouples in explosive charge
        16.3.1. Use thin wooden dowel to measure (record) depth of blind hole in explosive charge.
        16.3.2. Arrange thermocouple probe ends at proper distances for the desired depths in the hole. Temporarily secure the staggered TC ends by taping the bundle of TC wiring > 3 in. from the tip (where no epoxy will go).
        16.3.3. Insert TC bundle into hole to proper depth.
        16.3.4. Epoxy tubing assembly into explosive charge
            16.3.4.1. Use a syringe with a hypodermic needle tip to carefully inject epoxy into hole to pot tubing assembly into explosive charge

Experiment Procedure: Heavy Bucket PBX 9501 — SITX 2
M-6 Los Alamos National Laboratory Revision C (issued 10/12/20)

16.3.4.2. Endeavor to fill hole from bottom upward, to minimize trapped air
16.3.4.3. Endeavor to minimize puddling/beading on explosive charge (any epoxy out of the hole will impinge on the ability for the charge to rest tangentially in the cavity
16.3.5. Photograph the results after epoxy cures
17. Carefully arrange remaining loose upper TCs in preparation for inserting HE charge.
18. Ensure that charge, insert, and lid are close enough to bucket that charge can be inserted without disturbing insert or lid.
19. Place o-rings in grooves PRIOR TO INSERTING EXPLOSIVE INTO BUCKET
20. Lower explosive charge into cavity of bucket. Use gaff-tape straps to accomplish this.
21. Clean the mating surface where the insert will meet the bucket
22. THE STEPS WHICH FOLLOW—THOSE THAT INVOLVE HEAVY METAL PARTS—MUST BE EXECUTED WITH EXTREME CARE TO AVOID BREAKING CABLING
23. Install insert into bucket
23.1. Two people will be required for this step
23.1.1. One person protects and guides the thermocouple bundle through the hole in the insert
23.1.2. Second person manipulates the insert, with two hands, guided and directed by the first person
23.2. Lower insert onto top of bowl
23.3. After insert is positioned with hypodermic tubing protruding:
23.3.1. Screw insert vessel until bottomed out
23.3.2. One person maintains secure hold on protruding thermocouple wiring to prevent excessive rotation
23.4. Confirm depth of insert below mating face (measure & record)
23.5. PHOTOGRAPH
24. Thoroughly clean top mating surface of bucket, especially o-ring grooves
25. Clean mating surface of lid (the underside)
26. Lower lid flat onto top surface
26.1. Install guide rod jigs, one each on opposite sides of the bucket.
26.2. Install wedges
26.2.1. Ensure that o-rings remain properly positioned.
26.2.2. Purpose of the wedges is to allow lid to be lowered straight down over TC cable bundle without pinching cables between the lid and insert, and without pinching workers fingers between lid and bucket.
26.2.3. Thickness of wedges at edge of bucket where fingers will be removed should be 9/16 inch
26.2.4. Tape wedges to bucket with tape at outer edge where it can be easily removed after lid is resting atop wedges.
26.3. THREE people are required for this step
26.3.1. One person to protect and guide hypodermic tubing up through the hole in the insert, managing the optical and thermocouple wires
26.3.2. Second and third person lift and lower the lid into position, onto guide rails and to rest atop wedges, guided and directed by the first person
26.3.3. Lower lid until it rests on wedges
26.4. Carefully work wedges out, monitoring the TC cable in the vanishing gap, until lid rests on vessel and wedges are removed entirely.
26.5. Remove tape securing wedges
26.6. Remove wedges, working back and forth between the four wedges
27. Insert and tighten bolts (as much as possible—do not use impact wrench however—the chance of disturbing the position of the explosive charge is too great).
28. Install external thermocouples
28.1. First adhere small square of Kapton to bucket to electrically insulate TC bead
28.2. Tape TC bead to bucket using Kapton tape
28.3. Place small square of adhesive fiberglass sheet over each TC to partially insulate from heat tape
28.4. label and record TC locations as necessary
28.5. Carefully organize external TC cables
28.6. PHOTOGRAPH
29. Install heater tape
29.1. Use a piece of kapton to hold initial end of heat tape to bucket
29.2. Use piece of kapton to temporarily hold end of heat tape to bucket
29.3. Repeat for all four tapes.
29.4. Adjust heater tapes to be evenly spaced and fully tightened.
29.5. Place additional wraps of kapton around entire bucket to secure all tapes.
29.6. PHOTOGRAPH
30. Wire plug ends to all four heaters
31. Measure and record resistance of each heater
32. Prep bucket for transport
32.1. Arrange and secure TC cables and wires & heater cables

Experiment Procedure: Heavy Bucket PBX 9501 — SITX 3
M-6 Los Alamos National Laboratory Revision C (issued 10/12/20)

B. Pre-Test Preparations at the Firing Site

1. Check scope settings, phantom settings, delay generator, etc
2. Check dynamic transducer
   - 2.1. Examine dynamic transducer trace while on long-time mode, should observe slow drift—this confirms connection
   - 2.2. Switch dynamic transducer amp to short time mode
   - 2.3. Make sure it is in "operate" mode
   - 2.4. Confirm zeroed trace on scope
3. Weather-protect
   - 3.1. place cover on both pelican boxes
4. Confirm all network connections
5. Install shot on mound
   - 5.1. Drive shot to mound and roll into block house
   - 5.2. Wire up dynamic transducer
   - 5.3. Attach thermocouple plugs
   - 5.4. Attach heater power
6. Position bounce mirrors, cameras, lighting

C. Test Execution

1. Start data capture
   - 1.1. check settings
   - 1.2. Check thermocouples to known GOOD thermocouples
2. Connect heater power cords
3. Depart Mound
4. Set temperature profile as desired
5. Turn on the heaters
6. At the right time, fire the laser

D. Post-Test

1. Turn off temp controller
2. Save Data Files
   - 2.1. High-speed cameras
   - 2.2. Surveillance cameras
   - 2.3. DAQ temp and pressure
   - 2.4. Scope traces
3. Restart DAQ for temperature cooling curve
4. Allow experiment to cool overnight before approaching mound
5. After parts are cooled
   - 5.1. Approach bunker, do not yet ascend mound
   - 5.2. Turn off facility power to all devices that are located on the mound
6. May now ascend mound to examine

Appendix D Machining Quote

YEAMANS MACHINE SHOP INC.

QUOTE

10389

162 East Gate Drive
Los Alamos, NM 87544
(505) 662-9313 phone (505) 662-9806 fax
Email: yms@yeamansmachine.com

To: Matt Holmes
LANL
(505) 665-4107
Fax (505) 667-9809

PO:

YMS will provide the following parts and quantities per specification.

Item	Description	Qty	Unit Cost	Total Cost
1	Lid	3	$4,969.00	$14,907.00
2	Bowl V2	3	$12,263.00	$36,789.00
3	Insert V2	3	$3,598.00	$10,794.00
4	Base Plate	3	$941.00	$2,823.00
5	Custom Transducer Port	3	$673.00	$2,019.00
6	AE AP40	9	$180.00	$1,620.00
			Lot total:	**$68,952.00**

Delivery 14 weeks ARO

Quote Valid for 30 Days

Patrick Yeamans

Thursday, June 13, 2019
Date

10389

Appendix E Steel Material Certifications

3307
LID
BOWL V2

SCOT FORGE

105 Scot Drive, Clinton WI 53525-9029
Phone: 847/587-1000 Fax: 847/587-2000

PO #49627-2

MATERIAL CERTIFICATION

Cust # 503855
Heat # CJ162

Page 1 of 3

CJ162

SOLD TO		Material Cert Number: 540289-1-R0
		Revision Date: 05/20/2019

Item 4	Part Number: 49300
Material	AISI 4340 Aircraft Quality Steel in accordance with MIL-S-5000E, AMS-S-5000, AMS 2304B, AMS 6484E, AMS 6415U, AMS 6409E, AMS 2310F, AMS 2301K, ASTM A322-13(2018), A108-18 in lieu of A331 Capable of Boeing BMS 7-28G We take exception to DMS-1555
Thermal Process	Sub Critical Anneal, Normalize to 235 Maximum Brinell
Destructive Test	per Specification
Reference	Part Number: 49300
Finish	Rough Machine to sizes shown Straightness = 1/8" in 5 FT
Dimensions	OD Random Len (inches) 13 132 to 156
Surface	250 RMS Saw Cut

Heat Number	# of Pieces	Melting Mill:
CJ162	2	ELLWOOD QUALITY STEELS COMPANY

Note: Additional prefix letter stamped on product with heat number is for our inventory purposes only and not relevant to heat number.

Mill Chemistry (Wt. %)

C	Mn	P	S	Si	Ni	Cr	Mo	Cu	Al	V
0.41	0.73	0.011	0.013	0.23	1.67	0.82	0.22	0.19	0.033	0.009
Cb	**N**	**B**	**Ti**	**H**	**Ca**	**Sb**	**As**	**Sn**	**Pb**	
0.003	0.0060	<0.0005	0.001	0.00017	<0.001	<0.001	0.005	0.011	<0.001	

Cast Jominy

(In.)	1	2	3	4	5	6	7	8	9	10	12	14	16
(HRC)	57	57	57	56	56	56	56	56	55	55	55	55	54
18	20	24	28	32									
53	52	51	49	47									

Heat Treatment

Serial Number(s)	1 - 2	1 - 2
Treatment	Normalize	Sub-critical anneal
Temperature	1625 °F	1250 °F
Time	9.75 Hours	14.00 Hours

13 RD

The recording of false, fictitious or fraudulent statements or entries on this document may be punishable as a felony under Federal Statute.

Jerry Glessinger
Corporate Quality Assurance Manager
This certification has been created and reviewed in compliance with the Scot Forge QMS

3307

SCOT FORGE

105 Scot Drive, Clinton WI 53525-9029
Phone: 847/587-1000 Fax: 847/587-2000

PO #49627-2

MATERIAL CERTIFICATION

Cust # 503855
Heat # CJ162

Page 2 of 3

Material Cert Number
540289-1-R0

Mechanical Testing

Hardness

Serial Number(s)	HBW
2	207

Decarburization Exam

Test Number(s)	1
Decarb Result	DECARBFREE

Micro-Exam

Serial Number(s) 1

Date Tested	05/10/2019
Micro-Exam Test Type	Austenite Grain Size
Micro-Exam Specification	ASTM E112-13
Micro-Exam Method	Oxidation
Micro-Exam Etchant	Picral
Actual Grain Size	8
Micro-Exam Test Result	AUST. GS= 8
Total Magnification	100X
Objective Magnification	10X
Disposition	Pass

The recording of false, fictitious or fraudulent statements or entries on this document may be punishable as a felony under Federal Statute.

Jerry Glessinger
Corporate Quality Assurance Manager
This certification has been created and reviewed in compliance with the Scot Forge QMS

3307

SCOT FORGE

105 Scot Drive, Clinton WI 53525-9029
Phone: 847/587-1500 Fax: 847/587-2000

PO #49627-2

MATERIAL CERTIFICATION

Cust # 503855
Heat # CJ162

Page 3 of 3

Material Cert Number
540289-1-R0

Notes

4.93:1 FORGING REDUCTION FROM ORIGINAL INGOT

MELTED AND MANUFACTURED IN THE U.S.A.

CLEANLINESS INSPECTION PERFORMED PER AMS 2301K & 2304B
RESULTS: FREQUENCY=0.00 SEVERITY=0.00

JOMINY PERFORMED BY ELLWOOD QUALITY STEELS COMPANY
RESULTS FOUND ACCEPTABLE (SEE ATTACHED MILL CERTIFICATION)

540289-1: 5730 LBS WGT
540289-2: 5420 LBG WGT

CERTIFIES THAT THIS IS
A TRUE COPY OF THE ORIGINAL MILL TEST
REPORT NOW ON FILE
RECEIVED AND INSPECTED

MAY 31 2019

BY _____ - Q.C. MANAGER

Compliance Statements:

We certify that the material listed was not processed with mercury bearing instruments and/or equipment which might cause contamination, nor was mercury handled in the immediate vicinity during the manufacturing process. We also certify that the material was not processed or cleaned with low melting point materials as alloying constituents, i.e. lead, zinc, cadmium, tin, antimony, bismuth, sulfur, or their compounds. We certify that our production equipment and production areas are asbestos-free.

In accordance with the requirements of the Pressure Equipment Directive, all testing, inspection, and documentation is produced in accordance with EN 10204:2004 Type 3.1 and ISO 10474 Type 3.1.B.

Material provided has been produced by Scot Forge under an approved quality program as defined within the Scot Forge Quality Management System Manual, Revision 6, dated 8/23/2018.

The products supplied are in compliance with the quantity and quality requirements of the purchase order and specifications noted. The test reports represent the actual attributes of the items furnished and the test results are in full compliance with all applicable specifications and order requirements.

Jerry Glessinger
Corporate Quality Assurance Manager
This certification has been created and reviewed in compliance with the Scot Forge QMS

The recording of false, fictitious or fraudulent statements or entries on this document may be punishable as a felony under Federal Statute.

3308

INSERT V2

A0862J

Liberty Specialty Steels
7, Fox Valley Way
Stocksbridge
Sheffield
S36 2JA
Telephone: + 44 (0) 114 288 2361
Fax (main) : + 44 (0) 114 283 2079
Website : www.libertyspecialitysteels.com

INSPECTION CERTIFICATE/TYPE 3.1 to BS EN10204/LSS AIRCRAFT RELEASE PROCEDURE

Cast No. A0862J	Works Order No. C8827910	Date of Issue 12-DEC-2018
	Customer Order No. 49298-4(S49160)	Certificate No. 00708728/1
		Page No. 1 of 6

SPECIFICATIONS ASSOCIATED WITH THIS ORDER -
E4340 TO AMS6409 + (14) ADDITIONAL SPECS
SAE AMS 6409 REV E
SAE AMS 6415 REV U
SAE AMS 2301 REV.K 2015
SAE AMS 2304 REV.B 2015
SAE AMS 2310 REV.F 2015
BOEING BMS 7-28 REV.G
VOUGHT; AERONAUTICS CVA 1-585 REV.G
SAE AMS 6484 REV E
ASTM A322 REV 13 E4340;INCLUDING S13
ASTM A108 13 4340
ASTM A331 95 (R2000)
DOUGLAS; AIRCRAFT DMS 1555; GRADE B H
SAE AMS-STD-2154 REV C TYPE II; CLASS B
SAE AMS-S-5000 REV.A E4340 NOTICE
MIL-S-5000 E.NOTICE 1 E4340

CERTIFIES THAT THIS IS
A TRUE COPY OF THE ORIGINAL MILL TEST
REPORT NOW ON FILE
RECEIVED AND INSPECTED

DEC 1 8 2018

BY _____ Q.C. MANAGER

PRODUCT INFORMATION -
SIZE - 6.75"
QUANTITY/WEIGHT - 6 BARS 4.182 TONNES APPROX
LENGTHS 3.540/3.975M
IDENTITIES: 34 - B B1 2 21 TO TO1
CONDITION OF MATERIAL - COLD STR, NORMALISED, SM TURN, TEMPERED
STEELMAKING PROCESS/PROCESS OF MANUFACTURE - Electric VDG Ingot
CERTIFICATE OF COMPLIANCE NUMBER - 708728

HEAT TREATMENT OF MATERIAL -
Normalise at 899° C; for 01:00; Air Cooled.
Temper at 670° C; for 06:00; Air Cooled.

ANALYSIS -

Cast No	C %	Si %	Mn %	P %	S %	Cr %	Mo %	Ni %	Cu %	Sn %	Al %	Nb %	Ti %	V %
Cast Analysis														
A0862J	.415	.24	.78	.007	.0012	.90	.28	1.96	.12	.005	.031	<.001	.0009	.001

6 3/4 D

3308

LIBERTY STEEL

Liberty Specialty Steels
7, Fox Valley Way
Stocksbridge
Sheffield
S36 2JA
Telephone: + 44 (0) 114 288 2361
Fax (main) : + 44 (0) 114 283 2079
Website : www.libertyspecialitysteels.com

INSPECTION CERTIFICATE/TYPE 3.1 to BS EN10204/LSS AIRCRAFT RELEASE PROCEDURE

Cast No. A0862J	Works Order No. CB827910	Date of Issue 12-DEC-2018
	Customer Order No. 49298-4(S49160)	Certificate No. 00708728/1
		Page No. 2 of 6

Mechanical Test - Tested to ASTM E8 - 16a
Material Specification BMS 7-28
Sample Heat Treatment -
Normalise 899C for 01:00hr Air Cool in 10mm Dia
Harden 829C for 01:00hr Oil Quench
Temper 496C for 02:00hr Air Cool

	Test No.	Ingot Id	Ingot Pos.	Sample Pos.	Orient	Temp.	0.2% PS	U.T.S	R of A	Tensile G.L	Frac Pos.
Units						C	PSI	PSI	%	inches	
Result	3575562	34	T	Mid-Radial	Tr	RT	185000	197000	48.0	1.000	A
	3575563	34	T	Mid-Radial	Tr	RT	184000	195000	49.0	1.000	A
	3575564	34	B	Mid-Radial	Tr	RT	187000	197000	55.0	1.000	A
	3575565	34	B	Mid-Radial	Tr	RT	187000	198000	54.0	1.000	B

Mechanical Test - Tested to ASTM E8 - 16a
Material Specification DMS 1555
Sample Heat Treatment -
Normalise 899C for 01:00hr Air Cool in 12mm Dia
Harden 816C for 01:00hr Oil Quench start temp. 55C
Temper 246C for 02:00hr Air Cool
Second Temper 246C for 02:00hr Air Cool

	Test No.	Ingot Id	Ingot Pos.	Sample Pos.	Orient	Temp.	0.2% PS	U.T.S	Elong At Fr	R of A	Tensile G.L	Frac Pos.
Units						C	PSI	PSI	%	%	inches	
Result	3583492	33	T	Mid-Radial	Tr	RT	229000	269000	11.5	41.0	1.000	B
	3583493	33	T	Mid-Radial	Tr	RT	227000	268000	11.8	41.0	1.000	B
	3583494	33	T	Centre	Tr	RT	235000	269000	10.8	41.0	1.000	B
	3583495	33	T	Centre	Tr	RT	235000	271000	10.5	40.0	1.000	B
	3583496	33	B	Mid-Radial	Tr	RT	227000	268000	12.6	44.0	1.000	B
	3583497	33	B	Mid-Radial	Tr	RT	227000	268000	11.4	44.0	1.000	B
	3583498	33	B	Centre	Tr	RT	225000	268000	12.0	47.0	1.000	B
	3583499	33	B	Centre	Tr	RT	226000	268000	12.0	43.0	1.000	B

Mechanical Test - Tested to ASTM E8 - 16a
Material Specification AMS 6409
Sample Heat Treatment -
Normalise 899C for 01:00hr Air Cool in 10mm Dia
Harden 829C for 01:00hr Oil Quench
Temper 496C for 02:00hr Air Cool

	Test No.	Ingot Id	Ingot Pos.	Sample Pos.	Orient	Temp.	U.T.S	R of A	Tensile G.L	Frac Pos.
Units						C	KSI	%	inches	
Result	3575562	34	T	Mid-Radial	Tr	RT	197.0	48.0	1.000	A
	3575563	34	T	Mid-Radial	Tr	RT	195.0	49.0	1.000	A
	3575564	34	B	Mid-Radial	Tr	RT	197.0	55.0	1.000	A
	3575565	34	B	Mid-Radial	Tr	RT	198.0	54.0	1.000	B

3308

LIBERTY STEEL

Liberty Specialty Steels
7, Fox Valley Way
Stocksbridge
Sheffield
S36 2JA
Telephone: + 44 (0) 114 288 2361
Fax (main) : + 44 (0) 114 283 2079
Website : www.libertyspecialitysteels.com

INSPECTION CERTIFICATE/TYPE 3.1 to BS EN10204/LSS AIRCRAFT RELEASE PROCEDURE

Cast No. A0852J

Works Order No. CB827910
Customer Order No. 49298-4(S49160)

Date of Issue 12-DEC-2018
Certificate No. 00708728/1
Page No. 3 of 6

Mechanical Test - Tested to ASTM A370 - 17a
CVA-1-585
Sample Heat Treatment -
Normalise 899C for 01:00hr Air Cool in 12mm Dia
Harden 816C for 01:00hr Oil Quench start temp. 55C
Temper 246C for 02:00hr Air Cool
Second Temper 246C for 02:00hr Air Cool

	Test No.	Ingot Id	Ingot Pos.	Sample Pos.	Orient	Temp.	0.2% PS	U.T.S	Elong At Fr	R of A	Frac Pos.
Units						C	PSI	PSI	%	%	
Result	3583492	33	T	Mid-Radial	Tr	RT	229000	269000	12.0	41.0	B
	3583493	33	T	Mid-Radial	Tr	RT	227000	268000	12.0	41.0	B
	3583494	33	T	Centre	Tr	RT	235000	269000	11.0	41.0	B
	3583495	33	T	Centre	Tr	RT	235000	271000	11.0	40.0	B
	3583496	33	B	Mid-Radial	Tr	RT	227000	268000	13.0	44.0	B
	3583497	33	B	Mid-Radial	Tr	RT	227000	268000	11.0	44.0	B
	3583498	33	B	Centre	Tr	RT	225000	266000	12.0	47.0	B
	3583499	33	B	Centre	Tr	RT	226000	268000	12.0	43.0	B

Grain Size Test - Tested to ASTM E112 - 13 (Comparison Method)
MacQuaid Ehn Grain Size - Carburised at 925 Deg C 8 Hours Furnace Cooled.

Tested at a magnification of X100

	Test No.	Ingot Id	Ingot Pos.	G.Size	G.Size	No. Fields	Etchant
Result	3564937	31	M	8	7	10	Picral

Jominy End Quench Test - Tested to ASTM A255 - 10 (REAP 2014)
Sample Heat Treatment -
Normalise 871C for 01:00hr Air Cool in 35mm Dia
Austenitise 843C for 00:30hr Water Quench start temp. 19C in 25mm Dia

	Test No.	Ingot Id	Ingot Pos.	1/16"	2/16"	3/16"	4/16"	5/16"	6/16"	7/16"	8/16"	9/16"	10/16"	11/16"	12/16"	13/16"	14/16"	15/16"	16/16"
Units				HRc	HRc	HRc	HRc	HRc	HRc	HRc	HRc	HRc	HRc	HRc	HRc	HRc	HRc	HRc	HRc
Result	3575581	34	M	58.5	59.0	58.5	58.5	58.0	57.5	57.5	57.5	57.5	57.5	57.0	57.5	57.0	57.0	57.5	57.0

	Test No.	Ingot Id	Ingot Pos.	18/16"	20/16"	24/16"	28/16"	32/16"
Units				HRc	HRc	HRc	HRc	HRc
Result	3575581	34	M	56.5	57.0	56.5	56.5	56.5

Works Surface Hardness - Tested to ASTM E10 - 17

	Test No.	Ingot Id	Ingot Pos.	Hardness	Hardness
Units				HBW10/3000	HBW10/3000
Result	3575570			235	235

3308

LIBERTY STEEL

Liberty Specialty Steels
7, Fox Valley Way
Stocksbridge
Sheffield
S36 2JA
Telephone: + 44 (0) 114 288 2361
Fax (main) : + 44 (0) 114 283 2079
Website : www.libertyspecialtysteels.com

INSPECTION CERTIFICATE/TYPE 3.1 to BS EN10204/LSS AIRCRAFT RELEASE PROCEDURE

Cast No. A0862J	Works Order No. C0827910	Date of Issue 12-DEC-2018
	Customer Order No. 49298-4(S49160)	Certificate No. 00708728/1
		Page No. 4 of 6

Decarburisation Test - Tested to ASTM E1077 - 14
Magnification X100

	Test No.	Ingot Id	Ingot Pos.	Sample Pos.	Max Dec	Avg Dec	Etchant
Units					mm	mm	
Result	3575566		R	Edge	0.00	0.00	0.00

Magnetic Particle Inspection Test - Tested to ASTM E1444 - 2016e
AMS 2301

	Test No.	Ingot Id	Ingot Pos.	Sev	Freq
Result	3564918	11	T	0.00	0.00
	3564916	21	T	0.00	0.00
	3564920	31	T	0.00	0.00
	3564917	11	B	0.00	0.00
	3564919	21	B	0.00	0.00
	3564921	31	B	0.00	0.00

Magnetic Particle Inspection Test - Tested to ASTM E1444 - 2016e
AMS 2304

	Test No.	Ingot Id	Ingot Pos.	Sev	Freq
Result	3564918	11	T	0.00	0.00
	3564916	21	T	0.00	0.00
	3564920	31	T	0.00	0.00
	3564917	11	B	0.00	0.00
	3564919	21	B	0.00	0.00
	3564921	31	B	0.00	0.00

Hardness test - Tested to BS EN ISO 6506 - 1 2014

	Test No.	Ingot Id	Ingot Pos.	Mid Radial	Mid Radial
Units				HBW10/3000	HBW10/3000
Result	3575567		R	228	230

3308

LIBERTY STEEL

Liberty Speciality Steels
7, Fox Valley Way
Stocksbridge
Sheffield
S36 2JA
Telephone: + 44 (0) 114 288 2351
Fax (main) : + 44 (0) 114 283 2079
Website : www.libertyspecialitysteels.com

INSPECTION CERTIFICATE/TYPE 3.1 to BS EN10204/LSS AIRCRAFT RELEASE PROCEDURE

Cast No. A0862J	Works Order No. CS827910	Date of Issue 12-DEC-2018
	Customer Order No. 49298-4(S49160)	Certificate No. 00706728/1
		Page No. 5 of 6

Macroetch Test - Tested to ASTM E381 - 17

Result

Test No.	Ingot Id	Ingot Pos.	Class S	Class R	Class C
3564928	11	T	1	1	1
3564930	21	T	1	1	1
3564932	31	T	1	1	1
3564929	11	B	1	1	1
3564931	21	B	1	1	1
3564933	31	B	1	1	1

Ultrasonic Test - Tested to INTERNAL PROCEDURE CAR ALLOY OR MARTENSITIC STAINLESS STEELS
Satisfactory To procedure 7UD

Ultrasonic Test - Tested to SAE AMS-STD-2154 TYPE II (Contact Method)
Satisfactory to CLASS B STAMP

Ultrasonic Test - Tested to BS 6S 100:2010
Satisfactory to CLASS A HIGH STAMP

MISCELLANEOUS INFORMATION -
NO WELDING PERFORMED
SAE AMS6409 EXCEPT PARA.3.2.1-MATERIAL IN THE SOFT CONDITION, TYPICALLY < 20 ROCKWELL C.
MELTED & MANUFACTURED IN THE UK
BOEING VENDOR CODE NO. 561093
INGOT ROUTE
Airbus approval ref 224215 (Stocksbridge) and 270919 (Rotherham)
BAe Military Air Solutions approval held - please see BAE/AG/QC/SC10 For Grade Approval List
BAeSystems approval number RALOA/00118/3
GE Aviation S-400 Certified Materials Test Laboratory. AE supplier code T9313
GKN Aerospace approved
Hawker Beechcraft approval number 10104108 RAW
Quality System approved to GE S1000
Released in accordance with Agusta Helicopters SQA50
Rolls-Royce RR9000:SABRe approval number 01509 and 11499
Speciality steel UK has complied with all producer requirements of AS6279
The recording of false, fictitious or fraudulent statements or entries on the certificate may breach applicable law.
UKAS accredited Testing Laboratory No. 4337
Unless stated otherwise all Metallurgical and Mechanical testing is carried out at Liberty Speciality Steels.
Unless stated otherwise all laboratory heat treatments are carried out in Air.
Unless stated otherwise all tensiles are Round Proportional Tension Test Specimens.
CES STAMP NUMBER - 7
Material type tested satisfactorily
Method of Analysis
- Atomic Emission Spectroscopy (CES) tested at our Rotherham laboratory Si Mn P Cr Mo Ni Cu Sn Al Nb Ti V
Radioactivity < 0.1Bq/g on ladle sample.
% Elongation is measured after fracture.
This product is mercury free.
No weld repair carried out on this product.
Liberty Speciality Steels quality management system is certified to the following standards : ISO9001 and AS/EN9100.
Liberty Speciality Steels environmental system is certified to IS014001.
Material is melted and manufactured in the United Kingdom.

3308

INSERT V2

LIBERTY STEEL

Liberty Specialty Steels
7, Fox Valley Way
Stocksbridge
Sheffield
S36 2JA
Telephone: + 44 (0) 114 288 2361
Fax (main) : + 44 (0) 114 283 2079
Website : www.libertyspecialitysteels.com

INSPECTION CERTIFICATE/TYPE 3.1 to BS EN10204/LSS AIRCRAFT RELEASE PROCEDURE

Cast No. A0862J	Works Order No. CB627910	Date of Issue 12-DEC-2018
	Customer Order No. 49298-4(S49160)	Certificate No. 00708726/1
		Page No. 6 of 6

AUTHORISED SIGNATURE -
Certified by Liberty Specialty Steels that, unless otherwise stated above, the whole of the above mentioned materials have been manufactured, tested & inspected in accordance with the terms of the contract/order applicable thereto and conform fully to the standard/specifications quoted hereon.
Approved Signatory - Matthew Grice, Certification and Accreditation Manager

Signed.....

For Liberty Specialty Steels

End Of Certificate

ELLWOOD QUALITY STEELS COMPANY

A PENNSYLVANIA BUSINESS TRUST
700 MORAVIA STREET, NEW CASTLE, PA 16101

Page 1 of 1

EQS
(724) 658-6788
Telefax (724) 658-6802

CERTIFIED TEST REPORT

Date: 3/5/19

Report of Tests of: (3), 31" X 175" - Grade G43400XXX / 4340 Ingot(s)

For Company: Scot Forge
8001 Winn Rd
Spring Grove, IL 60081

Customer's Order: 137163
Date of Order: 2/25/19
Our Shop Order: 142690
Specification: G43400XXX REV.4

CHEMICAL ANALYSIS

Heat #	C	Mn	P	S	Si	Ni	Cr	Mo	V	Cu	Al	Hppm	Ti	As
CJ162	.41	.73	.011	.013	.23	1.67	.82	.22	.009	.19	.033	1.7	.001	.005
	Sn	Pb	B	Sb	Nb	Ca	N							
	.011	<.001	<.0005	<.001	.003	<.001	.0060							

Jominy: CJ162 (Cast) per ASTM A255

J-Position	1	2	3	4	5	6	7	8	9	10	11	12	13	14	15	16	18	20	22	24	26	28	30	32
Rc Hardness	57	57	57	56	56	56	56	56	55	55	55	55	55	55	54	54	53	52	52	51	50	49	49	47

Jominy was austenitized at a temperature of 1550 degrees F.

The material was melted using the electric furnace-ladle refined-vacuum degassed process and was subsequently bottom poured.

The material is capable of meeting AMS S-5000.

The material is capable of meeting SAE J404.

The material is capable of meeting FED MIL-S-5000E.

The material has been melted using a fine grain melt practice of 5 or finer per ASTM E112.

The material meets the requirements of Scot Forge specification #104 Rev. 4 dtd. 9/12/18.

The material has been aluminum deoxidized.

Capable of 20ppm max. Oxygen.

The material was produced in accordance with the EQS Quality Manual dtd. 5/27/16, Rev. 3 which meets the intent of the latest revisions to ISO 9001:2015, ISO 10012-1, MIL-I-45208, NCA-3800, and 10-CFR-50 App. B for quality assurance, inspection and calibration systems.

This material was produced in the U.S.A.

The material is capable of meeting the inclusion content requirements of ASTM A866.

I certify that the reported results and statements of the certificate represent the actual attributes of the material furnished and are in full compliance with all purchase order/ specification requirements. The recording of false, fictitious or fraudulent statements or entries on this document may be punishable as a felony under Federal Statutes. During the manufacturing process, tests, and inspections, the material did not come in direct contact with mercury or any of its compounds nor with any mercury containing device employing a single boundary of containment. No welding or weld repair was performed on this material. The material was produced free of radioactive elements.

Gregory J. Morgan
Quality Engineer

Appendix F Heat Treatment Certification

HDHT
HIGH DESERT HEAT TREATING

CERTIFICATE OF COMPLIANCE

High Desert Heat Treating LLC.
709 W 1st Street Bldg 5A (Bay C)
Ogden Business Depot, Ogden UT 84404

This is to certify that the goods described below have been treated in accordance with the customers requirements.

Customer:	Yeamans Machine Shop		
P.O#	10389		
Part Number:	Lid	Bowl V2	Insert V2
Quantity:	3 ea	3 ea	3 ea
Material:	4340	4340	4340
Process Performed:	Austenitize and Temper		
Specification Required:	Dwg # Lid	Dwg # Bowl V2	Dwg # Insert V2
Hardness Required:	36-40 HRC	36-40 HRC	36-40 HRC
Actual Hardness:	38-39 HRC	38-40 HRC	38-39 HRC
QTY. Tested	66%	66%	66%

Notes:

Hardness Test Performed By: Cooper Griffin Date: 9/12/2019

Signiture:

Quality
M Alex Bloemen

Date: 9/12/2019

Document Created By: Alex Bloemen: Effective 01 Dec 2014
D 00120 R1 6/1/2015

Appendix G Miscellaneous Datasheets

Pressures to 150,000 psi (10342 bar)

Parker Autoclave Engineers high pressure fittings Series F and SF are the industry standard for pressures to 150,000 psi (10342 bar). Utilizing Parker Autoclave Engineers high pressure coned-and-threaded connections, these fittings are correlated with Series 30SC, 43SC, 30VM, 40VM, 60VM, 100VM, and 150V valves and Parker Autoclave Engineers high pressure tubing.

Connection Components

All Parker Autoclave Engineers valves and fittings are supplied complete with appropriate glands and collars. To order these components separately, use order numbers listed. When using plug, collar is not required.

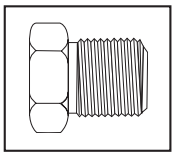

Gland
AGL ( )

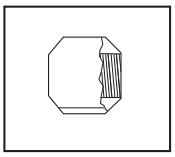

Collar
ACL ( )

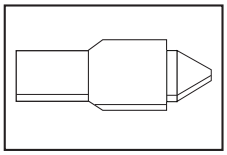

Plug
AP ( )

Add tube size ( )
1/4" - 40
5/16" - 50
3/8" - 60
9/16" - 90
1" - 160

Example:
9/16" Gland - AGL (90)

To ensure proper fit use Parker Autoclave Engineers tubing.

Note: Special material glands may be supplied with four flats in place of standard hex.

Connection Type	Gland	Collar	Plug	Connection Components (Industry Standard)
F250C F375C F562C F562C40 40F562C-312	AGL( )	ACL( )	AP( )	Parker Autoclave Engineer's high pressure fittings 1/4, 3/8 and 9/16 connection components to 60,000 psi (4137 bar). For use with 30VM, 40VM, 60VM valves and fittings.
F1000C43	CGLX160	CCLX160	43CP160	Parker Autoclave Engineer's high pressure 1" connection components to 43,000 psi (2965 bar) for use with 30SC, 43Y valves, and fittings.
F312C150	CGL50	CCL50	CP50	Parker Autoclave Engineer's ultra high pressure 5/16 connection components to 150,000 psi (10342 bar) for use with 100VM and 150V valve and fittings.
	100CGL40 100CGL60	100CCL40 100CCL60	100CP40 100CP60	Parker Autoclave Engineer's 100,000 psi (6895 bar) connection components utilize our 5/16" connection for 1/4" and 3/8" tubing. (See Note*)

PRIMASHEET® 1000 Flexible Sheet Explosive (DETASHEET® Flexible Explosive)

PRODUCT TECHNICAL DATA SHEET

DESCRIPTION:

PRIMASHEET® 1000 Flexible Sheet Explosive (DETASHEET® Flexible Explosive) is a waterproof PETN-based (63% nominal) flexible sheet explosive. It is manufactured as a continuous roll of varying lengths and thicknesses for a wide range of applications. It is type classified and qualified to MIL-PRF-46676 for use by United States Military and International Forces.

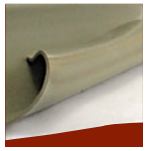

APPLICATION:

Due to its consistent performance and properties, PRIMASHEET® 1000 fulfills a wide variety of uses in military demolition applications and commercial explosive hardening of metals. Both commercial and military configurations are available.

- Breaching
- Military demolition
- Ordnance disposal
- Metal hardening
- Metal forming and welding
- Skin severance charge

PROPERTIES:

- VOD: 7,100 m/s (nominal)
- Density: 1.44 g/cc (nominal)
- Operating temperature: -40°F to 165°F (-40°C to 74°C)
- Bullet-impact insensitive
- Compliant with Montreal Protocol

ENSIGN-BICKFORD AEROSPACE & DEFENSE COMPANY

www.EBA-D.com

Rev. 1

EBAD Ensign-Bickford Aerospace & Defense

EX-9304026
Explosive, Blasting, Type D, UN0084
1.1D

PRIMASHEET® 1000 Flexible Sheet Explosive (DETASHEET® Flexible Explosive)

SPECIFICATIONS:

NATIONAL STOCK NUMBER	DODIC	WEIGHT	THICKNESS (NOMINAL)		ROLLS PER BOX	WEIGHT PER ROLL		ROLL LENGTH	
		gm/in²	in	mm		lb	kg	ft	m
1375-01-565-8411	M994	C 1	0.042	1	2	10	4.5	38	11.6
1375-01-565-2743	M993	C 1.5	0.062	1.5	2	10	4.5	24	7.2
1375-01-562-3014	M980	C 2	0.083	2	2	20	9.1	38	11.6
1375-01-562-3220	M981	C 3	0.125	3	2	20	9.1	25	7.6
1375-01-568-2740	M982	C 4	0.166	4	2	20	9.1	19	5.8
1375-01-568-2737	M983	C 5	0.208	5	2	20	9.1	15	4.6
1375-01-562-3225	M984	C 6	0.250	6	2	20	9.1	13	4.0
1375-01-568-2729	M985	C 7	0.291	7	2	20	9.1	11	3.4
1375-01-568-2716	M986	C 8	0.333	8	2	20	9.1	9	2.7

OPERATION:

Demolition/Breaching—PRIMASHEET® 1000 is an excellent tool for general demolition applications. It can be easily cut to any desired shape and applied with adhesive or incorporated into a charge holder. The flexible sheet can be applied as strips directly on the target or used to improvise linear shape charges.

Metal Hardening—PRIMASHEET® 1000 finds extensive use in hardening metals. Manganese steels can be hardened by detonating the flexible sheet in contact with the metal surface. This high-velocity hardening technique is used extensively in the railroad industry for metal track switches. Explosive joining and forming of metals can also be accomplished with PRIMASHEET® 1000.

ENSIGN-BICKFORD AEROSPACE & DEFENSE COMPANY
640 HOPMEADOW STREET, P.O. BOX 429, SIMSBURY, CT 06070, USA www.EBA-D.com

Rev. 1

Cleared for Open Publication by the Office of Security Review, Department of Defense 05/30/17 **17-S-1756**

RP-2
EBW DETONATOR

RP-2 EBW Detonator

P/N 167-4379

The RP-2 is a high precision Exploding Bridgewire Detonator manufactured by RISI which features close tolerance electrode spacing, precise bridgewire attachment, high quality loading sleeves and a rigidly controlled crystallization process of the PETN explosive and loading operation. Density is controlled through consistency of crystalline structure, precision weighing and class 'A' dies and tooling.

The result is a detonator with a transmission line simultaniety standard deviation of less than .035 microsecond. While some applications may not require this degree of timing or safety, users may want to take advantage of the high degree of reliability present in this detonator.

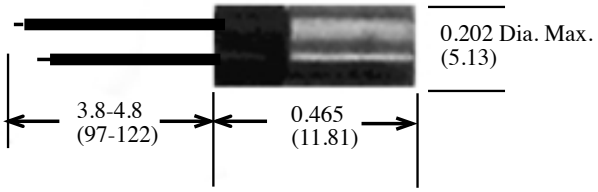

RP-2 EXPLOSIVE TRAIN

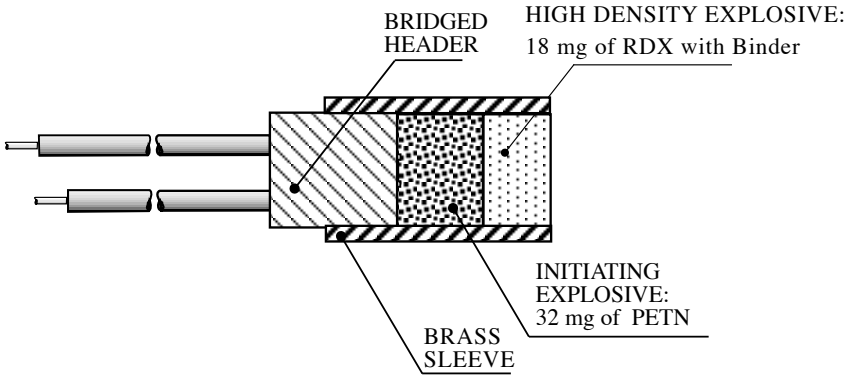

RP-2 Firing Parameters

- Threshold Burst Current: 220 amps
- Threshold Voltage: Approx. 500 volts
- Threshold Voltage Std. Deviation: 25 volts maximum
- Function Time: 1.65 μsec. typical
- Function Time Simultaneity Standard Deviation: 0.035 μsec Max.

Caution: While EBW and EFI Initiators are inherently less susceptible to accidental detonation during handling and set-up than devices containing primary explosives, electrical and electronic firing systems are sensitive to transient electrical energies which could cause premature triggering or firing. The blasting area must be clear of personnel and equipment before the detonator leads are connected to any RISI Firing System. Only approved RISI Firing Systems should ever be used to initiate or detonate any explosive product manufactured and authorized for sale by RISI.

Pressure

KISTLER
measure. analyze. innovate.

Quartz High-Pressure Sensor

Type 6213B...

for Ballistic Pressure Measurement to 10 000 bar

Front sealing high pressure sensor for ballistic and hydraulic pressure measurements up to 10 000 bar.

- Extremely high life
- Good long-time stability
- Excellent linearity

Description
Front sealed diaphragm, therefore very low mechanical and thermal stress of the sensor, no mounting gap (small dead volume) and a laregely reduced surface pressure in the sealing part.

Easy handling, through M12x1 damaging through mounting torque barely possible.
Measuring element out of quartz crystal. Therefore, high stability of the sensitivity and no drift through pyroelectricity. The optimized shape through machined diaphragm.

Thanks to patented Anti-Strain construction, the sensor is not critical to different tightening torques and mounting conditions. It excels by its excellent linearity of ≤±0,5 %, an extremely high life and a good long-time stability.

Application
Use for all ballistic measurements and measuring configurations and as a reference sensor. Despite its extremely large measuring range, the sensor is best suited for measuring relatively low pressures of several hundred bar.

Based on its accurate performance, highly suitable to be used as reference sensor for calibration setup (version 6213BK with linearity >±0,3 %FSO.

Type 6213B

Type 6213BA, short version

Technical Data

System		
Measuring range	bar	0 ... 10 000
Calibrated range	bar	0 ... 8 000
Calibrated partial range	bar	0 ... 1 000
Overload	bar	11 000
Threshold	bar	<0,02
Sensitivity	pC/bar	–1,2
Natural frequency	kHz	>150
Rise time	µs	2
Linearity	%FSO	≤±0,5
for range and partial range (typical)	%FSO	<±0,3
Acceleration sensivity	bar/g	<0,005
Shock resistance axial	g	25 000
transverse	g	10 000
Temperature coefficient of sensitivity	%/°C	≤±0,02
Operating temperature range	°C	–50 ... 200
Capacitance Type 6213B	pF	≈5,5
Type 6213BA	pF	≈60
Insulation resistance at 20 °C	Ω	$>10^{13}$
Tightening torque	N·m	40
Weight	g	18

1 bar = 10^5 Pa (Pascal) = 10^5 N · m^{-2} = 1,0197... at = 14,503... psi;
1 g = 9,80665 m · s^{-2}; 1 N·m = 0,73756... lbft; 1 g = 0,03527... oz

6213B_000-042e-12.10

KISTLER
measure. analyze. innovate.

Dimensions and Mounting Bore Type 6213B

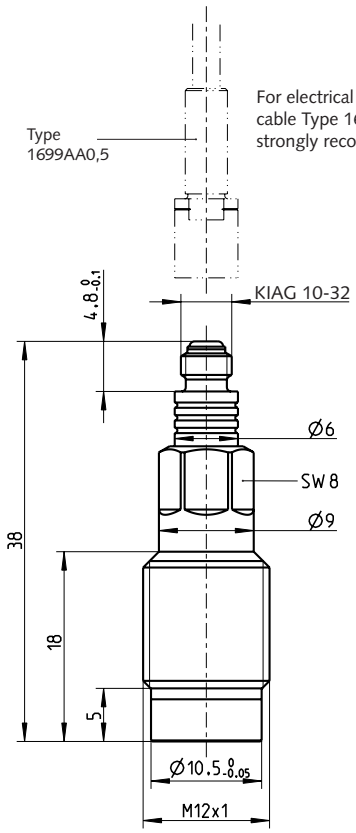

Fig. 1: Dimensions Type 6213B

Dimensions and Mounting Bore Type 6213BA

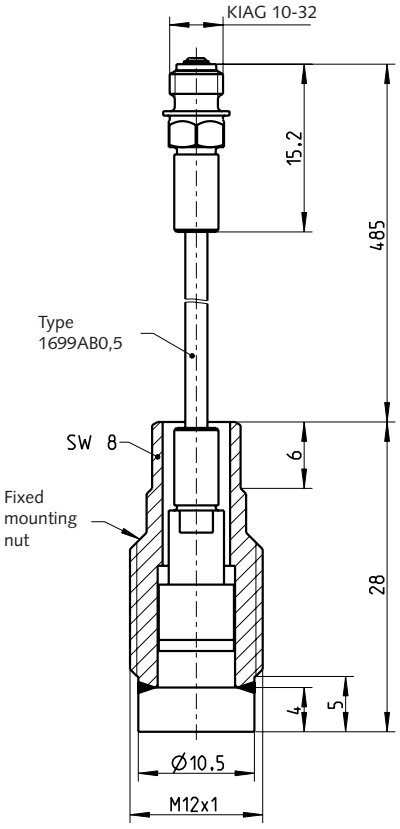

Fig. 2: Dimensions Type 6213BA

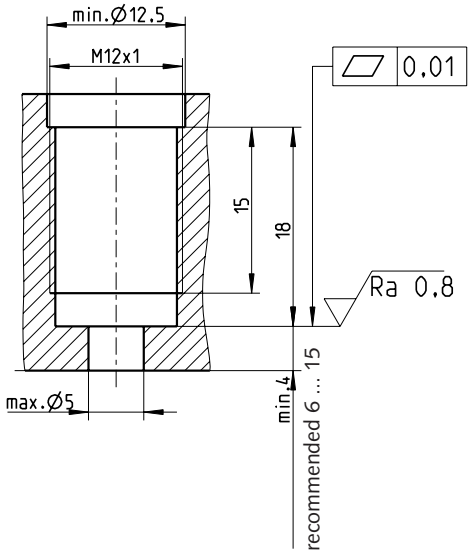

Fig. 3: Mounting bore Type 6213B and 6213BA

KISTLER
measure. analyze. innovate.

Mounting

To mount the sensor, a threaded hole M12x1 with accurately machined contact face, which has been finished with the surface finishing tool Type 1300A23, is sufficient (Fig. 3). The sensor can be fitted without special thermal protection, using only the sealing ring Type 1100 (Fig. 4).

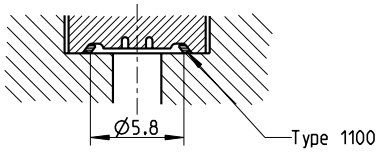

Fig. 4: Direct mounting

The front seal allows the use of an additional attachment. Fig. 5 shows the installation with thermal protection shield Type 6563A and thermal protective plate Type 1181A to reduce thermal shock error. For measurements in which the sensor is exposed to heat over the entire pressure profile (e.g. in pressure bombs and cartridge chambers).

Fig. 6 shows the installation with diaphragm protector Type 6564. Recommended for measurements at the case mouth and along the measuring barrel as protection against mechanical damage from metal fragments and powder particles. It is essential to follow the operating instructions when machining the measuring hole and for installation.

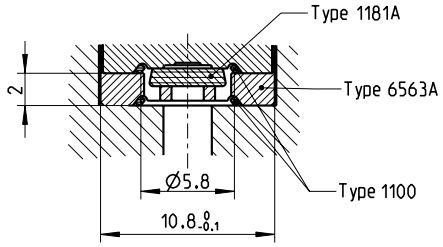

Fig. 5: Mounting with thermal protective plate (Type 1181) and thermal protection shield (Type 6563A)

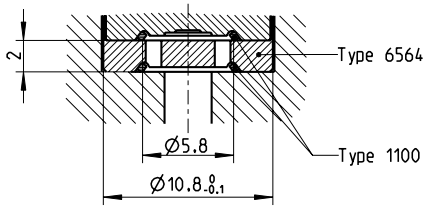

Fig. 6: Mounting with diaphragm protection (Type 6564)

Accessories Included	Type/Art. No.
• Sealing ring, 10 pieces	1100
• Lubrication grease, 1 piece	1063

Optional Accessories	Type/Art. No.
• Thermal protective plate	1181A
• Thermal protection shield	6563A
• Diaphragm protection	6564
• Sealing joint	1100
• Locking tappet	6467
• Adapter to pressure generator Type 6906	6923A
• Connection cable to Type 6213B, (KIAG 10-32 pos./KIAG 10-32 neg.)	1699AA0,5
• HT connection cable	1631C...
• Special drilling tool	1341
• Screw tap M12x1	1355
• Surface finishing tool	1300A23
• Torque wrench	1371B
• Tubular socket wrench hex. 8mm	1373

Ordering Key

Type 6213B ☐

Quartz high-pressure sensor	–
Quartz high-pressure sensor with additional accessories included Types 1341, 1355, 1300A23 + 1373	1
Short version with integr. cable	A
Selected high-pressure quartz sensor with linearity ≤0,3 %	K

6213B_000-042e-12.10

CLEARCO

Order Toll Free: 800 533-5823

Product Information

DPDM-400 High Temperature Silicone Heat Transfer Fluid

Operating Temperature Range: 25°C to 250°C (open system) / 25°C to 300°C (closed system)

DPDM-400 High Temperature Silicone Heat Transfer Fluid has a service life of 25°C to 300°C.

DPDM-400 High Temperature Silicone Heat Transfer Fluid is a clear, colorless silicone fluid that is classified as a Dimethyl-Diphenylsiloxane (CAS # 68083-14-7) with a viscosity of 400cSt @ 25°C. It is formulated for use as a heat transfer medium for high temperature ranging from 25ºC to 300ºC (closed system*).

DPDM-400 High Temperature Silicone Heat Transfer Fluid is characterized by its high flash point, high service temperature range, and low vapor pressure, high resistance to oxidation, high dielectric strength and hydrophobic nature (insoluble in water). It has a high VTC (viscosity-to-temperature coefficient) so its viscosity will lower quickly when heated, allowing for the fluid to be easily pumped.

DPDM-400 High Temperature Silicone Heat Transfer Fluid has a Thermal Conductivity value of 0.00032g/cal/cm/sec °C. Its specific heat value is 0.35 (cal/g °C @ 25°C.)

When compared to polydimethylsiloxane fluids (PSF-Fluids), DPDM-400 exhibits much higher thermal stability. Although it is more expensive, it will provide a very long service life.

Applications include: high temp heat transfer, high temperature open system baths, high temperature closed system baths, constant temperature baths, high temperature circulating baths, high temp closed loop baths, high temperature heat transfer baths, high temperature fluids for laboratory research apparatus and instruments.

* Closed system baths are systems from which air has been excluded.

Features

- Excellent High Temp Performance
- Service range: 25°C to 315°C (closed system)
- High Oxidation Resistance
- Non-Flammable
- High Temperature bath fluid for laboratory research apparatus and instruments.
- High Dielectric strength –dielectric fluid in capacitors
- High Temperature heat transfer applications
- Compatible with virtually all o-rings, gaskets, valves, seals, and hoses *
- VOC Exempt

Not recommended for silicone o-rings where the fluid may cause swelling

Properties

Appearance: clear, colorless, odorless fluid

Pour Point °C……-30°C
Flashpoint……315°C

Specific Gravity……1.07
Refractive index……1.505

Volatility, , % wt loss
24 hours @ 150°C……max 0.3%

Thermal
Expansion (cc/cc/C)……..0.00073

Dielectric Properties
Breakdown Voltage (KV/2.5mm)….>50
Dielectric Constant (50 Hz)……2.88
Dissipation Factor (50 Hz)……<0.0005

Thermal Gel Time (open system)
@ 250°C……1,500 to 2,000 hours
@ 260°C……>200 hours

Specific Heat
@ 25C……0.35 cal/g°C, 25°C

Thermal Conductivity
(cal/cm/sec °C)……0.00032

Thermal Expansion
(cc/cc/C)……0.00073

Surface Tension
(dynes/cm)…..25.2

Viscosity/Temp Specs.

Viscosity/Temp Coefficient……0.82

Viscosity @25°C…..400cSt (mm2/sec)

Viscosity @ temperature
@250°C……..7cSt (mm2/sec)
@ 200°C……..11cSt
@100°C……...46cSt
@50°C……167cSt
@25°C……400cSt
@ 0°C……1,770cSt
@ -25°C……24,800cSt

Packaging

1-gallon…….. 4kg / 8.8lb
5-gallon pail……20kg / 44 lb
55-gallon drum ……..200kg quote upon request

F.O.B. Phila, PA 19135 U.S.A.

For More Information, Contact:

Clearco Products Co., Inc.
3430 G. Progress Drive
Bensalem, PA 19020
Tel: 215 639-2640
Fax: 215 639-2919
Email: info@clearcoproducts.com
Web: www.clearcoproducts.com